MOLECULAR INTERFACES TO ELECTRONIC MATERIALS

by

Rose Emily Ruther

A dissertation submitted in partial fulfillment of

the requirements for the degree of

Doctor of Philosophy

(Chemistry)

at the

UNIVERSITY OF WISCONSIN-MADISON

2012

Date of final oral examination: 5/14/2012

The dissertation is approved by the following members of the Final Oral Committee:

Robert Hamers, Professor, Chemistry
John Wright, Professor, Chemistry
Franz Himpsel, Professor, Physics
Shannon Stahl, Professor, Chemistry
Padma Gopalan, Associate Professor, Materials Science

Molecular Interfaces to Electronic Materials

Rose Emily Ruther

Under the supervision of Professor Robert J. Hamers

University of Wisconsin-Madison

Abstract

The ability to introduce specific molecular groups to the surfaces of semiconductors holds great promise in photovoltaics, catalysis, sensing, and molecular electronics. This thesis describes the covalent functionalization of ZnO and diamond surfaces with a variety of different organic, inorganic, and organometallic groups.

The first part of this thesis investigates the photochemical grafting of organic alkenes on the $(10\bar{1}\,0)$ surface of single crystal ZnO and ZnO nanorods. The molecular layers are shown to be conformal to the underlying ZnO with a thickness controlled by the illumination time. The ability to perform multi-step synthetic chemistry on the ZnO surface is demonstrated.

The second part of this thesis looks at the formation of redox-active diamond surfaces. A combination of photochemical grafting and click chemistry (copper catalyzed azide alkyne cycloaddition) is used to couple inorganic and organometallic complexes to the diamond surface. A model ruthenium complex $[Ru(tpy)_2]$ tethered to the surface demonstrate remarkable stability to potential cycling out to very strongly oxidizing potentials (1.5 V vs. NHE). The electron transfer rate between diamond electrodes and surface-tethered ferrocene is also measured using electrochemical impedance spectroscopy. The electron transfer rate is shown to decrease with increasing surface coverage but is found to be independent of chain length. Electron transfer rates are generally fast, typically 10^3-10^4 s^{-1}.

Acknowledgements

Many people have contributed to this thesis. I would like to thank Bob for his patience and tremendous enthusiasm for science. I would like to thank the Hamers group, past and present. Your friendship and insight have kept me going. Thanks to Jeremy Streifer and Xiaoyu Wang for teaching me about the XPS, Monica Usrey and Kacie Louis for teaching me about football, Yizheng Tan for being a great labmate, Ryan Franking for caring more about my projects than I sometimes did, Heesuk Kim and Bin Sun for making me feel welcome in the group from day one, and Jixin Chen for being happy to help with anything and everything.

I would like to thank my many wonderful collaborators who have enriched my own projects and allowed me to contribute to and learn from theirs. Thanks to Adam Powell, James Gerken, Matt Rigsby, Shu Yao, Michael Nippe, Jennifer Laaser, Wei Xiong, Randy Mehlenbacher, Peerasak Paoprasert, and Peter Cook. You made my work more fun, more interesting, and more productive.

Thanks to all of my wonderful students, Alex Huhn, Sohil Shah, Connor Firth, Nigel Becknell, and Josh Thiede. I learned more from you than you did from me. You bring energy and creativity into the lab and remind me that science is actually pretty cool sometimes.

Finally, many thanks to my family, especially my grandparents who loved school.

Table of Contents

Chapter 1

Introduction and Background

1.1 Surface Modification of Semiconductor Materials

The ability to introduce specific molecular groups to the surfaces of semiconductors holds great promise in photovoltaics,[1-3] catalysis,[4] sensing,[5-7] and molecular electronics.[8, 9] For example, the ability to form stable, biomolecular layers on thin film diamond electrodes has led to extremely robust biosensors.[7, 10, 11] Similarly, the integration of chromophores[1, 12] and selective molecular catalysts[13-15] onto metal oxide surfaces is of interest for renewable energy. These emerging technologies require surface chemistries that are stable under harsh conditions such as elevated temperature, light-exposure, high salt concentrations, and extreme pH. Optimally, the chemistry should also be versatile and function with a variety of different semiconducting substrates and molecular groups. Two chemistries that meet these criteria are the photochemical grafting of alkenes[16] and the copper catalyzed azide alkyne cycloaddition (CuAAC) or "click chemistry".[17, 18] Photochemical grafting of alkenes has been shown to form stable, functional organic layers on a variety of semiconducting substrates.[7, 19] One limitation of this chemistry, though, is the use of deep UV light which limits the direct grafting of light-sensitive species. Click chemistry is a highly versatile coupling reaction that can be used to overcome some of the limitations of the photochemical grafting approach.[20-24] By developing a route to either an azide or alkyne modified surface, one can in principle click any number of different molecules onto the electrode. This two-step approach offers the advantage of greater synthetic simplicity and also extends the variety of complexes that are able to be attached to the surface.[20, 21]

1.2 Photochemical Grafting of Alkenes

Photochemical grafting of alkenes has proven to be a very versatile chemistry for modifying different semiconductor surfaces. The first studies investigated the reactivity of alkenes with the surface of hydrogen-terminated silicon and found that the reaction could be initiated by radicals, heat, or light.[25-28] A surface silicon to carbon bond was shown to form.[28, 29] For photochemical grafting, the reaction was proposed to proceed through either the photodesorption of surface hydrogen[29] or electrophilic sites generated by surface excitons.[26] More recently, a photoemission process was proposed.[30]

Photochemical grafting of alkenes was shown to work for the other Group IV semiconductors, germanium[31] and diamond.[32] In the case of diamond, a highly stable carbon to carbon bond is formed at the surface.[7] More recently, the approach has been extended to form molecular layers on amorphous carbon,[6, 33] gallium nitride,[34] silica,[35] silicon carbide[36], silicon nitride,[36] and titanium dioxide.[19, 37] On titanium dioxide the photochemically grafted layers are highly stable, likely due to the formation of cross-links between adjacent molecules.[38]

1.3 Click Chemistry

Since its discovery ten years ago "click" chemistry has emerged as a very popular method for coupling specific groups to surfaces.[17, 18, 20-24, 39] Click reactions are a class of reactions described by Sharpless that fulfill several reaction conditions including selectivity, large thermodynamic driving force, and gentle reaction conditions.[17] The most widely used example of a click reaction is the copper-catalyzed azide-alkyne cycloaddition (CuAAC). In this reaction, a primary alkyne reacts with a terminal azide to create a 1,4-disubstituted 1,2,3-triazole

linkage via a [3+2] Huisgen cycloaddition. The reaction is tolerant to a variety of different solvent conditions (including water), insensitive to pH, highly specific, fast, and high-yielding. The CuAAC has recently been adapted to link molecules to surfaces including gold,[20, 21] silicon,[24] and carbon.[23, 39]

1.4 Introduction to ZnO

ZnO is a direct wide band gap (~3.3 eV) semiconductor with many desirable properties including high carrier mobility, biocompatibility, piezoelectricity, and high transparency.[40, 41] The combination of good electrical properties with good optical properties makes ZnO very promising as a transparent conducting oxide (TCO) for display applications.[42-44] Almost all commercial TCO films are made of indium tin oxide (ITO). While ITO has very low resistivity and good optical properties, indium is not very abundant and the cost is increasing. ZnO is an abundant, low-cost alternative. ZnO has the extra advantage that is solution processable at low temperatures which may make it compatible with low cost plastic displays.[45, 46] One of the biggest challenges to realizing ZnO-based TCO is the susceptibility of ZnO to degradation from humidity and thermal stress.[47, 48]

ZnO is also attractive as a replacement for TiO_2 in dye-sensitized solar cells and hybrid polymer solar cells.[2, 3, 12, 49, 50] ZnO has much higher carrier mobility than TiO_2 and is more easily grown in a variety of different nanoscale structures.[51-54] However, the carboxylic acid dye-chemistry developed for TiO_2 solar cells is incompatible with ZnO which is much more easily etched.[55, 56] Electron injection from dye molecules into ZnO is slower and recombination rates are higher compared to TiO_2. This has been attributed to its lower density of states and lower dielectric constant which insufficiently screens separated charges.[57, 58]

1.5 Introduction to Diamond

Diamond has many technologically important properties including extreme hardness, tunable conductivity, chemical resistance, high thermal conductivity, high electron and hole mobilities, and optical transparency.[59, 60] Diamond has a wide band gap of 5.5 eV and offers many advantages for electronic applications under harsh environmental conditions. While intrinsic diamond is an insulator, diamond can be doped with boron to become a semimetal. The insulator to metal transition is observed at around 10^{20} B•cm^{-3}.[61]

Synthetic diamonds grown at high pressures and high temperature (HPHT diamond) have been made on a commercial scale since the 1950s.[62] Pressures of 50,000 – 100,000 atm and temperatures of 1500-2000 °C are used. Significant advances in diamond growth by CVD occurred in the 1980s.[60] Diamond grown by CVD is comparable in purity and properties to HPHT diamond, but offers the ability to coat large surface areas at low pressures (typically 10-100 torr) and somewhat lower temperatures (typically 800-1000°C).[62] Diamond thin films are typically grown from a dilute mixture of methane in hydrogen using either hot-filament or microwave discharge CVD. [60, 62] Boron doping can be accomplished by introducing a boron-containing gas such as B_2H_6 or using solid state sources such as boron nitride.[63] Diamond films can be grown on a variety of substrates, the most common being silicon, molybdenum, tungsten platinum, and quartz.[64]

The ability to produce diamond at lower cost, over large surface areas, and on a variety of substrates has led to its commercial use in water disinfection and wastewater treatment. Boron-doped diamond electrochemically generates reactive oxygen species such as hydroxyl radicals

that efficiently degrade toxic organic materials.[65-72] Diamond is an excellent choice for this application because it is extremely stable even at extreme pH and electrical potential. While sp^2 bonded carbon corrodes at elevated temperatures and in harsh chemical environments, diamond electrodes offer extreme corrosion resistance.[64, 73, 74]

1.6 Surface Attached Redox Probes

Surface-tethered redox active probes have been used extensively to investigate the mechanism of electron transfer through a molecular layer.[75] Many factors influence the electron transfer rate including the structure of the monolayer[76-79], the nature of the substrate[80], the density of redox active groups[81-84], and the choice of electrolyte, solvent, and pH.[85-87] Many studies have been performed on thiol SAMs on gold where the chain length in the monolayer is systematically varied. The electron transfer rate has been found to decrease exponentially with increasing distance or chain length:[78, 88-95]

$$k°_{app}=k°\exp(-\beta d)$$

where $k°_{app}$ is the apparent rate constant, β is the tunneling parameter, and d is the distance between the electrode and the redox couple. The value of the tunneling parameter β has been shown to depend on the conjugation of the spacer and the environment of the redox couple which reflect changes in tunneling rate and mechanism.[78, 95]

A few studies have not found an exponential dependence on rate constant with the length of the spacer.[79, 85, 96-101] Electron transfer rates that are independent of chain length have been explained by a rate-limiting step that is not electron tunneling. Rather, conformational changes[99-101], counterion motion[79, 102], or electron hopping between redox centers[97, 98] determine the electron transfer rate. Redox active probes have also been investigated on some surfaces other

than gold,[39, 80, 84, 96, 97, 103-105] but no detailed studies has investigated electron transfer through redox-active monolayers on diamond.

1.7 Surface Attached Catalysts

Recent years have witnessed great progress in the synthesis of molecules able to catalyze a wide range of oxidation and reduction reactions. The integration of electrochemically active molecular complexes with electrodes has great potential for the development of electrocatalytic interfaces for applications such as water splitting,[4, 106, 107] organic synthesis,[108-110] and solar energy.[1, 111, 112] The ability to use catalysts directly tethered to electrodes offers several advantages over traditional homogenous catalysis and electrocatalysis. Direct attachment of catalysts to electrode surfaces eliminates the use of stoichiometric oxidizing or reducing agents. A minimal amount of catalyst is needed because all catalysts are electrochemically active and no catalysts are wasted in the solution. Moreover, the ability to carefully tune the potentials may maximize reaction selectivity and catalyst stability.[113, 114]

In practice the integration of molecular redox catalysts onto electrodes has been limited by a number of practical issues, such as the general difficulty of tethering molecular systems to conductive solids and the need for highly stable surface linkages. Most monolayer chemistries and electrode materials fail under harsh conditions. For example, molecular ligands such as carboxylic acids can be readily protonated and desorb under acidic conditions[19, 115], while most common metal oxides are not stable under basic conditions. Thiol-based self-assembled monolayers on gold are unstable in organic solvents, in the presence of common anions like Cl^-, and at strongly oxidizing or reducing potentials.[116-121] While ruthenium catalysts have been successfully attached to metal oxide electrodes through phosphonic acids[113, 114, 122], the necessary

deprotection of the phosphonic acid esters requires very harsh chemistry (3 days at 110°C in 4 M HCl) which limits the types of complexes that can be attached this way.

Carbon-based materials have been widely used as electrode materials for electroanalytical measurements.[123] While sp^2-hybridized materials such as graphite, glassy carbon, and carbon nanotubes are oxidized at modest potentials (>0.6 V vs NHE at pH=1)[124, 125]and rapidly corrode at potentials >1 V vs. NHE,[125, 126] multiple studies have shown that diamond surfaces are stable to ~ 1.7 V vs. NHE.[63, 73, 74] Boron-doped diamond is a nearly ideal electrode due to its high conductivity, wide potential window, high stability, and low and stable background currents.[59, 63, 64, 73, 74, 124, 127] Boron-doped diamond electrodes can also be transparent, making them an excellent choice for spectroelectrochemistry.[64, 128]

Virtually all previous work on electrochemistry of diamond electrodes has used the "bare" electrodes, either terminated with hydrogen or oxidized. The use of covalent chemistry to link molecular catalysts to conductive electrodes can combine the high intrinsic stability and high electrical conductivity of diamond with the selectivity of molecular catalysts.

1.8 Scope of this Thesis

This thesis describes the functionalization of ZnO and diamond surfaces. Chapter 2 investigates the photochemical grafting of organic alkenes on the surface of single crystal ZnO and ZnO nanorods. The molelcular layers are characterized using FTIR, XPS, and AFM. The ability to perform multi-step synthetic chemistry on the ZnO surface is demonstrated. Chapter 3 looks at the formation of redox-active diamond surfaces. A combination of photochemical grafting and click chemistry is used to couple a model ruthenium-based redox couple to the surface. The diamond electrodes demonstrates remarkable stability to potential cycling out to

very strongly oxidizing potentials (1.5 V vs. NHE). Chapter 4 investigates the electron transfer rate between diamond electrodes and surface-tethered ferrocene. The electron transfer rate is measured for different chain lengths and for different surface coverage of organic groups. The electron transfer rate is shown to decrease with increasing surface coverage but surprisingly is found to be independent of chain length. Finally, chapter 5 concludes with some remarks about possible directions for future studies.

1.9 References

1. Grätzel, M., Dye-sensitized solar cells. *Journal of Photochemistry and Photobiology C: Photochemistry Reviews* **2003,** 4, 145.

2. Yip, H. L.; Hau, S. K.; Baek, N. S.; Ma, H.; Jen, A. K. Y., Polymer solar cells that use self-assembled-monolayer-modified ZnO/Metals as cathodes. *Advanced Materials* **2008,** 20, 2376.

3. Monson, T. C.; Lloyd, M. T.; Olson, D. C.; Lee, Y. J.; Hsu, J. W. P., Photocurrent Enhancement in Polythiophene- and Alkanethiol-Modified ZnO Solar Cells. *Advanced Materials* **2008,** 20, 4755.

4. Concepcion, J. J.; Jurss, J. W.; Brennaman, M. K.; Hoertz, P. G.; Patrocinio, A. O. T.; Murakami Iha, N. Y.; Templeton, J. L.; Meyer, T. J., Making Oxygen with Ruthenium Complexes. *Accounts of Chemical Research* **2009,** 42, 1954.

5. Baker, S. E.; Tse, K. Y.; Hindin, E.; Nichols, B. M.; Clare, T. L.; Hamers, R. J., Covalent functionalization for biomolecular recognition on vertically aligned carbon nanofibers. *Chemistry of Materials* **2005,** 17, 4971.

6. Sun, B.; Colavita, P. E.; Kim, H.; Lockett, M.; Marcus, M. S.; Smith, L. M.; Hamers, R. J., Covalent photochemical functionalization of amorphous carbon thin films for integrated real-time biosensing. *Langmuir* **2006,** 22, 9598.

7. Yang, W. S.; Auciello, O.; Butler, J. E.; Cai, W.; Carlisle, J. A.; Gerbi, J.; Gruen, D. M.; Knickerbocker, T.; Lasseter, T. L.; Russell, J. N.; Smith, L. M.; Hamers, R. J., DNA-modified nanocrystalline diamond thin-films as stable, biologically active substrates. *Nature Materials* **2002,** 1, 253.

8. Gardner, T. J.; Frisbie, C. D.; Wrighton, M. S., Systems for Orthogonal Self-Assembly of Electroactive Monolayers on Au and ITO - An Approach to Molecular Electronics. *Journal of the American Chemical Society* **1995,** 117, 6927.

9. Fan, F. R. F.; Yang, J. P.; Cai, L. T.; Price, D. W.; Dirk, S. M.; Kosynkin, D. V.; Yao, Y. X.; Rawlett, A. M.; Tour, J. M.; Bard, A. J., Charge transport through self-assembled monolayers of compounds of interest in molecular electronics. *Journal of the American Chemical Society* **2002,** 124, 5550.

10. Radadia, A. D.; Stavis, C. J.; Carr, R.; Zeng, H.; King, W. P.; Carlisle, J. A.; Aksimentiev, A.; Hamers, R. J.; Bashir, R., Control of Nanoscale Environment to Improve Stability of Immobilized Proteins on Diamond Surfaces. *Advanced Functional Materials* **2011**, 21, 1040.

11. Stavis, C.; Clare, T. L.; Butler, J. E.; Radadia, A. D.; Carr, R.; Zeng, H.; King, W. P.; Carlisle, J. A.; Aksimentiev, A.; Bashir, R.; Hamers, R. J., Surface functionalization of thin-film diamond for highly stable and selective biological interfaces. *Proceedings of the National Academy of Sciences of the United States of America* **2011**, 108, 983.

12. Law, M.; Greene, L. E.; Johnson, J. C.; Saykally, R.; Yang, P. D., Nanowire dye-sensitized solar cells. *Nature Materials* **2005,** 4, 455.

13. Kim, Y. I.; Atherton, S. J.; Brigham, E. S.; Mallouk, T. E., Sensitized Layered Metal-Oxide-Semiconductor Particles for Photochemical Hydrogen Evolution from Nonsacrificial Electron-Donors. *Journal of Physical Chemistry* **1993,** 97, 11802.

14. Youngblood, W. J.; Lee, S.-H. A.; Kobayashi, Y.; Hernandez-Pagan, E. A.; Hoertz, P. G.; Moore, T. A.; Moore, A. L.; Gust, D.; Mallouk, T. E., Photoassisted Overall Water Splitting in a Visible Light-Absorbing Dye-Sensitized Photoelectrochemical Cell. *Journal of the American Chemical Society* **2009,** 131, 926.

15. Maeda, K.; Eguchi, M.; Lee, S.-H. A.; Youngblood, W. J.; Hata, H.; Mallouk, T. E., Photocatalytic Hydrogen Evolution from Hexaniobate Nanoscrolls and Calcium Niobate Nanosheets Sensitized by Ruthenium(II) Bipyridyl Complexes. *Journal of Physical Chemistry C* **2009,** 113, 7962.

16. Wang, X.; Landis, E. C.; Franking, R.; Hamers, R. J., Surface Chemistry for Stable and Smart Molecular and Biomolecular Interfaces via Photochemical Grafting of Alkenes. *Accounts of Chemical Research* **2010**, 43, 1205.

17. Kolb, H. C.; Finn, M. G.; Sharpless, K. B., Click chemistry: Diverse chemical function from a few good reactions. *Angewandte Chemie International Edition* **2001,** 40, 2004.

18. Rostovtsev, V. V.; Green, L. G.; Fokin, V. V.; Sharpless, K. B., A stepwise Huisgen cycloaddition process: Copper(I)-catalyzed regioselective "ligation" of azides and terminal alkynes. *Angewandte Chemie International Edition* **2002,** 41, 2596.

19. Franking, R. A.; Landis, E. C.; Hamers, R. J., Highly Stable Molecular Layers on Nanocrystalline Anatase TiO2 through Photochemical Grafting. *Langmuir* **2009,** 25, 10676.

20. Collman, J. P.; Devaraj, N. K.; Chidsey, C. E. D., "Clicking" functionality onto electrode surfaces. *Langmuir* **2004,** 20, 1051.

21. Collman, J. P.; Devaraj, N. K.; Eberspacher, T. P. A.; Chidsey, C. E. D., Mixed azide-terminated monolayers: A platform for modifying electrode surfaces. *Langmuir* **2006,** 22, 2457.

22. Devadoss, A.; Chidsey, C. E. D., Azide-modified graphitic surfaces for covalent attachment of alkyne-terminated molecules by "click" chemistry. *Journal of the American Chemical Society* **2007,** 129, 5370.

23. Evrard, D.; Lambert, F.; Policar, C.; Balland, V.; Limoges, B., Electrochemical Functionalization of Carbon Surfaces by Aromatic Azide or Alkyne Molecules: A Versatile Platform for Click Chemistry. *Chemistry - A European Journal* **2008,** 14, 9286.

24. Marrani, A. G.; Dalchiele, E. A.; Zanoni, R.; Decker, F.; Cattaruzza, F.; Bonifazi, D.; Pratoc, M., Functionalization of Si(100) with ferrocene derivatives via "click" chemistry. *Electrochimica Acta* **2008,** 53, 3903.

25. Linford, M. R.; Fenter, P.; Eisenberger, P. M.; Chidsey, C. E. D., Alkyl Monolayers On Silicon Prepared From 1-Alkenes And Hydrogen-Terminated Silicon. *Journal of the American Chemical Society* **1995,** 117, 3145.

26. Stewart, M. P.; Buriak, J. M., Exciton-mediated hydrosilylation on photoluminescent nanocrystalline silicon. *Journal of the American Chemical Society* **2001,** 123, 7821.

27. Hovis, J. S.; Liu, H. B.; Hamers, R. J., Cycloaddition chemistry of 1,3-dienes on the silicon(001) surface: Competition between [4+2] and [2+2] reactions. *Journal of Physical Chemistry B* **1998,** 102, 6873.

28. Terry, J.; Linford, M. R.; Wigren, C.; Cao, R. Y.; Pianetta, P.; Chidsey, C. E. D., Determination of the bonding of alkyl monolayers to the Si(111) surface using chemical-shift, scanned-energy photoelectron diffraction. *Applied Physics Letters* **1997,** 71, 1056.

29. Cicero, R. L.; Linford, M. R.; Chidsey, C. E. D., Photoreactivity of unsaturated compounds with hydrogen-terminated silicon(111). *Langmuir* **2000,** 16, 5688.

30. Wang, X.; Ruther, R. E.; Streifer, J. A.; Hamers, R. J., UV-Induced Grafting of Alkenes to Silicon Surfaces: Photoemission versus Excitons. *Journal of the American Chemical Society* **2010**, 132, 4048.

31. Choi, K.; Buriak, J. M., Hydrogermylation of alkenes and alkynes on hydride-terminated Ge(100) surfaces. *Langmuir* **2000,** 16, 7737.

32. Strother, T.; Knickerbocker, T.; Russell, J. N.; Butler, J. E.; Smith, L. M.; Hamers, R. J., Photochemical functionalization of diamond films. *Langmuir* **2002,** 18, 968.

33. Colavita, P. E.; Sun, B.; Tse, K. Y.; Hamers, R. J., Photochemical grafting of n-alkenes onto carbon surfaces: the role of photoelectron ejection. *Journal of the American Chemical Society* **2007,** 129, 13554.

34. Kim, H.; Colavita, P. E.; Metz, K. M.; Nichols, B. M.; Sun, B.; Uhlrich, J.; Wang, X. Y.; Kuech, T. F.; Hamers, R. J., Photochemical functionalization of gallium nitride thin films with molecular and biomolecular layers. *Langmuir* **2006,** 22, 8121.

35. ter Maat, J.; Regeling, R.; Yang, M.; Mullings, M. N.; Bent, S. F.; Zuilhof, H., Photochemical Covalent Attachment of Alkene-Derived Monolayers onto Hydroxyl-Terminated Silica. *Langmuir* **2009,** 25, 11592.

36. Rosso, M.; Giesbers, M.; Arafat, A.; Schroen, K.; Zuilhof, H., Covalently Attached Organic Monolayers on SiC and Si_xN_4 Surfaces: Formation Using UV Light at Room Temperature. *Langmuir* **2009,** 25, 2172.

37. Li, B.; Franking, R.; Landis, E. C.; Kim, H.; Hamers, R. J., Photochemical Grafting and Patterning of Biomolecular Layers onto TiO2 Thin Films. *ACS Applied Materials & Interfaces* **2009,** 1, 1013.

38. Franking, R. Development of the TiO_2-Organic Interface and Mechanistic Studies of Photochemical Grafting on TiO_2. Thesis. University of Wisconsin - Madison, 2011.

39. Landis, E. C.; Hamers, R. J., Covalent Grafting of Redox-Active Molecules to Vertically Aligned Carbon Nanofiber Arrays via "Click" Chemistry. *Chemistry of Materials* **2009,** 21, 724.

40. Ozgur, U.; Alivov, Y. I.; Liu, C.; Teke, A.; Reshchikov, M. A.; Dogan, S.; Avrutin, V.; Cho, S. J.; Morkoc, H., A comprehensive review of ZnO materials and devices. *Journal of Applied Physics* **2005,** 98, 041301.

41. Look, D. C., Recent advances in ZnO materials and devices. *Materials Science and Engineering B - Solid State Materials for Advanced Technology* **2001,** 80, 383.

42. Suzuki, A.; Matsushita, T.; Wada, N.; Sakamoto, Y.; Okuda, M., Transparent conducting Al-doped ZnO thin films prepared by pulsed laser deposition. *Japanese Journal of Applied Physics* **1996,** 35, L56.

43. Agura, H.; Suzuki, A.; Matsushita, T.; Aoki, T.; Okuda, M., Low resistivity transparent conducting Al-doped ZnO films prepared by pulsed laser deposition. *Thin Solid Films* **2003,** 445, 263.

44. Ginley, D. S.; Bright, C., Transparent conducting oxides. *MRS Bulletin* **2000,** 25, 15.

45. Park, M. S.; Lee, D. H.; Bae, E. J.; Kim, D.-H.; Kang, J. G.; Son, D.-H.; Ryu, S. O., Fabrication of Indium Gallium Zinc Oxide (IGZO) TFTs Using a Solution-Based Process. *Molecular Crystals and Liquid Crystals* **2010**, 529, 137.

46. Clatot, J.; Campet, G.; Zeinert, A.; Labrugere, C.; Rougier, A., Room temperature transparent conducting oxides based on zinc oxide thin films. *Applied Surface Science* **2011**, 257, 5181.

47. Minami, T.; Miyata, T.; Yamamoto, T., Stability of transparent conducting oxide films for use at high temperatures. *Journal of Vacuum Science & Technology A - Vacuum Surfaces and Films* **1999,** 17, 1822.

48. Minami, T.; Kuboi, T.; Miyata, T.; Ohtani, Y., Stability in a high humidity environment of TCO thin films deposited at low temperatures. *Physica Status Solidi A - Applications and Materials Science* **2008,** 205, 255.

49. O'Regan, B.; Schwartz, D. T.; Zakeeruddin, S. M.; Grätzel, M., Electrodeposited nanocomposite n-p heterojunctions for solid-state dye-sensitized photovoltaics. *Advanced Materials* **2000,** 12, 1263.

50. Beek, W. J. E.; Wienk, M. M.; Kemerink, M.; Yang, X. N.; Janssen, R. A. J., Hybrid zinc oxide conjugated polymer bulk heterojunction solar cells. *Journal of Physical Chemistry B* **2005,** 109, 9505.

51. Yan, H. Q.; He, R. R.; Pham, J.; Yang, P. D., Morphogenesis of one-dimensional ZnO nano- and microcrystals. *Advanced Materials* **2003,** 15, 402.

52. Vayssieres, L., Growth of arrayed nanorods and nanowires of ZnO from aqueous solutions. *Advanced Materials* **2003,** 15, 464.

53. Wang, Z.; Qian, X. F.; Yin, J.; Zhu, Z. K., Large-scale fabrication of tower-like, flower-like, and tube-like ZnO arrays by a simple chemical solution route. *Langmuir* **2004,** 20, 3441.

54. Wang, Z. L., Functional oxide nanobelts: Materials, properties and potential applications in nanosystems and biotechnology. *Annual Review of Physical Chemistry* **2004,** 55, 159.

55. Keis, K.; Lindgren, J.; Lindquist, S. E.; Hagfeldt, A., Studies of the adsorption process of Ru complexes in nanoporous ZnO electrodes. *Langmuir* **2000,** 16, 4688.

56. Taratula, O.; Galoppini, E.; Wang, D.; Chu, D.; Zhang, Z.; Chen, H. H.; Saraf, G.; Lu, Y. C., Binding studies of molecular linkers to ZnO and MgZnO nanotip films. *Journal of Physical Chemistry B* **2006,** 110, 6506.

57. Asbury, J. B.; Hao, E.; Wang, Y. Q.; Ghosh, H. N.; Lian, T. Q., Ultrafast electron transfer dynamics from molecular adsorbates to semiconductor nanocrystalline thin films. *Journal of Physical Chemistry B* **2001,** 105, 4545.

58. Nemec, H.; Rochford, J.; Taratula, O.; Galoppini, E.; Kuzel, P.; Polivka, T.; Yartsev, A.; Sundstrom, V., Influence of the Electron-Cation Interaction on Electron Mobility in Dye-Sensitized ZnO and TiO(2) Nanocrystals: A Study Using Ultrafast Terahertz Spectroscopy. *Physical Review Letters* **2010**, 104, 197401.

59. Xu, J. S.; Granger, M. C.; Chen, Q. Y.; Strojek, J. W.; Lister, T. E.; Swain, G. M., Boron-doped diamond thin-film electrodes. *Analytical Chemistry* **1997,** 69, A591.

60. Angus, J. C.; Hayman, C. C., Low-Pressure, Metastable Growth of Diamond and Diamondlike Phases. *Science* **1988,** 241, 913.

61. Lagrange, J. P.; Deneuville, A.; Gheeraert, E., Activation energy in low compensated homoepitaxial boron-doped diamond films. *Diamond and Related Materials* **1998,** 7, 1390.

62. Celii, F. G.; Butler, J. E., Diamond Chemical Vapor-Deposition. *Annual Review of Physical Chemistry* **1991,** 42, 643.

63. Martin, H. B.; Argoitia, A.; Landau, U.; Anderson, A. B.; Angus, J. C., Hydrogen and oxygen evolution on boron-doped diamond electrodes. *Journal of the Electrochemical Society* **1996,** 143, L133.

64. Hupert, M.; Muck, A.; Wang, R.; Stotter, J.; Cvackova, Z.; Haymond, S.; Show, Y.; Swain, G. M., Conductive diamond thin-films in electrochemistry. *Diamond and Related Materials* **2003,** 12, 1940.

65. Ruiz, E. J.; Arias, C.; Brillas, E.; Hernandez-Ramirez, A.; Peralta-Hernandez, J. M., Mineralization of Acid Yellow 36 azo dye by electro-Fenton and solar photoelectro-Fenton processes with a boron-doped diamond anode. *Chemosphere* **2011**, 82, 495.

66. Mascia, M.; Vacca, A.; Polcaro, A. M.; Palmas, S.; Ruiz, J. R.; Da Pozzo, A., Electrochemical treatment of phenolic waters in presence of chloride with boron-doped diamond (BDD) anodes: Experimental study and mathematical model. *Journal of Hazardous Materials* **2010**, 174, 314.

67. Polcaro, A. M.; Vacca, A.; Mascia, M.; Palmas, S.; Ruiz, J. R., Electrochemical treatment of waters with BDD anodes: kinetics of the reactions involving chlorides. *Journal of Applied Electrochemistry* **2009,** 39, 2083.

68. Gonzalez, T.; Dominguez, J. R.; Palo, P.; Sanchez-Martin, J.; Cuerda-Correa, E. M., Development and optimization of the BDD-electrochemical oxidation of the antibiotic trimethoprim in aqueous solution. *Desalination* **2011**, 280, 197.

69. Gonzalez, T.; Dominguez, J. R.; Palo, P.; Sanchez-Martin, J., Conductive-diamond electrochemical advanced oxidation of naproxen in aqueous solution: optimizing the process. *Journal of Chemical Technology and Biotechnology* **2011**, 86, 121.

70. Dominguez, J. R.; Gonzalez, T.; Palo, P.; Sanchez-Martin, J., Electrochemical Advanced Oxidation of Carbamazepine on Boron-Doped Diamond Anodes. Influence of Operating Variables. *Industrial & Engineering Chemistry Research* **2010**, 49, 8353.

71. Palma-Goyes, R. E.; Guzman-Duque, F. L.; Penuela, G.; Gonzalez, I.; Nava, J. L.; Torres-Palma, R. A., Electrochemical degradation of crystal violet with BDD electrodes: Effect of electrochemical parameters and identification of organic by-products. *Chemosphere* **2010**, 81, 26.

72. Butron, E.; Juarez, M. E.; Solis, M.; Teutli, M.; Gonzalez, I.; Nava, J. L., Electrochemical incineration of indigo textile dye in filter-press-type FM01-LC electrochemical cell using BDD electrodes. *Electrochimica Acta* **2007,** 52, 6888.

73. Swain, G. M., Electrically Conducting Diamond Thin Films: Advanced Electrode Materials for Electrochemical Technologies. Electroanalytical Chemistry: A Series of Advances. Vol. 22, p 181-277.

74. Swain, G. M., The Susceptibility to Surface Corrosion in Acidic Fluoride Media - A Comparison of Diamond, HOPG, And Glassy Carbon Electrodes. *Journal of the Electrochemical Society* **1994,** 141, 3382.

75. Finklea, H. O., Electrochemistry of organized monolayers of thiols and related molecules on electrodes. Electroanalytical Chemistry: A Series of Advances. Vol. 19, p 109-335.

76. Chidsey, C. E. D.; Bertozzi, C. R.; Putvinski, T. M.; Mujsce, A. M., Coadsorption of Ferrocene-Terminated and Unsubstituted Alkanethiols on Gold - Electroactive Self-Assembled Monolayers. *Journal of the American Chemical Society* **1990,** 112, 4301.

77. Hockett, L. A.; Creager, S. E., Redox Kinetics for Ferrocene Groups Immobilized in Impermeable and Permeable Self-Assembled Monolayers. *Langmuir* **1995,** 11, 2318.

78. Finklea, H. O.; Liu, L.; Ravenscroft, M. S.; Punturi, S., Multiple electron tunneling paths across self-assembled monolayers alkanethiols with attached ruthenium(II/III) redox centers. *Journal of Physical Chemistry* **1996,** 100, 18852.

79. Sumner, J. J.; Creager, S. E., Redox kinetics in monolayers on electrodes: Electron transfer is sluggish for ferrocene groups buried within the monolayer interior. *Journal of Physical Chemistry B* **2001,** 105, 8739.

80. Liu, G. Z.; Liu, J. Q.; Bocking, T.; Eggers, P. K.; Gooding, J. J., The modification of glassy carbon and gold electrodes with aryl diazonium salt: The impact of the electrode materials on the rate of heterogeneous electron transfer. *Chemical Physics* **2005,** 319, 136.

81. Hauquier, F.; Ghilane, J.; Fabre, B.; Hapiot, P., Conducting ferrocene monolayers on nonconducting surfaces. *Journal of the American Chemical Society* **2008,** 130, 2748.

82. Blauch, D. N.; Saveant, J. M., Dynamics of Electron Hopping in Assemblies of Redox Centers - Percolation and Diffusion. *Journal of the American Chemical Society* **1992,** 114, 3323.

83. Roth, K. M.; Gryko, D. T.; Clausen, C.; Li, J. Z.; Lindsey, J. S.; Kuhr, W. G.; Bocian, D. F., Comparison of electron-transfer and charge-retention characteristics of porphyrin-containing self-assembled monolayers designed for molecular information storage. *Journal of Physical Chemistry B* **2002,** 106, 8639.

84. Roth, K. M.; Yasseri, A. A.; Liu, Z. M.; Dabke, R. B.; Malinovskii, V.; Schweikart, K. H.; Yu, L. H.; Tiznado, H.; Zaera, F.; Lindsey, J. S.; Kuhr, W. G.; Bocian, D. F., Measurements of electron-transfer rates of charge-storage molecular monolayers on Si(100). Toward hybrid molecular/semiconductor information storage devices. *Journal of the American Chemical Society* **2003,** 125, 505.

85. Hong, H. G.; Park, W., Unusual electron tunneling constant for long range electron transfer in hydroquinone (H(2)Q)-terminated self-assembled monolayers on gold in alkaline solution. *Bulletin of the Korean Chemical Society* **2005,** 26, 1885.

86. Forster, R. J.; Faulkner, L. R., Electrochemistry Of Spontaneously Adsorbed Monolayers - Effects of Solvent, Potential, and Temperature on Electron-Transfer Dynamics. *Journal of the American Chemical Society* **1994,** 116, 5453.

87. Ravenscroft, M. S.; Finklea, H. O., Kinetics of Electron-Transfer to Attached Redox Centers on Gold Electrodes in Nonaqueous Electrolytes. *Journal of Physical Chemistry* **1994,** 98, 3843.

88. Dubois, L. H.; Nuzzo, R. G., Synthesis, Structure, and Properties of Model Organic-Surfaces. *Annual Review of Physical Chemistry* **1992,** 43, 437.

89. Sachs, S. B.; Dudek, S. P.; Hsung, R. P.; Sita, L. R.; Smalley, J. F.; Newton, M. D.; Feldberg, S. W.; Chidsey, C. E. D., Rates of interfacial electron transfer through pi-conjugated spacers. *Journal of the American Chemical Society* **1997,** 119, 10563.

90. Finklea, H. O.; Hanshew, D. D., Electron-Transfer Kinetics In Organized Thiol Monolayers With Attached Pentaammine(Pyridine)Ruthenium Redox Centers. *Journal of the American Chemical Society* **1992,** 114, 3173.

91. Smalley, J. F.; Feldberg, S. W.; Chidsey, C. E. D.; Linford, M. R.; Newton, M. D.; Liu, Y. P., The Kinetics of Electron-Transfer through Ferrocene-Terminated Alkanethiol Monolayers on Gold. *Journal of Physical Chemistry* **1995,** 99, 13141.

92. Rowe, G. K.; Carter, M. T.; Richardson, J. N.; Murray, R. W., Consequences of Kinetic Dispersion on the Electrochemistry of an Adsorbed Redox-Active Monolayer. *Langmuir* **1995,** 11, 1797.

93. Brevnov, D. A.; Finklea, H. O.; Van Ryswyk, H., Ac voltammetry studies of electron transfer kinetics for a redox couple attached via short alkanethiols to a gold electrode. *Journal of Electroanalytical Chemistry* **2001,** 500, 100.

94. Weber, K.; Hockett, L.; Creager, S., Long-range electronic coupling between ferrocene and gold in alkanethiolate-based monolayers on electrodes. *Journal of Physical Chemistry B* **1997,** 101, 8286.

95. Creager, S.; Yu, C. J.; Bamdad, C.; O'Connor, S.; MacLean, T.; Lam, E.; Chong, Y.; Olsen, G. T.; Luo, J. Y.; Gozin, M.; Kayyem, J. F., Electron transfer at electrodes through conjugated "molecular wire" bridges. *Journal of the American Chemical Society* **1999,** 121, 1059.

96. Landis, E. C.; Hamers, R. J., Covalent Grafting of Ferrocene to Vertically Aligned Carbon Nanofibers: Electron-transfer Processes at Nanostructured Electrodes. *Journal of Physical Chemistry C* **2008,** 112, 16910.

97. Riveros, G.; Meneses, S.; Escobar, S.; Garin, C.; Chornik, B., Electron Transfer Rates of Alkyl-Ferrocene Molecules Forming Incomplete Monolayer on Silicon Electrodes. *Journal of the Chilean Chemical Society* **2010**, 55, 61.

98. Riveros, G.; Garin, C.; Meneses, S.; Escobar, S., Silicon Modification with Molecules Derived from Ferrocene: Effect of the Crystallographic Orientation of Silicon in the Electron-Transfer Rates. *Molecular Crystals And Liquid Crystals* **2010**, 521, 187.

99. Feng, Z. Q.; Imabayashi, S.; Kakiuchi, T.; Niki, K., Long-range electron-transfer reaction rates to cytochrome c across long- and short-chain alkanethiol self-assembled monolayers: Electroreflectance studies. *Journal of the Chemical Society - Faraday Transactions* **1997,** 93, 1367.

100. Avila, A.; Gregory, B. W.; Niki, K.; Cotton, T. M., An electrochemical approach to investigate gated electron transfer using a physiological model system: Cytochrome c

immobilized on carboxylic acid-terminated alkanethiol self-assembled monolayers on gold electrodes. *Journal of Physical Chemistry B* **2000,** 104, 2759.

101. Niki, K.; Sprinkle, J. R.; Margoliash, E., Intermolecular biological electron transfer: an electrochemical approach. *Bioelectrochemistry* **2002,** 55, 37.

102. Amatore, C.; Maisonhaute, E.; Schollhorn, B.; Wadhawan, J., Ultrafast voltammetry for probing interfacial electron transfer in molecular wires. *Chemphyschem* **2007,** 8, 1321.

103. Guldi, D. M.; Marcaccio, M.; Paolucci, D.; Paolucci, F.; Tagmatarchis, N.; Tasis, D.; Vazquez, E.; Prato, M., Single-wall carbon nanotube-ferrocene nanohybrids: Observing intramolecular electron transfer in functionalized SWNTs. *Angewandte Chemie International Edition* **2003,** 42, 4206.

104. Yasseri, A. A.; Syomin, D.; Loewe, R. S.; Lindsey, J. S.; Zaera, F.; Bocian, D. F., Structural and electron-transfer characteristics of O-, S-, and Se-tethered porphyrin monolayers on Si(100). *Journal of the American Chemical Society* **2004,** 126, 15603.

105. Li, C. Q.; Ren, B. Y.; Zhang, Y.; Cheng, Z. Y.; Liu, X. X.; Tong, Z., A Novel Ferroceneylazobenzene Self-Assembled Monolayer on an ITO Electrode: Photochemical and Electrochemical Behaviors. *Langmuir* **2008,** 24, 12911.

106. Liu, F.; Concepcion, J. J.; Jurss, J. W.; Cardolaccia, T.; Templeton, J. L.; Meyer, T. J., Mechanisms of water oxidation from the blue dimer to photosystem II. *Inorganic Chemistry* **2008,** 47, 1727.

107. Wasylenko, D. J.; Ganesamoorthy, C.; Henderson, M. A.; Koivisto, B. D.; Osthoff, H. D.; Berlinguette, C. P., Electronic Modification of the [Ru(II)(tpy)(bpy)(OH(2))](2+) Scaffold: Effects on Catalytic Water Oxidation. *Journal of the American Chemical Society* **2010,** 132, 16094.

108. Tucker, J. W.; Narayanam, J. M. R.; Krabbe, S. W.; Stephenson, C. R. J., Electron Transfer Photoredox Catalysis: Intramolecular Radical Addition to Indoles and Pyrroles. *Organic Letters* **2010**, 12, 368.

109. Ischay, M. A.; Anzovino, M. E.; Du, J.; Yoon, T. P., Efficient visible light photocatalysis of [2+2] enone cycloadditions. *Journal of the American Chemical Society* **2008,** 130, 12886.

110. Murray, R. W., Chemically Modified Electrodes. Electroanalytical Chemistry: A Series of Advances. Vol. 13, p 191-368.

111. Kalyanasundaram, K., Photophysics, Photochemistry and Solar-Energy Conversion with Tris(Bipyridyl)Ruthenium(Ii) and its Analogs. *Coordination Chemistry Reviews* **1982,** 46, 159.

112. Campagna, S.; Puntoriero, F.; Nastasi, F.; Bergamini, G.; Balzani, V., Photochemistry and Photophysics of Coordination Compounds I. Vol. 280. Springer-Verlag Berlin: 2007.

113. Liu, F.; Cardolaccia, T.; Hornstein, B. J.; Schoonover, J. R.; Meyer, T. J., Electrochemical oxidation of water by an adsorbed mu-oxo-bridged Ru complex. *Journal of the American Chemical Society* **2007,** 129, 2446.

114. Chen, Z.; Concepcion, J. J.; Jurss, J. W.; Meyer, T. J., Single-Site, Catalytic Water Oxidation on Oxide Surfaces. *Journal of the American Chemical Society* **2009,** 131, 15580.

115. Bishop, L. M.; Yeager, J. C.; Chen, X.; Wheeler, J. N.; Torelli, M. D.; Benson, M. C.; Burke, S. D.; Pedersen, J. A.; Hamers, R. J., A Citric Acid-Derived Ligand for Modular Functionalization of Metal Oxide Surfaces via "Click" Chemistry. *Langmuir* **2012**, 28, 1322.

116. Schlenoff, J. B.; Li, M.; Ly, H., Stability and self-exchange in alkanethiol monolayers. *Journal of the American Chemical Society* **1995,** 117, 12528.

117. Everett, W. R.; Welch, T. L.; Reed, L.; Fritschfaules, I., Potential-Dependent Stability of Self-Assembled Organothiols on Gold Electrodes in Methylene-Chloride. *Analytical Chemistry* **1995,** 67, 292.

118. Boubour, E.; Lennox, R. B., Stability of omega-functionalized self-assembled monolayers as a function of applied potential. *Langmuir* **2000,** 16, 7464.

119. Stapleton, J. J.; Harder, P.; Daniel, T. A.; Reinard, M. D.; Yao, Y. X.; Price, D. W.; Tour, J. M.; Allara, D. L., Self-assembled oligo(phenylene-ethynylene) molecular electronic switch monolayers on gold: Structures and chemical stability. *Langmuir* **2003,** 19, 8245.

120. Flynn, N. T.; Tran, T. N. T.; Cima, M. J.; Langer, R., Long-term stability of self-assembled monolayers in biological media. *Langmuir* **2003,** 19, 10909.

121. Willey, T. M.; Vance, A. L.; van Buuren, T.; Bostedt, C.; Terminello, L. J.; Fadley, C. S., Rapid degradation of alkanethiol-based self-assembled monolayers on gold in ambient laboratory conditions. *Surface Science* **2005,** 576, 188.

122. Jurss, J. W.; Concepcion, J. C.; Norris, M. R.; Templeton, J. L.; Meyer, T. J., Surface Catalysis of Water Oxidation by the Blue Ruthenium Dimer. *Inorganic Chemistry* **2010**, 49, 3980.

123. McCreery, R. L., Advanced carbon electrode materials for molecular electrochemistry. *Chemical Reviews* **2008,** 108, 2646.

124. Swain, G. M.; Ramesham, R., The Electrochemical Activity Of Boron-Doped Polycrystalline Diamond Thin-Film Electrodes. *Analytical Chemistry* **1993,** 65, 345.

125. Choo, H.-S.; Kinumoto, T.; Jeong, S.-K.; Iriyama, Y.; Abe, T.; Ogumi, Z., Mechanism for electrochemical oxidation of highly oriented pyrolytic graphite in sulfuric acid solution. *Journal of the Electrochemical Society* **2007,** 154, B1017.

126. Besenhard, J. O.; Fritz, H. P., The Electrochemistry Of Black Carbons. *Angewandte Chemie International Edition In English* **1983,** 22, 950.

127. Granger, M. C.; Witek, M.; Xu, J. S.; Wang, J.; Hupert, M.; Hanks, A.; Koppang, M. D.; Butler, J. E.; Lucazeau, G.; Mermoux, M.; Strojek, J. W.; Swain, G. M., Standard electrochemical behavior of high-quality, boron-doped polycrystalline diamond thin-film electrodes. *Analytical Chemistry* **2000,** 72, 3793.

128. Zak, J. K.; Butler, J. E.; Swain, G. M., Diamond optically transparent electrodes: Demonstration of concept with ferri-ferrocyanide and methyl viologen. *Analytical Chemistry* **2001,** 73, 908.

Chapter 2

Formation of Smooth, Conformal Molecular Layers on Zinc Oxide Surfaces by Photochemical Grafting

The work in the following chapter was published in an article in *Langmuir*, volume 27, issue 17, pages 10604-10614.

2.1 Introduction

ZnO is a direct wide band gap (~3.3 eV) semiconductor with many desirable properties including high carrier mobility, biocompatibility, piezoelectricity, high transparency, and relatively simple growth technologies as both bulk single crystals and nanoscale structures. ZnO is of interest for numerous applications including photovoltaics,[1-4] sensors,[5-10] ultraviolet light detectors,[11,12], and light-emitting diodes.[13-15] Surface functionalization is a promising strategy to tune the electronic and optoelectronic properties of ZnO based devices.[16-20] However, only a few different covalent surface functionalizations have been developed for ZnO and many of these remain controversial. Common anchoring groups for metal oxides such as phosphonic acids and carboxylic acids do not bind to ZnO in all cases[21,22] and the extent of binding seems to depend highly on the experimental conditions.[21-23] Perhaps more importantly, ZnO is only stable over a rather narrow range of pH values.[24,25] Consequently, many of the strategies used to functionalize more robust oxides such as TiO_2 can be difficult or impossible to use with ZnO. For example, the acidic protons within phosphonic acids and carboxylic acids can etch the ZnO surface. A deeper understanding of the surface chemistry is complicated by the fact that many studies of ZnO surface functionalization have used only nanoparticles or nanocrystalline films[23,27,28] that expose

multiple crystal faces. The reactivity of different crystal faces of ZnO is known to be quite different,[29,30] and the lack of a well-defined surface makes it difficult to compare experiments in different laboratories. While the surface chemistry of bulk single crystals of ZnO has been explored in some detail, these studies focused almost exclusively on small molecules in ultra high vacuum,[29-33] where the absence of water and associated solvation may substantially alter reactivity.

The photochemical grafting of organic alkenes has been used to form covalent bonds to semiconductor surfaces including silicon,[2] germanium,[3] and various forms of carbon.[36-40] Recently this method has also been extended to ionic semiconductors to form stable, functional layers on gallium nitride[4] and titanium dioxide.[42,43] Here we investigate the photochemical grafting of alkenes to the ZnO $(10\bar{1}\,0)$ nonpolar surface. Experiments are performed on both bulk single crystal surfaces and on single crystal nanorods that predominantly expose the $(10\bar{1}\,0)$ face. Fourier-transform infrared spectroscopy (FTIR), x-ray photoelectron spectroscopy (XPS), and atomic force microscopy (AFM) on atomically-flat ZnO single crystals show that alkenes can be photochemically attached to ZnO to form highly uniform, molecular layers with little or no detectable alteration of the underlying structure. The impact of the organic layer on electronic properties is evaluated with flatband potential measurements based on both capacitance and photoresponse. We show that alkenes bearing a second functional group can be successfully grafted and further reacted, providing a versatile approach to tailor the ZnO surface for improved electronic interfaces.

2.2 Experimental

2.2.1 Preparation of ZnO Nanorods

ZnO nanorods were grown using a seeded growth method similar to a previously published procedure.[1] Nanorods were grown on silicon substrates that were coated with 100 nm of titanium to improve reflectivity for FTIR measurements. Seeding was accomplished by dip-coating the substrates in an ethanolic suspension of ZnO quantum dots prepared according to a previously published procedure.[44] ZnO nanorods were grown at 90^{o}C in aqueous solutions of 25 mM zinc nitrate (Aldrich) and 25 mM hexamethylenetetramine (Aldrich). This procedure grew nanorods typically 200 – 300 nm in length and ~ 50 nm in diameter. Subsequent to growth the nanorods were annealed in air at 500^{o}C for 30 minutes to remove any surface-bound organic material.

2.2.2 Preparation of ZnO Bulk Single Crystals

ZnO wafers with $(10\bar{1}0)$ orientation (MTI and CrysTec GmbH) were annealed at 1100^{o}C in a ceramic ZnO box (99.999%, Kurt J. Lesker Company) for 3 hours to produce a surface with well-defined terraces and steps.[45]

2.2.3 Photochemical Grafting of Alkenes

Fig. 2.1 shows the following compounds that were used for surface modification: 1-dodecene (Sigma), trifluoroacetic acid protected 10-aminodec-1-ene (TFAAD, Almac Sciences), methyl 10-undecenoate (UAME, Sigma), and methyl 10-undecanoate ("Saturated-UAMA", Sigma). ZnO samples were placed in a nitrogen-purged, Teflon reaction cell with a UV grade fused silica window. The neat liquid alkene was added to wet the surface, and a UV grade fused

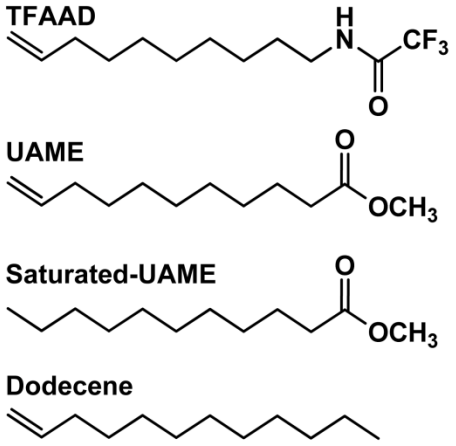

Figure 2.1: Molecules used for photochemical grafting

silica cover was placed on top of the sample to reduce evaporation. The samples were illuminated with a low pressure mercury lamp (254 nm, ~10 mW/cm^2). After reaction the samples were soaked for approximately 1 hour each in heptane, isopropanol, and methanol to remove physisorbed reagents. Samples were stored in isopropanol in the dark between measurements. Samples were rinsed with fresh isopropanol and blown dry with nitrogen immediately before characterization.

2.2.4 Characterization

Infrared spectra were collected on a Bruker Vertex 70 FTIR spectrometer. All spectra were collected with a resolution of 4 cm^{-1}. FTIR spectra of neat liquids were collected in transmission mode using salt plates. FTIR spectra of ZnO nanorods were collected in reflection mode using a VeeMaxII variable angle specular reflectance accessory with a wire grid polarizer. All reflection spectra were collected with p-polarized light at an incident illumination angle of 50^o off normal. FTIR of functionalized ZnO nanorods were taken with an annealed unfunctionalized sample as the background. Sloping baselines were removed to improve the clarity of the spectra.

XPS was performed using a monochromatic Al Kα source (1486.6 eV photon energy) with an analyzer resolution of between 0.1 and 0.2 eV and an electron takeoff angle of 45^o. Peak areas were calculated by fitting the raw data to Voigt functions after a baseline correction. Peak energies were shifted to make the primary C(1s) peak of the organic alkyl chain of TFAAD lie at 285 eV;[46] all other peaks were shifted by the same amount. AFM images were collected in contact mode with a Multimode, Nanoscope IV (Veeco) using silicon AFM probes with a force constant of 0.2 N/m (Budget Sensors). Impedance data were collected using a potentiostat

(Solartron 1287) and an impedance analyzer (Solartron 1260) with Zplot software (Scribner Associates, Inc.). Impedance data were collected in a three electrode cell using ZnO nanorods as the working electrode. The counter electrode was a platinum wire. The nonaqueous Ag/Ag+ reference electrode consisted of a silver wire immersed in a solution of 0.01 M $AgNO_3$ and 0.1 M $LiClO_4$ in acetonitrile. Measurements were performed in the dark at room temperature in 0.1 M $LiClO_4$ in acetonitrile. Mott Schottky plots were obtained by fitting the impedance data to a simple series RC circuit. A Kalrez O-ring pressing against the working electrode limited the exposed area to 0.64 cm^2; all reported values for the capacitance are normalized to this area.

Photoresponse measurements were performed in the same three electrode cell as described for the impedance measurements. Light from a 250 W quartz tungsten halogen lamp (Ushio) was passed through a monochromator (Acton Research Corporation, SpectraPro 275) and focused onto the working ZnO electrode. Before entering the cell the light was chopped with an optical chopper. The signal from the chopper was fed to the reference channel of a lock-in amplifier (Stanford Research Systems, SR830). The polarization of the working electrode was controlled by a potentiostat (Solarton 1287). The potentiostat also measured the current passing through the working electrode as the voltage drop across a 1000 Ω resistor. This voltage was fed into the signal channel of the lock-in amplifier. A Matlab interface was used to sweep the polarization of the working electrode at a rate of 2 mV/s and measure the photocurrent simultaneously.

2.3 Results

2.3.1 Characterization of ZnO Surfaces

Fig. 2.2a shows an SEM image of the ZnO nanorods. Well defined crystal faces can clearly be identified. The sidewalls of the nanorods, which comprise ~90% of the surface area, expose the nonpolar $(10\bar{1}0)$ surface.[47] XPS spectra of annealed ZnO nanorods can be found in the supporting information (Fig. S7). Fig. 2.2b shows an AFM image of the $(10\bar{1}\,0)$ surface of a bulk single crystal after annealing. Fig. 2.2c shows an AFM height profile over the region indicated by the red line in Fig. 2.2b; these data show that the abrupt features in Fig. 2.2b correspond to height changes of 0.23 nm, which is within experimental error equivalent to the 0.28 nm expected for single atomic steps on this surface.

2.3.2 Covalent Grafting of Organic Layers to ZnO $(10\bar{1}0)$

Fig. 2.3 shows infrared spectra of ZnO nanorods after grafting for 16 h with each of the alkenes depicted in Fig. 2.1. While FTIR is difficult to quantify accurately, the intensity of the C-H stretching modes in the 2800-3000 cm^{-1} range is expected to be proportional to the surface coverage because all three molecules have approximately the same number of C-H units.

TFAAD and UAME show strong peaks at 2856 cm^{-1} and 2927 cm^{-1} that arise from the CH_2 symmetric and asymmetric stretches of the alkyl chain, while dodecene shows almost no absorbance in this range. Consequently, the data in Fig. 2.3 show that TFAAD and UAME both graft to the ZnO nanorods, while dodecene does not graft to a significant extent. To confirm that the alkene group is necessary for surface grafting, we performed experiments comparing the grafting of UAME and its analog with all C-C bonds saturated, methyl decanoate ("saturated-UAME") (see Fig. 2.1 for structure). Fig. 2.4a shows infrared spectra of ZnO nanorods after

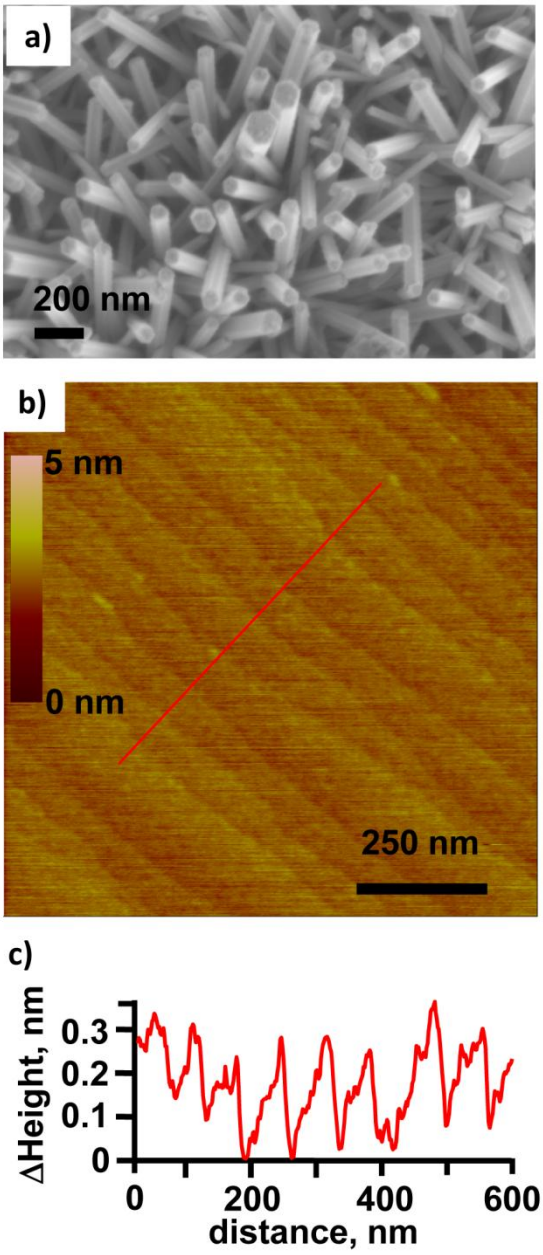

Figure 2.2: (a) SEM image of ZnO nanorods. (b) AFM image of the $(10\bar{1}0)$ surface of an annealed ZnO single crystal. (c) Height profile taken along line shown in (b).

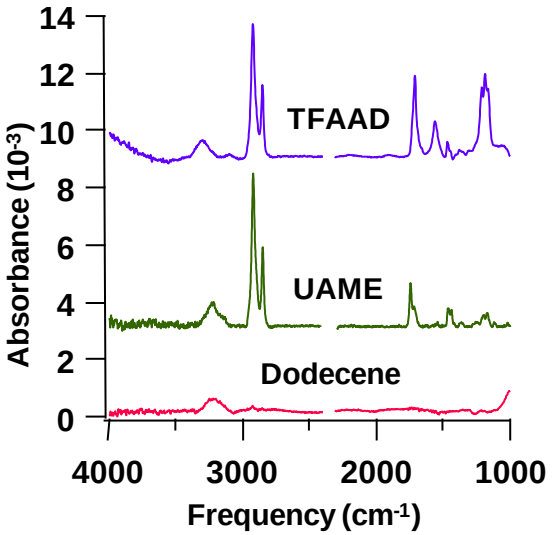

Figure 2.3: FTIR spectra of ZnO nanorods after grafting with the alkenes shown in Fig. 2.1

grafting for ~16 h with these molecules, along with a transmission spectrum of the pure UAME reactant liquid. While grafting of UAME leads to substantial intensity of the C-H modes, the IR spectrum of the sample that was illuminated while in contact with the analogous saturated compound shows no significant IR absorption. This difference in reactivity between these molecules establishes that the unsaturated alkene group is necessary for reaction.

A more detailed analysis shows that the alkene group is directly involved in the surface reaction. The spectrum of the UAME neat liquid displays two infrared features that arise from the vinyl group: one peak at 3078 cm^{-1} from the alkene C-H vibration, and a second peak at 1641 cm^{-1} from the C=C stretching vibrations of the terminal alkene.[48] Fig. 2.4b and Fig. 2.4c show these regions at higher resolution for neat UAME and for ZnO nanorods after grafting with UAME. In both cases, the vibrational modes that are associated with the unsaturated C=C bonds are clearly present in the reactant liquid but are absent after grafting to ZnO. Thus, we conclude that the alkene group is directly involved in surface bonding. Fig. 2.4d shows a spectrum of the region where -OH groups are observed on ZnO surfaces.[49] Because the absorbances of the -OH groups are very small (note the difference in vertical scale of Fig. 2.4d compared with 2.4a-2.4c), we corrected this spectrum for atmospheric water absorption[50,51] and also show the spectrum of water vapor in this region. Surface -OH peaks (all negative) are observed at 3687, 3676, and possibly a smaller peak at 3610 cm^{-1}. These peaks are similar to those reported previously on single-crystalline and nanocrystalline ZnO surfaces.[49,52,53] Since these peaks are all negative, we conclude that grafting of UAME to the ZnO surface is accompanied by a loss of surface -OH groups.

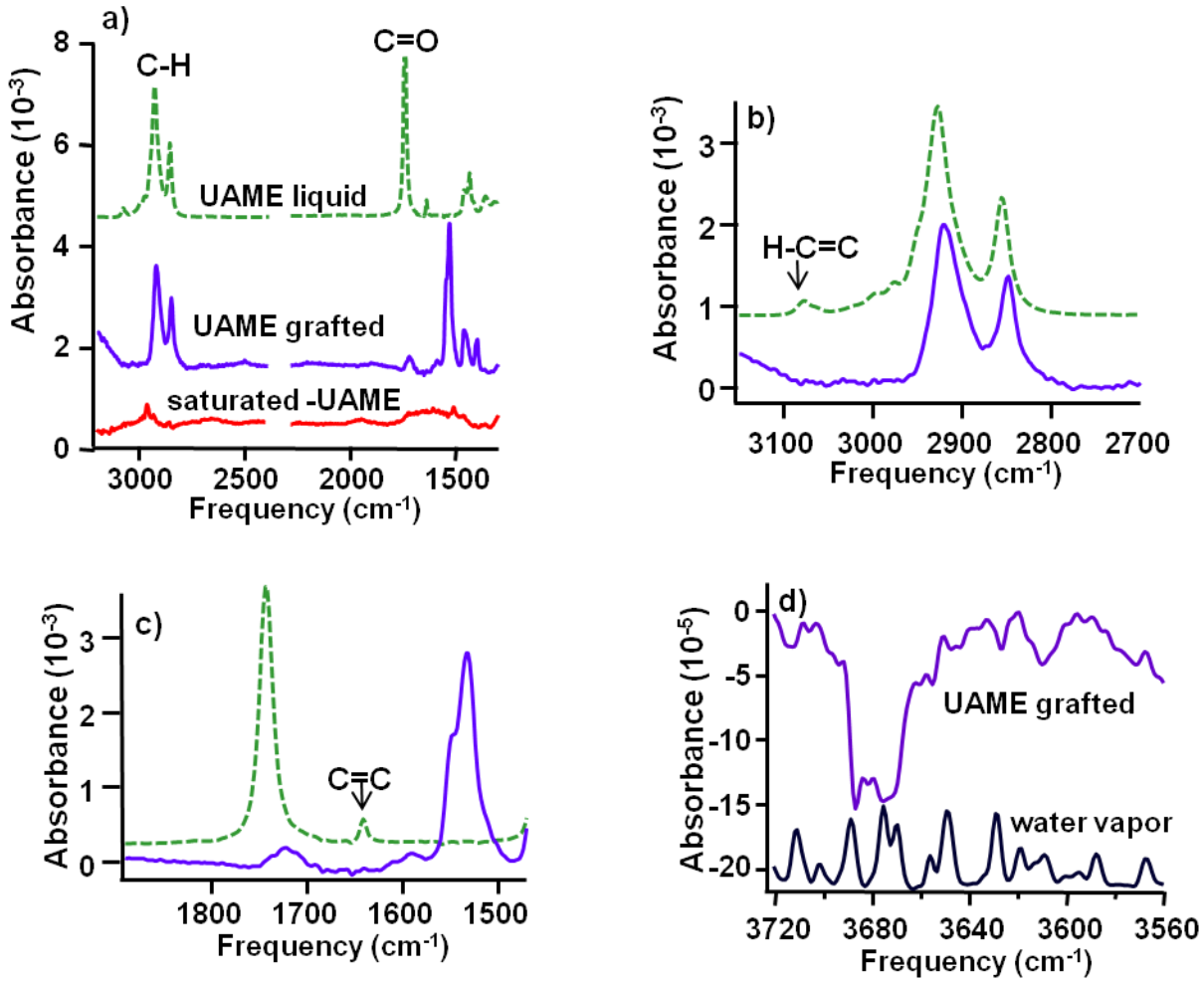

Figure 2.4: (a) FTIR spectra of neat liquid UAME, UAME grafted to ZnO nanorods, and the analog of UAME without the vinyl group grafted to ZnO nanorods. (b) Magnified view of the C-H stretching region. The vinylic C-H stretch present in the neat liquid is absent after grafting. (c) Magnified view of the C=C stretching region. The C=C stretch present in the neat liquid is absent after grafting. (d) Magnified view of the –OH stretching region. An FTIR spectrum of water vapor is also shown for comparison. For clarity the absorbance of the neat liquid in a-c has been rescaled to be of comparable intensity to the absorbance of the surface-bound molecules.

One notable factor in the FTIR spectra in Fig. 2.4 is that the carbonyl stretch observed at 1743 cm^{-1} for the reactant liquid is somewhat variable between different samples. In most cases the predominant feature is a single peak at 1743 cm^{-1} (identical to that observed for the neat parent compound), with a shoulder near 1718 cm^{-1} that is likely due to the free carboxylic acid. In some cases this peak is replaced by a very strong mode at 1531 cm^{-1} and a weaker shoulder at 1591 cm^{-1} that are characteristic of the symmetric and asymmetric stretches of carboxylates bound to ZnO.[22] Repeated studies indicate that trace amounts of water and environmental humidity have a strong effect on the bonding configuration by inducing hydrolysis of the ester to the free acid, similar to prior results on TiO_2.[42] Molecules that are bound to the surface via the alkene group without further hydrolysis yield the ester mode at 1743 cm^{-1}; subsequent hydrolysis to expose the carboxylic acid group gives rise to the broader peak at 1718 cm^{-1}. If the carboxylate group interacts with the surface it yields modes at 1531 and 1591 cm^{-1}; in this case it is possible that some molecules may bind in an inverted configuration, with possible cross-linking of the alkene groups. However, in the more commonly observed case where grafting yields the ester and/or free acid, the absence of the olefinic stretch in the grafted UAME and the fact that the methyl ester without a terminal alkene group (saturated-UAME) does not graft both show that the UAME binds to the surface via the terminal vinyl group.

The kinetics of the photochemical grafting reaction were followed with XPS using annealed bulk single crystals exposing $(10\bar{1}0)$ surfaces. Molecular coverages were calculated including effects of attenuation in the organic layer, using direct measurements of the attenuation factor in the organic film. Attenuation due to the organic layer was corrected for by using the Zn(3p) peak area of clean samples showing a minimum of carbon contamination. The Zn(3p)

peak was chosen because the relatively high kinetic energy of Zn(3p) photoelectrons leads to reduced inelastic scattering in the organic layer.

Fig. 2.5a shows the coverage of UAME on ZnO ($10\bar{1}0$) as a function of illumination time. While some UAME bonds via physisorption without illumination (t=0), illumination with UV light induces additional grafting that eventually reaches a coverage of UAME of ~ 4 x 10^{14} molecules/cm^2 after ~25 hours. For comparison, studies of crystalline n-alkanes show that the minimum area needed for an alkyl chain is 18.5 Å[54], which corresponds to a maximum coverage of 5.4 x 10^{14} alkyl chains/cm^2. While we do not expect molecules with the bulkier ester group to pack as efficiently, the coverage of UAME is roughly comparable to that expected for a single monolayer. Fig. 2.5b shows an AFM image of a ZnO ($10\bar{1}0$) single crystal; the individual steps and flat terraces can be clearly seen, demonstrating the molecular layers graft uniformly across the surface.

2.3.3 Grafting of TFAAD to ZnO

The grafting of TFAAD to ZnO was investigated as a general route to enable multistep chemistry on the surface via coupling to surface amino groups. After grafting TFAAD to the surface, the trifluoroacetamide (TFA) group can be deprotected under relatively mild conditions to yield primary amine groups. These primary amine groups can then be used as a starting point for further modification.

Fig. 2.6a shows FTIR of neat liquid TFAAD, ZnO nanorods reacted 16 h with TFAAD, and TFAAD-modified nanorods after deprotection of the TFA group. The most intense modes associated with the TFA group are the carbonyl stretch of the amide group at 1707 cm^{-1} and three closely spaced modes from C-F vibrations of the $–CF_3$ group at 1211, 1188, and 1167 cm^{-1}.

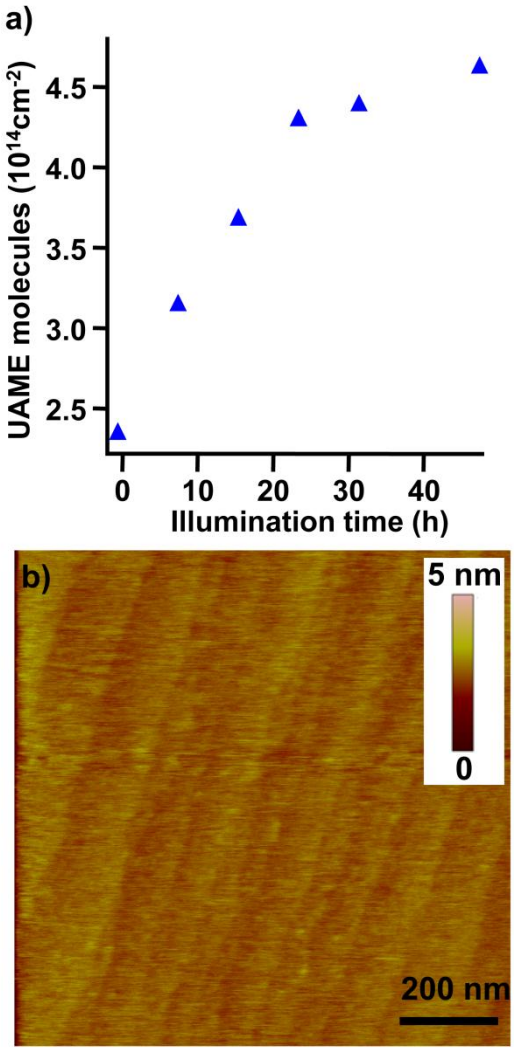

Figure 2.5: a) Density of UAME molecules on single crystal ZnO($10\bar{1}0$) as a function of illumination time measured by XPS. b) AFM image of UAME layer after 16 hours of grafting on ZnO($10\bar{1}0$) surface. Single-height steps are clearly visible across the image through the molecular layer.

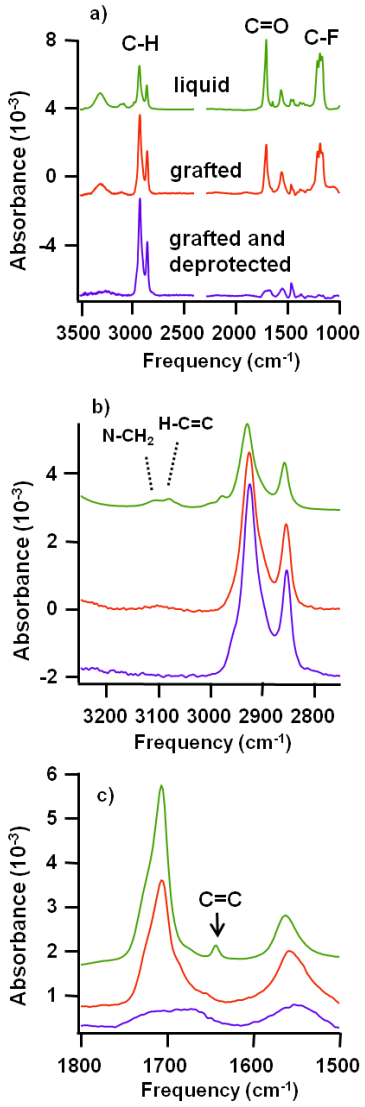

Figure 2.6: (a) FTIR spectra of neat liquid TFAAD, TFAAD grafted to ZnO nanorods for 16 h, and TFAAD that has been deprotected after grafting. (b) Magnified view of the C-H stretching region. The vinylic C-H stretch present in the neat liquid is absent after grafting. (c) Magnified view of the C=C stretching region. The C=C stretch present in the neat liquid is absent after grafting. For clarity the absorbance of the neat liquid in a-c has been rescaled to be of comparable intensity to the absorbance of the surface-bound molecules.

These signatures of the protecting group are clearly seen in the spectrum of TFAAD grafted to nanorods and are markedly reduced in intensity after the deprotection step, as expected for a successful deprotection step.

Fig. 2.6b is an enlarged view of the C-H stretching region of the neat TFAAD and TFAAD grafted to ZnO nanorods both before and after deprotection. The peaks at 2929 and 2858 cm^{-1} from the aliphatic chain are of approximately the same intensity both before and after deprotection, indicating that the photochemically grafted layers are stable under the deprotection conditions. The band at 3080 cm^{-1} associated with the terminal alkene is absent after grafting. The broad peak at 3106 cm^{-1} has been previously assigned to an overtone of the amide II band.[55] It is observed weakly in the spectrum of the grafted molecule and is completely absent after the deprotection step, which removes the trifluoroacetate group. Fig. 2. 6c is an enlarged view of the C=C stretching region of the neat TFAAD and TFAAD grafted to ZnO nanorods. The band at 1643 cm^{-1} attributed to the C=C stretching vibrations of the terminal alkene is absent after grafting. These infrared data show TFAAD grafts to the surface via the terminal alkene group, and that the TFA protecting group can be subsequently deprotected with high efficiency.

As a complement to FTIR studies, we used XPS to characterize the grafting and subsequent deprotection of TFAAD on ZnO surfaces. Fig. 2.7 shows the C(1s), N(1s), and F(1s) regions of ZnO nanorods grafted with TFAAD for 21 hours, an identical sample after the deprotection step, and a control sample that was exposed to TFAAD for 46 hrs without illumination. The main C(1s) peak from the alkyl chain of the TFAAD molecule was shifted to lie at the standard calibration energy of 285 eV,[46] and other peaks were shifted accordingly. Before deprotection higher binding energy C(1s) peaks are present at 293.5 and 289 eV,

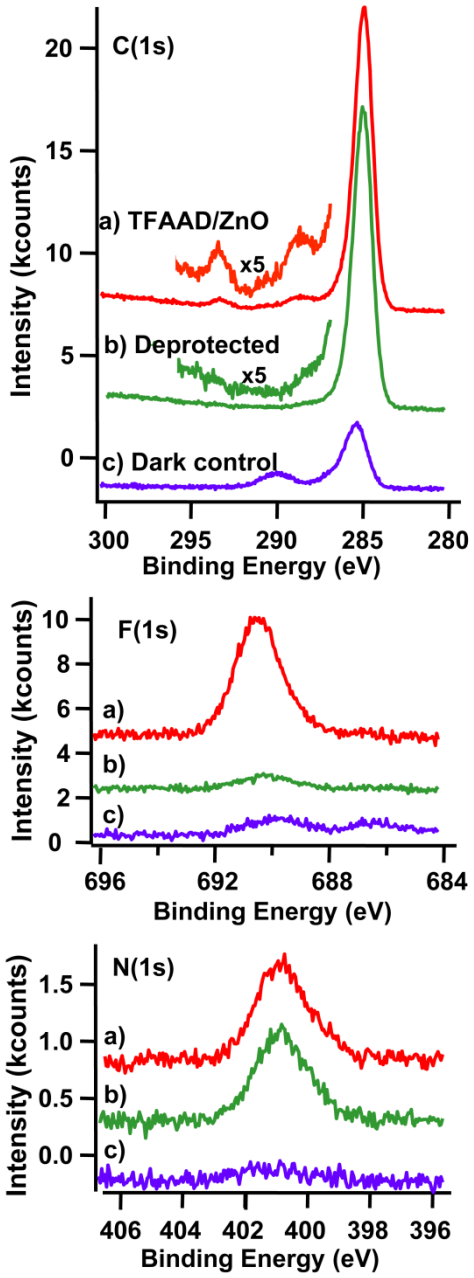

Figure 2.7: XPS data of the C(1s), F(1s), and N(1s) regions of TFAAD grafted to ZnO nanorods for 21 h. (a) XPS after grafting of TFAAD (b) XPS after deprotection of TFAAD. (c) dark controls, showing XPS data of a control sample that was exposed to TFAAD for 46 h but not illuminated.

corresponding to the C atoms of the CF_3 group and the carbonyl group respectively. The F(1s) region of TFAAD grafted to ZnO shows a peak at 690.7 eV and the N(1s) region shows a single peak at 400.8 eV. Upon deprotection the F(1s) peak nearly vanishes, while the N(1s) peak remains nearly unaffected. These XPS data further establish that TFAAD can be grafted and subsequently deprotected with high efficiency.

2.3.4 TFAAD Multilayer Formation

While grafting of UAME is self-terminating near one monolayer, quantitative analysis of the XPS data for TFAAD (see below) show that the coverage of this molecule is significantly more than a single monolayer. Recent studies of photochemical grafting of alkenes to other surfaces have shown that a key step in the reaction is the photoemission of electrons from the sample into the adjacent liquid, and that TFAAD grafts exceptionally well because the TFA group is a good electron acceptor; however, these good electron-accepting abilities also enhance the possibility of additional reactions that lead to multilayer formation.[56] Multilayer films can have some advantages over true monolayer films, such as a higher density of functional groups and/or improved stability, provided that the multilayer formation can be controlled.

To characterize multilayer formation, we used atomic force microscopy (AFM) to measure the roughness of the surfaces. The thickness of the layers was evaluated using both AFM and XPS. One of the most striking features of the photochemical grafting is the smoothness of the surface even when forming multilayers. Fig. 2.8a shows an AFM image of a ZnO $(10\bar{1}\,0)$ surface that was annealed in air, covered with liquid TFAAD, and illuminated for 48 hours to form a very thick molecular layer. A patch of the organic layer was then removed by increasing the AFM set-point voltage, which increases the force between the tip and the sample

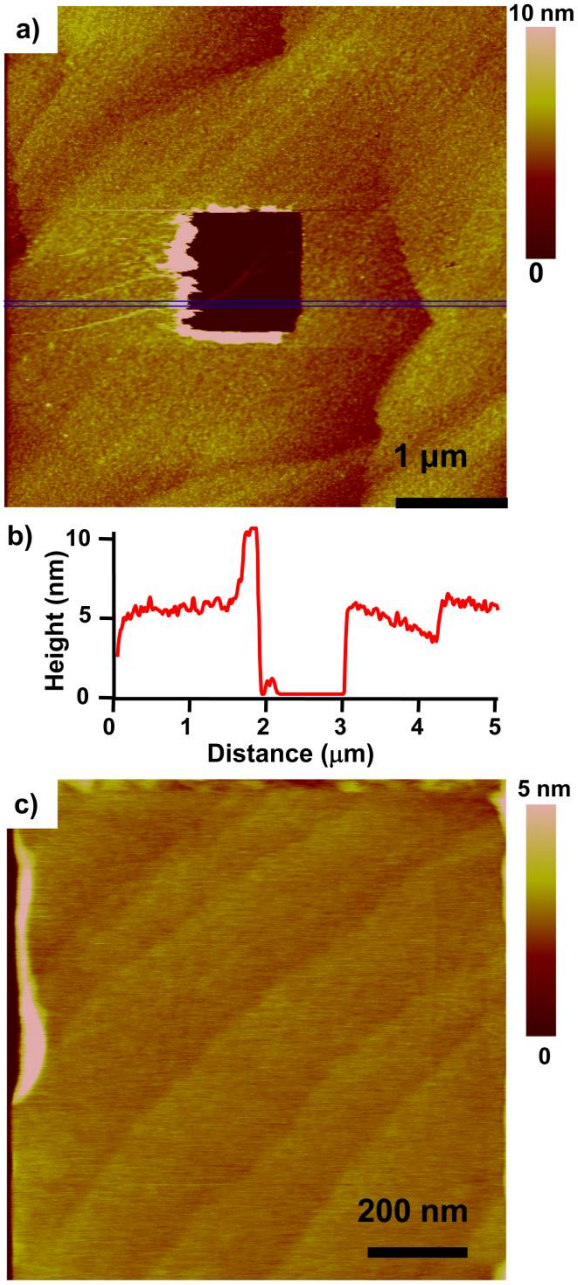

Figure 2.8: (a) AFM image of ZnO ($10\bar{1}0$) after grafting with TFAAD for 48h. The center square is where the TFAAD layer has been removed by scratching with the AFM tip. (b) Height profile along the line shown in (a). (c) Magnified view of (a) taken where the TFAAD layer has been removed.

and induces removal of the layer when a smaller area is scanned. The sample was then re-imaged over a larger area, yielding the image in Fig. 2.8a and the height profile shown in Fig. 2.8b. The height profile shows that the multilayer film is ~5 nm thick but still has a roughness of < 1 nm RMS. Fig. 8c shows an AFM image obtained within the area of removal (i.e., from within the dark square in Fig. 8a). In Fig. 2.8c single-height steps of the ZnO surface are easily revealed, demonstrating that grafting does not significantly alter the structure of the ZnO surface.

Fig. 2.9 compares the thickness of the layer measured with AFM to the effective coverage calculated from XPS measurements of the C(1s) and Zn(3p) peak areas. The XPS data yield effective molecular densities as high as ~$3x10^{15}$ molecules/cm^2. This is significantly higher than the maximum packing density of ~ $4x10^{14}$ molecules/cm^2 found for self-assembled monolayers on gold,[57,58] demonstrating that the grafting process yields multilayers. Fig. 2.9 also show the thickness of the molecular layers obtained from AFM measurements like those shown in Fig. 2.8. The AFM data demonstrate formation of multilayers up to ~5 nm thickness.

One remarkable aspect of the multilayer formation is that the resulting surfaces are remarkably smooth and uniform across the surface. Fig. 2.10 shows AFM images of a freshly annealed ZnO single crystal, and ZnO single crystals that were reacted for 8 and 24 hours with TFAAD, which should result in layers approximately 1 nm and 4 nm thick, respectively (based on Fig. 2.9). The average surface roughness measured over a 25 μm-line is 0.17 nm for the freshly annealed sample. The roughness increases to only 0.36 and 0.51 nm for the 8 and 24 hour reactions respectively.

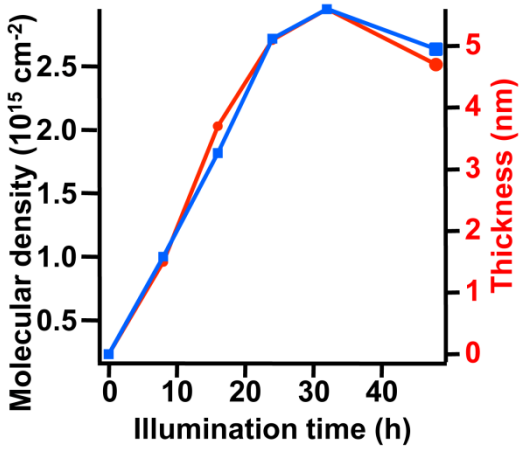

Figure 2.9: Left axis: Density of TFAAD molecules on single-crystal ZnO ($10\bar{1}0$) as a function of illumination time measured by XPS. Right axis: Thickness of the TFAAD layer as a function of illumination time measured by AFM scratching experiments.

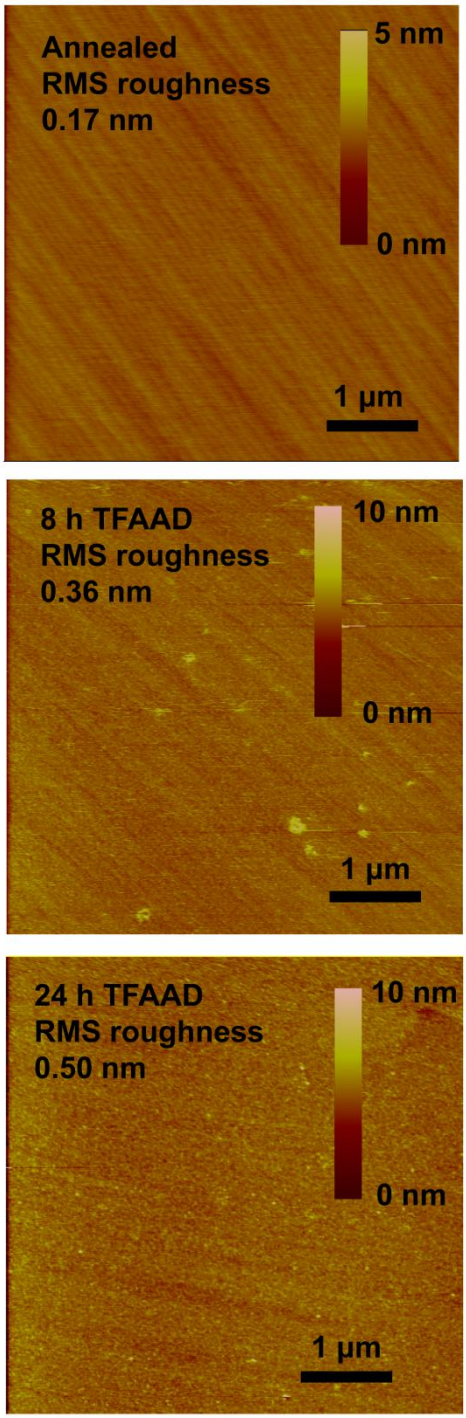

Figure 2.10: AFM images taken of ZnO (10$\bar{1}$0) (a) after annealing (b) after grafting TFAAD 8 h (c) after grafting TFAAD 24 h

2.3.5 Multistep Surface Functionalization

One motivation for grafting of TFAAD and other molecules to ZnO is to serve as starting points for subsequent chemistry to tailor the properties of the ZnO surfaces. For example, hydrophobic or hydrophilic ligands can control wetting and solubility properties, while functional groups such as amines can be used for subsequent covalent chemistry. Previous studies have shown that TFAAD molecules grafted to surfaces of TiO_2 and diamond could be deprotected to yield primary amine groups than can then be used in subsequent chemical steps to graft even more complex molecules to surfaces.[36,43,59] We evaluated whether similar chemistry could be applied to the much more delicate ZnO surface. Of especially great interest is the question of whether multilayer formation leads to an increase in the number density of functional groups at the surface or whether multilayer formation leads to inaccessible or inactive functional groups.

The XPS data in Fig. 2.7 shows the C(1s), N(1s), and F(1s) regions of ZnO nanorods grafted with TFAAD for 21 hours before and after deprotection. Deprotection leads to >90% loss of the F(1s) peak and the high binding-energy C(1s) peak near 293 eV, while the N(1s) signal remains unaltered within the error of the measurement. These results show that >90% of the protected amine groups are chemically accessible and can be successfully deprotected even in a multilayer structure.

To further demonstrate that the primary amine groups formed during the deprotection step are accessible and available for further surface modification, amine-terminated ZnO nanorods were reacted with methyl-4-formylbenzoate (MFB). This molecule was chosen as a model system because it can react with primary amine groups as depicted in Fig. 2.11a, and

because both the aldehyde group and the methyl ester group have clear IR signatures. ZnO nanorods functionalized with the deprotected TFAAD were reacted with a 1.5% solution of methyl-4-formylbenzoate (Aldrich) in a 1:1 (by volume) mixture of cyanoborohydride coupling buffer (Aldrich) and isopropanol for 2 hours at room temperature. The samples were then rinsed with isopropanol and soaked overnight in deionized water. Fig. 2.11b shows reflectance infrared spectra of ZnO nanorods after deprotection and after subsequent reaction with MFB.

The bottom trace in Fig. 2.11b shows the infrared spectrum of pure methyl-4-formylbenzoate. Several modes are of particular importance. The two vibrational modes at 1685 cm^{-1} and 1202 cm^{-1} arise from the aldehyde group. The 1685 cm^{-1} mode arises from the C=O stretch,[60,61] while the mode at 1202 cm^{-1} is similar to a very strong mode in benzaldehyde at 1206 cm^{-1} that has been attributed to the in-plane CHO stretch.[60] The methyl ester group gives rise to a characteristic C=O stretching mode at 1724 cm^{-1}. Comparing the spectra of the deprotected surface (top trace) and the neat MFB (bottom trace) with that of the surface adduct shows several changes. In particular, the two peaks at 1685 and 1202 cm^{-1} that are characteristic of the aldehyde group are absent, but the sharp peak at 1724 cm^{-1} that is characteristic of the methyl ester is clearly present. These changes demonstrate that the aldehyde group of MFB reacts with the amino-functionalized ZnO surface to form the secondary amine, but the ester group remains unaffected.

As an additional control we used infrared spectroscopy to characterize the interaction of MFB with a ZnO surface that had TFAAD grafted to it but which did not undergo the deprotection procedure. The resulting spectra showed no significant change upon exposure to MFB. Thus, we conclude that even when coverage is in the multilayer regime, the amino

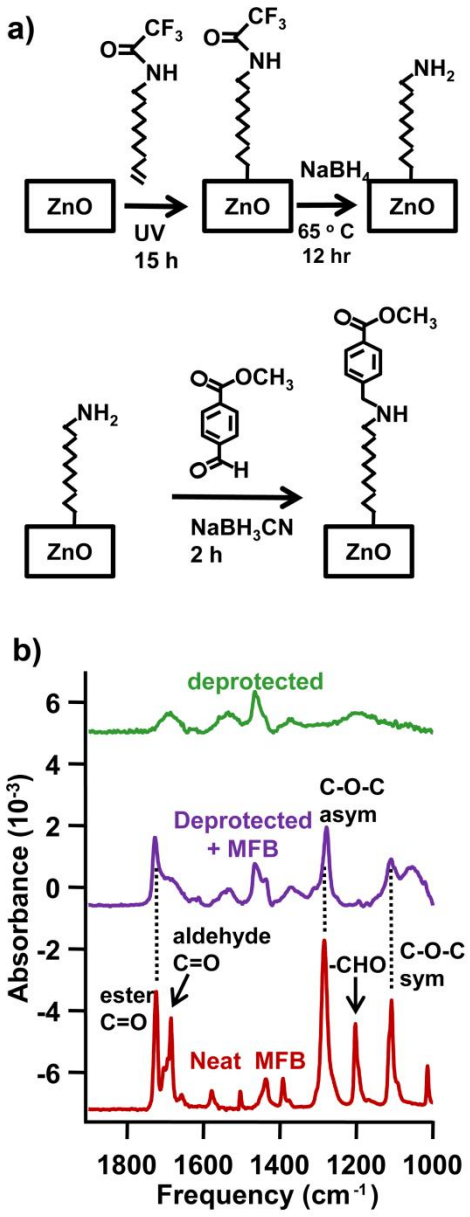

Figure 2.11: (a) Reaction scheme for multi-step chemistry on ZnO nanorods. (b) FTIR of ZnO nanorods taken after grafting and deprotection of TFAAD (top trace), after reaction with methyl-4-formylbenzoate (middle trace), and spectrum of neat methyl-4-formylbenzoate for comparison (lower trace).

functional groups of the TFAAD-grafted surface are highly accessible and can be successfully coupled with additional reactive groups such as aldehydes. This suggests that the multilayer structure must have a relatively high degree of porosity that permits diffusion of reactants into the structure.

2.3.6 Effect of TFAAD on Surface Flatband Potential

In order to investigate whether grafting of molecular layers significantly impacted the surface electronic structure, we performed differential capacitance (Mott-Schottky) analysis of the flatband potentials of bare ZnO nanorods and nanorods functionalized with TFAAD, in contact with solutions of $LiClO_4$ in acetonitrile.

Conventional electrical measurements showed some curvature and considerable frequency dispersion, making it difficult to unambiguously assign a flatband potential. For this reason photoresponse measurements, which are less sensitive to surface states and adsorbed species[62], were also taken (Fig. 2.12). In this case the samples are weakly illuminated with light having a wavelength of 350 nm (photon energy above the bandgap), creating electron-hole pairs in the sample; the response of the resulting photocurrent is measured as a function of the sample potential. Data are shown for bare and functionalized samples at optical chopping frequencies of 10 and 1000 Hz. In contrast to the differential capacitance (Mott-Schottky) measurements, the frequency dispersion in the photocurrent was minimal in the frequency range between 2 and 1000 Hz. In the absence of significant surface recombination, the onset of photocurrent is approximately the flatband potential.[63] Our measurements showed that all samples had a flatband potential of approximately -0.45 V vs. a Ag/Ag^+ reference electrode. These measurements clearly show no significant change in the flatband potential after photochemical grafting.

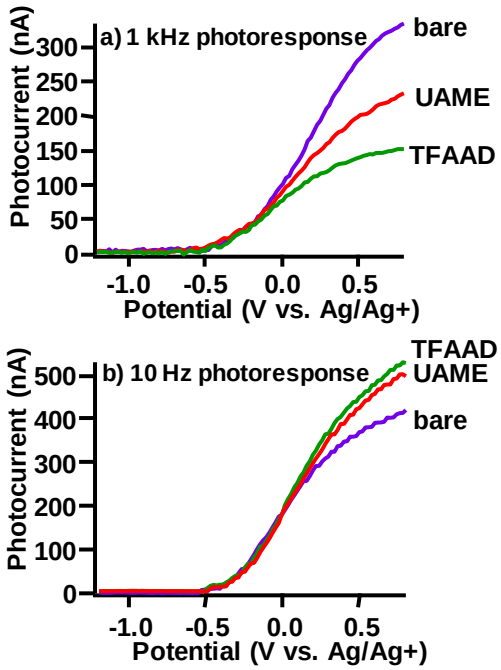

Figure 2.12: Photoresponse measurements for bare ZnO nanorods and nanorods functionalized for 16 h with TFAAD and UAME taken at (a) 1 kHz optical chopping frequency and (b) 10 Hz optical chopping frequency.

2.4 Discussion

Our results show that organic alkenes can form covalent bonds to ZnO under illumination with UV light, and that the resulting layers can be used as a basis for multistep chemistry on the ZnO surface. Our results show that for UAME the reaction self-terminates at one monolayer, while with TFAAD the reaction continues slowly, leading to multilayer formation. Perhaps surprisingly, multilayers formed from molecules bearing a suitable reactive group (such as TFAAD, which contains a protected primary amine group) retain full activity of all functional groups within the film. Thus, by using a molecule such as TFAAD it is possible to increase further the number of functional groups available on the surface.

2.4.1 Dependence on Molecular Structure

The results above show that having an olefinic group is necessary but not sufficient for facile grafting of alkenes to the surface, and that the terminal functional group plays an important role in controlling the grafting reaction. Overall the dependence on molecular structure we observe on ZnO is similar to that observed in previous studies on carbon,[64] silicon,[65] and TiO_2.[42] In all cases, grafting of simple alkenes such as 1-dodecene is very inefficient. Methyl esters such as UAME are more efficient and self-terminate at one monolayer, while the trifluoroacetamide group of TFAAD leads to highly efficient grafting and even a propensity toward multilayer formation. Previous studies on silicon,[65] diamond,[66] and amorphous carbon[56,64] have reported a general trend in photochemical grafting reactivity, with simple alkenes exhibiting lowest reactivity, esters having higher reactivity, and TFAAD more reactive yet. A key conclusion from these previous studies is that the photochemical grafting of alkenes using UV light is initiated by photoemission of the electrons from the substrate into the adjacent reactant fluid, leaving the

surface with positively-charged (cationic) sites that then undergo nucleophilic attack by the electron-rich alkene group.[64] A comparison of the extent of grafting of different molecules with density functional calculations of the their electron acceptor states showed that the rate of grafting is directly correlated with the electron affinity of the reactant molecules.[64] TFAAD has the highest grafting efficiency because it has a low-lying electron acceptor group, while dodecene is a poor electron acceptor and therefore grafts poorly. UAME has an electron affinity intermediate between those of dodecene and TFAAD, and therefore grafts better than dodecene but not as well as TFAAD and self-terminates near one monolayer.

A second important result from the previous studies is that while above-bandgap illumination can create surface holes, the steady-state concentration near the surface is controlled by a competition between excitation and recombination, resulting in a relatively low concentration of surface holes and a low rate of grafting.[65,67] In contrast, illuminating at very short wavelengths is highly efficient because photoelectron ejection is essentially an irreversible process, provided that there are acceptor states in the reactant liquid to facilitate photoemission. Such acceptor states can be introduced as part of the molecular structure (by using molecules such as TFAAD that have terminal groups that are good electron acceptors) or by introducing a secondary electron acceptor into the reactant mixture or on the surface.[56]

2.4.2 Surface Sites for Grafting

Our FTIR data (Fig. 2.4d) show that grafting is accompanied by loss of surface hydroxyl groups. Previous studies have shown that under ambient conditions, the reaction of the bare ZnO surface with water leaves the surface terminated with a high concentration of surface hydroxyl groups and strongly adsorbed water molecules that hydrogen-bond to the surface and to these –

OH groups.[49,52] In a previous study of TiO_2,[68] we proposed that the alkenes reacted at surface hydroxyl groups because -OH groups can act as hole traps. In this scenario, illumination with ultraviolet light ejects photoelectrons into the adjacent reactive alkene, leaving the surface with an excess of holes that become localized on the -OH groups. These cationic sites then undergo nucleophilic attack by the alkene group of the reactant molecules.

Our results suggest that bonding of the alkenes to the ZnO surface likely involves surface –OH groups. While a detailed mechanism at this point is highly speculative, we propose that the surface –OH groups may become partially positively charged, making them susceptible to nucleophilic attack by the organic alkene and linking the molecule to the surface via formation of new C-O bonds at the surface, similar to the process depicted in Fig. 2.13. More than one type of –OH group can be present and the determination of specific bonding configurations at the surface is difficult; Fig. 13 is intended to be merely illustrative of the general pathway and is not intended to reflect any specific form of surface hydroxyl group or particular bonding geometry. While peaks in the 3500-3700 cm^{-1} range are generally agreed to arise from -OH groups,[49] the molecular origin of specific peaks is complicated by the frequent presence of adsorbed H_2O on ZnO surfaces. Studies on single-crystal ZnO($10\bar{1}0$) surfaces have shown that the peak near 3672 cm^{-1} arises from surface -OH groups that are interacting with coadsorbed water molecules, while a peak near 3687 cm^{-1} has been attributed to -OH stretches of chemisorbed water molecules.[49] These frequencies are in good agreement with the negative peaks that we observe (~3676 and 3687 cm^{-1}) in Fig. 4d,[52] but a more detailed interpretation is not currently possible.

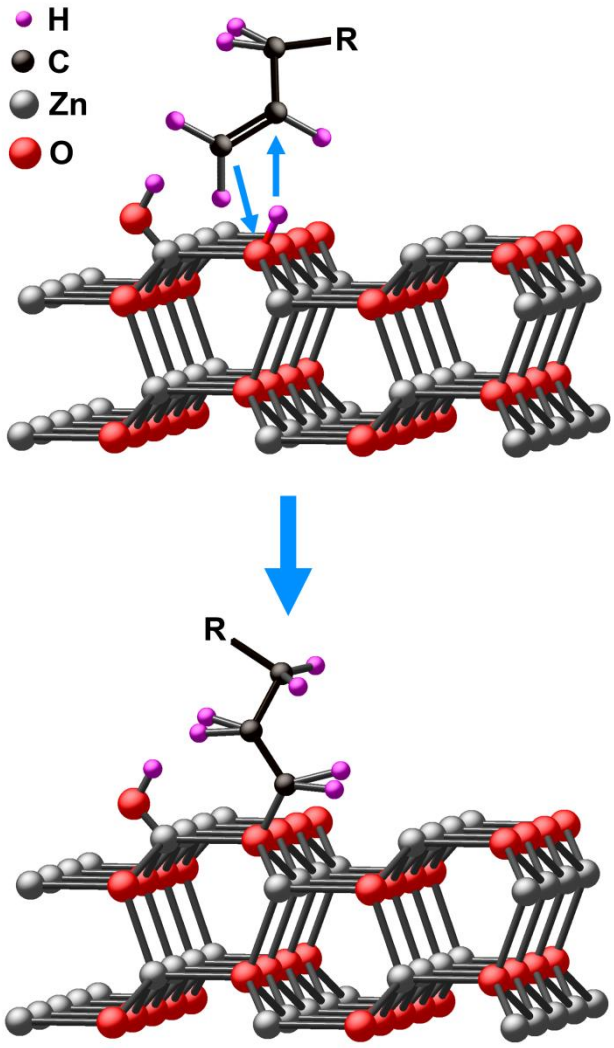

Figure 2.13: Schematic illustrating one potential way to form new C-O covalent linkage during the photochemical grafting of an alkene to ZnO. Surface hydroxyl groups are proposed to act as hole traps that facilitate nucleophilic attack by the alkene. While several types of –OH groups may be present, the figure illustrates only one possible reaction.

2.4.3 Multilayer vs. Monolayer Formation

In the case of TFAAD, we also observe clear evidence for multilayer formation. However, multilayer formation is not observed for UAME. While polymerization might be induced by the formation of radical sites near the molecule-ZnO interface, prior studies have shown that trifluoromethyl compounds can be susceptible to electron-induced degradation.[56,69-71] XPS measurements show that F/C ratio remains constant during grafting, indicating the there is no significant loss of material via electron-stimulated desorption processes. Electron-induced reaction of the TFA group would be expected to cleave the bond between the N atom and the CF_3CO group, leaving the remaining molecule as the primary amine (just as the deprotection step does) and leaving CF_3CO^- anions. While speculative, we believe the most likely pathway for multilayer formation would be if the electron-induced degradation of the TFA groups produces CF_3CO^- or other reactive groups that are able to initiate some additional cross-linking, perhaps by abstracting protons from alkyl chains of nearby TFAAD molecules. Further studies will be needed to establish a detailed mechanism for multilayer formation.

Perhaps the most surprising aspect of the multilayer formation is that the amino groups remain accessible for both deprotection and subsequent chemical functionalization, here demonstrated by the ability to react an aldehyde to the deprotected amine groups. This clearly suggests that the multilayer formation likely involves forming crosslinks between carbon atoms that are part of the alkyl chain. In addition to enabling multilayer formation, such crosslinks may contribute substantially to the overall stability of the photochemically grafted films, in much the same way that crosslinks enhance the stability of siloxane monolayers on surfaces.[72]

2.4.4 Comparison with Alternative Functionalization Methods

Currently the two most common methods to functionalize the ZnO surface are binding of carboxylic acids[4,22,25] and the use of silane chemistry,[22,73] although there is increasing interest in the use of phosphonic acids.[24,26] Carboxylic acids do not bind in all cases and successful binding depends on a number of factors including the surface preparation and properties, the solution pH, and the number, position, and acidity of the COOH groups.[22] One limitation of carboxylic acid binding is the potential for the acidic anchoring group to etch ZnO by forming a complex with Zn ions.[23] The grafting of alkenes avoids this problem because it requires no acidic protons. The binding of trimethoxy and triethoxy silanes is an alternative method that does not etch ZnO. One drawback of this approach, though, is the difficulty to control the surface coverage. Oligomerization in the bulk of the solution often leads to multilayer films and inhomogeneous deposition onto the surface. Efforts to reduce multilayer formation with n-butylamine catalyst resulted in only submonolayer coverages.[73] With photochemical grafting, however, the coverage of photochemically grafted alkenes can be controlled by varying the illumination time. For UAME the reaction rate appears to stop after ~ 1 monolayer coverage (~ 4×10^{14} molecules/cm^2) has been reached. While the reaction with TFAAD does not terminate at a single monolayer, AFM shows that even here the molecular layer is uniform with a thickness controlled by the illumination time. Our results further show successful deprotection to the primary amine and further reaction to form a secondary amine. In principle this type of reaction can be extended to introduce a variety of different surface groups to ZnO.

2.4.5 Influence on Surface Electronic Structure

The impact of the photochemically grafted molecules on the electronic properties of ZnO was investigated with flatband potential measurements. Measurements of the differential capacitance (Mott Schottky plots) deviate from the ideal Mott Schottky model, which includes only the space charge capacitance and bulk resistance of the semiconductor.[63] Capacitance measurements of metal oxide semiconductors can be strongly affected by surface states, with trapping and de-trapping of the states giving rise to frequency dispersion in the Mott-Schottky plots. The electronic properties can also depend strongly on sample history[74] since different sample preparation procedures may yield different types of defects. There may also be additional contributions because of the use of nanorod samples rather than planar samples.[75-77] However, an important observation of our work is that the sub-surface band-bending of the ZnO nanorods can be manipulated through the application of an external potential after functionalization. This implies that the functionalization does not adversely impact the space-charge layer of the ZnO (by, for example, adding defects that might pin the Fermi level), an important consideration for the potential application of functionalized ZnO in applications such as organic electronics or chemical/biological sensing.

Our results show that the differential capacitance of functionalized nanorods is consistently larger than that of annealed samples. If the molecular layer is modeled as an additional, voltage-independent capacitance in series with the space charge capacitance, the molecular layer should have no impact on the slope of the Mott-Schottky plot, but may only result in a (generally small) shift in the flatband potential[78]. Similarly, were the molecular layer to introduce a voltage-independent change in surface dipole, one would expect a shift in flatband

potential but no change in the slope of the Mott-Schottky plot.[63] Surface states are known to give rise to an additional capacitance in parallel with the space charge capacitance. If the energy of the surface state is not discrete, but rather distributed, surface states may contribute to the parallel capacitance over a considerable voltage range.[63] While the change in differential capacitance after grafting does suggest changes in surface states, it is clear that there is no shift in the flatband potential as measured by photoresponse. Further studies will be needed to fully understand how photochemically grafted films impact the electronic structure of ZnO nanorods and electronic transport processes across the interface.

2.5 Conclusion

We have demonstrated that organic alkenes will graft to the surface of ZnO under UV illumination. This method produces layers that are highly uniform and robust to subsequent modification steps, providing a versatile pathway to multistep chemical functionalization of ZnO surfaces and of ZnO nanostructures such as nanorods and nanoparticles. These results provide an attractive method to tailor the surface of ZnO. Our results suggest that the functionalization does not significantly impact the flat-band potential and that the sub-surface band-bending can still be easily manipulated through the application of an external field after functionalization. This suggests that photochemically grafted layers may provide an attractive method for functionalizing ZnO surfaces for application such as chemical/biological sensing, and or organic-inorganic hybrid structures such as solar cells.

2.6 References

(1) Law, M.; Greene, L. E.; Johnson, J. C.; Saykally, R.; Yang, P. D., Nanowire dye-sensitized solar cells. *Nature Materials* **2005**, 4, 455.

(2) O'Regan, B.; Schwartz, D. T.; Zakeeruddin, S. M.; Grätzel, M., Electrodeposited nanocomposite n-p heterojunctions for solid-state dye-sensitized photovoltaics. *Advanced Materials* **2000**, 12, 1263.

(3) Beek, W. J. E.; Wienk, M. M.; Kemerink, M.; Yang, X. N.; Janssen, R. A., Hybrid zinc oxide conjugated polymer bulk heterojunction solar cells. *Journal of Physical Chemistry B* **2005**, 109, 9505.

(4) Rossini, J. E.; Huss, A. S.; Bohnsack, J. N.; Blank, D. A.; Mann, K. R.; Gladfelter, W. L., Binding and Static Quenching Behavior of a Terthiophene Carboxylate on Monodispersed Zinc Oxide Nanocrystals. *Journal of Physical Chemistry C* **2011**, 115, 11.

(5) Fan, Z. Y.; Lu, J. G., Gate-refreshable nanowire chemical sensors. *Applied Physics Letters* **2005**, 86, 277.

(6) Li, Q. H.; Liang, Y. X.; Wan, Q.; Wang, T. H., Oxygen sensing characteristics of individual ZnO nanowire transistors. *Applied Physics Letters* **2004**, 85, 6389.

(7) Mitra, P.; Chatterjee, A. P.; Maiti, H. S., ZnO thin film sensor. *Materials Letters* **1998**, 35, 33.

(8) Wan, Q.; Li, Q. H.; Chen, Y. J.; Wang, T. H.; He, X. L.; Li, J. P.; Lin, C. L., Fabrication and ethanol sensing characteristics of ZnO nanowire gas sensors. *Applied Physics Letters* **2004**, 84, 3654.

(9) Xu, J. Q.; Pan, Q. Y.; Shun, Y. A.; Tian, Z. Z., Grain size control and gas sensing properties of ZnO gas sensor. *Senors and Actuators B - Chemical* **2000**, 66, 277.

(10) Zhang, Y. S.; Yu, K.; Jiang, D. S.; Zhu, Z. Q.; Geng, H. R.; Luo, L. Q., Zinc oxide nanorod and nanowire for humidity sensor. *Applied Surface Science* **2005**, 242, 212.

(11) Liu, Y.; Gorla, C. R.; Liang, S.; Emanetoglu, N.; Lu, Y.; Shen, H.; Wraback, M., Ultraviolet detectors based on epitaxial ZnO films grown by MOCVD. *Journal of Electronic Materials* **2000**, 29, 69.

(12) Basak, D.; Amin, G.; Mallik, B.; Paul, G. K.; Sen, S. K., Photoconductive UV detectors on sol-gel-synthesized ZnO films. *Journal of Crystal Growth* **2003**, 256, 73.

(13) Saito, N.; Haneda, H.; Sekiguchi, T.; Ohashi, N.; Sakaguchi, I.; Koumoto, K., Low-temperature fabrication of light-emitting zinc oxide micropatterns using self-assembled monolayers. *Advanced Materials* **2002**, 14, 418.

(14) Konenkamp, R.; Word, R. C.; Godinez, M., Ultraviolet electroluminescence from ZnO/polymer heterojunction light-emitting diodes. *Nano Letters* **2005**, 5, 2005.

(15) Nadarajah, A.; Word, R. C.; Meiss, J.; Konenkamp, R., Flexible inorganic nanowire light-emitting diode. *Nano Letters* **2008**, 8, 534.

(16) Lao, C. S.; Li, Y.; Wong, C. P.; Wang, Z. L., Enhancing the electrical and optoelectronic performance of nanobelt devices by molecular surface functionalization. *Nano Letters* **2007**, 7, 1323.

(17) Lao, C. S.; Park, M. C.; Kuang, Q.; Deng, Y. L.; Sood, A. K.; Polla, D. L.; Wang, Z. L., Giant enhancement in UV response of ZnO nanobelts by polymer surface-functionalization. *Journal of the American Chemical Society* **2007**, 129, 12096.

(18) Zhou, J.; Gu, Y. D.; Hu, Y. F.; Mai, W. J.; Yeh, P. H.; Bao, G.; Sood, A. K.; Polla, D. L.; Wang, Z. L., Gigantic enhancement in response and reset time of ZnO UV nanosensor by utilizing Schottky contact and surface functionalization. *Applied Physics Letters* **2009**, 94, 191103.

(19) Richters, J. P.; Voss, T.; Wischmeier, L.; Ruckmann, I.; Gutowski, J., Influence of polymer coating on the low-temperature photoluminescence properties of ZnO nanowires. *Applied Physics Letters* **2008**, 92, 011103.

(20) Yip, H. L.; Hau, S. K.; Baek, N. S.; Ma, H.; Jen, A. K. Y., Polymer solar cells that use self-assembled-monolayer-modified ZnO/Metals as cathodes. *Advanced Materials* **2008**, 20, 2376.

(21) Liu, D.; Wu, W.; Qiu, Y.; Yang, S.; Xiao, S.; Wang, Q. Q.; Ding, L.; Wang, J., Surface functionalization of ZnO nanotetrapods with photoactive and electroactive organic monolayers. *Langmuir* **2008**, 24, 5052.

(22) Taratula, O.; Galoppini, E.; Wang, D.; Chu, D.; Zhang, Z.; Chen, H. H.; Saraf, G.; Lu, Y. C., Binding studies of molecular linkers to ZnO and MgZnO nanotip films. *Journal of Physical Chemistry B* **2006**, 110, 6506.

(23) Keis, K.; Lindgren, J.; Lindquist, S. E.; Hagfeldt, A., Studies of the adsorption process of Ru complexes in nanoporous ZnO electrodes. *Langmuir* **2000**, 16, 4688.

(24) Hotchkiss, P. J.; Malicki, M.; Giordano, A. J.; Armstrong, N. R.; Marder, S. R., Characterization of phosphonic acid binding to zinc oxide. *Journal of Materials Chemistry* **2011**, 21, 3107.

(25) Zhang, B. B.; Kong, T.; Xu, W. Z.; Su, R. G.; Gao, Y. H.; Cheng, G. S., Surface Functionalization of Zinc Oxide by Carboxyalkylphosphonic Acid Self-Assembled Monolayers. *Langmuir* **2010**, 26, 4514.

(26) Perkins, C. L., Molecular Anchors for Self-Assembled Monolayers on ZnO: A Direct Comparison of the Thiol and Phosphonic Acid. *Journal of Physical Chemistry C* **2009**, 113, 18276.

(27) Garcia, M. A.; Merino, J. M.; Pinel, E. F.; Quesada, A.; de la Venta, J.; Gonzalez, M. L. R.; Castro, G. R.; Crespo, P.; Llopis, J.; Gonzalez-Calbet, J. M.; Hernando, A., Magnetic properties of ZnO nanoparticles. *Nano Letters* **2007**, 7, 1489.

(28) Marczak, R.; Werner, F.; Gnichwitz, J. F.; Hirsch, A.; Guldi, D. M.; Peukert, W., Communication via Electron and Energy Transfer between Zinc Oxide Nanoparticles and Organic Adsorbates. *Journal of Physical Chemistry C* **2009**, 113, 4669.

(29) Halevi, B.; Vohs, J. M., Reactions of CH_3SH and $(CH_3)_2S_2$ on the $(000\bar{1})$ and (0001) surfaces of ZnO. *Journal of Physical Chemistry B* **2005**, 109, 23976.

(30) Vohs, J. M.; Barteau, M. A., Structure Sensitivity, Selectivity, and Adsorbed Intermediates in the Reactions of Acetone and 2-Propanol on the Polar Surfaces of Zinc-Oxide. *Journal of Physical Chemistry* **1991**, 95, 297.

(31) Vohs, J. M.; Barteau, M. A., Formation of Stable Alkyl and Carboxylate Intermediates in the Reactions of Aldehydes on the Zno(0001) Surface. *Langmuir* **1989**, 5, 965.

(32) Cheng, W. H.; Kung, H. H., Interaction of CO, CO_2 and O_2 with Non-Polar, Stepped and Polar Zn Surfaces of ZnO. *Surface Science* **1982**, 122, 21.

(33) Schiek, M.; Al-Shamery, K.; Kunat, M.; Traeger, F.; Woll, C., Water adsorption on the hydroxylated H-(1x1) O-ZnO(0001) surface. *Physical Chemistry Chemical Physics* **2006**, 8, 1505.

(34) Cicero, R. L.; Linford, M. R.; Chidsey, C. E. D., Photoreactivity of unsaturated compounds with hydrogen-terminated silicon(111). *Langmuir* **2000**, 16, 5688.

(35) Choi, K.; Buriak, J. M., Hydrogermylation of alkenes and alkynes on hydride-terminated Ge(100) surfaces. *Langmuir* **2000**, 16, 7737.

(36) Yang, W. S.; Auciello, O.; Butler, J. E.; Cai, W.; Carlisle, J. A.; Gerbi, J.; Gruen, D. M.; Knickerbocker, T.; Lasseter, T. L.; Russell, J. N.; Smith, L. M.; Hamers, R. J., DNA-modified nanocrystalline diamond thin-films as stable, biologically active substrates. *Nature Materials* **2002**, 1, 253.

(37) Strother, T.; Knickerbocker, T.; Russell, J. N.; Butler, J. E.; Smith, L. M.; Hamers, R. J., Photochemical functionalization of diamond films. *Langmuir* **2002**, 18, 968.

(38) Baker, S. E.; Tse, K. Y.; Hindin, E.; Nichols, B. M.; Clare, T. L.; Hamers, R. J., Covalent functionalization for biomolecular recognition on vertically aligned carbon nanofibers. *Chemistry of Materials* **2005**, 17, 4971.

(39) Nichols, B. M.; Butler, J. E.; Russell, J. N.; Hamers, R. J., Photochemical functionalization of hydrogen-terminated diamond surfaces: A structural and mechanistic study. *Journal of Physical Chemistry B* **2005**, 109, 20938.

(40) Sun, B.; Colavita, P. E.; Kim, H.; Lockett, M.; Marcus, M. S.; Smith, L. M.; Hamers, R. J., Covalent photochemical functionalization of amorphous carbon thin films for integrated real-time biosensing. *Langmuir* **2006**, 22, 9598.

(41) Kim, H.; Colavita, P. E.; Metz, K. M.; Nichols, B. M.; Sun, B.; Uhlrich, J.; Wang, X. Y.; Kuech, T. F.; Hamers, R. J., Photochemical functionalization of gallium nitride thin films with molecular and biomolecular layers. *Langmuir* **2006**, 22, 8121.

(42) Franking, R. A.; Landis, E. C.; Hamers, R. J., Highly Stable Molecular Layers on Nanocrystalline Anatase TiO2 through Photochemical Grafting. *Langmuir* **2009**, 25, 10676

(43) Li, B.; Franking, R.; Landis, E. C.; Kim, H.; Hamers, R. J., Photochemical Grafting and Patterning of Biomolecular Layers onto TiO_2 Thin Films. *ACS Applied Materials and Interfaces* **2009**, 1, 1013.

(44) Wood, A.; Giersig, M.; Hilgendorff, M.; Vilas-Campos, A.; Liz-Marzan, L. M.; Mulvaney, P., Size effects in ZnO: The cluster to quantum dot transition. *Australian Journal of Chemistry* **2003**, 56, 1051.

(45) Kobayashi, A.; Ohta, J.; Fujioka, H., Characteristics of Single Crystal ZnO Annealed in a Ceramic ZnO Box and Its Application for Epitaxial Growth. *Japanese Journal of Applied Physics* **2006**, 45, 5724.

(46) Wagner, C. D.; Naumkin, A. V.; Kraut-Vass, A.; Allison, J. W.; Powell, C. J.; Rumble, J. R., Jr.: NIST X-ray Photoelectron Spectroscopy Database. NIST Standard Reference Database 20, Version 3.4 (Web Version), 2003, available from http://srdata.nist.gov/xps/

(47) Vayssieres, L., Growth of arrayed nanorods and nanowires of ZnO from aqueous solutions. *Advanced Materials* **2003**, 15, 464.

(48) Socrates, G.: *Infrared and Raman Characteristic Group Frequencies*; 3rd ed.; John Wiley and Sons, Ltd., 2001.

(49) Noei, H.; Qiu, H. S.; Wang, Y. M.; Loffler, E.; Woll, C.; Muhler, M., The identification of hydroxyl groups on ZnO nanoparticles by infrared spectroscopy. *Physical Chemistry Chemical Physics* **2008**, 10, 7092.

(50) Martens, H.; Bruun, S. W.; Adt, I.; Sockalingum, G. D.; Kohler, A., Pre-processing in biochemometrics: correction for path-length and temperature effects of water in FTIR bio-spectroscopy by EMSC. J*ournal of Chemometrics* **2006**, 20, 402.

(51) Bruun, S. W.; Kohler, A.; Adt, I.; Sockalingum, G. D.; Manfait, M.; Martens, H., Correcting attenuated total reflection-Fourier transform infrared spectra for water vapor and carbon dioxide. *Applied Spectroscopy* **2006**, 60, 1029.

(52) Noei, H.; Qiu, H. S.; Wang, Y. M.; Muhler, M.; Woll, C., Hydrogen Loading of Oxide Powder Particles: A Transmission IR Study for the Case of Zinc Oxide. *ChemPhysChem* **2010**, 11, 3604.

(53) Kähler, K.; Holz, M. C.; Rohe, M.; Strunk, J.; Muhler, M., Probing the Reactivity of ZnO and Au/ZnO Nanoparticles by Methanol Adsorption: A TPD and DRIFTS Study. *ChemPhysChem* **2010**, 11, 2521.

(54) Ewen, B.; Strobl, G. R.; Richter, D., Phase-Transitions in Crystals of Chain Molecules - Relation Between Defect Structures and Molecular Motion in the 4 Modifications of *n*-$C_{33}H_{68.}$ *Faraday Discussions* **1980**, 69, 19.

(55) McLachlan, R. D.; Nyquist, R. A., An infrared study of some α-substituted secondary amides in solution. *Spectrochimica Acta* **1964**, 20, 1397.

(56) Colavita, P. E.; Streifer, J. A.; Sun, B.; Wang, X. Y.; Warf, P.; Hamers, R. J., Enhancement of photochemical grafting of terminal alkenes at surfaces via molecular mediators: The role of surface-bound electron acceptors. *Journal of Physical Chemistry C* **2008**, 112, 5102.

(57) Bindu, V.; Pradeep, T., Characterisation of alkanethiol ($C_nH_{2n+1}SH$, n = 3, 4, 6, 8, 10, 12 and 18) self assembled monolayers by X-ray photoelectron spectroscopy. *Vacuum* **1998**, 49, 63.

(58) Alves, C. A.; Smith, E. L.; Porter, M. D., Atomic Scale Imaging Of Alkanethiolate Monolayers At Gold Surfaces With Atomic Force Microscopy. *Journal of the American Chemical Society* **1992**, 114, 1222.

(59) Stavis, C.; Clare, T. L.; Butler, J. E.; Radadia, A. D.; Carr, R.; Zeng, H. J.; King, W. P.; Carlisle, J. A.; Aksimentiev, A.; Bashir, R.; Hamers, R. J., Surface functionalization of thin-film diamond for highly stable and selective biological interfaces. *Proceedings of the National Acadamy of Science of the United States of America* **2011**, 108, 983.

(60) Zwarich, R.; Smolarek, J.; Goodman, L., Assignment of Out-of-Plane Vibrational Modes in Benzaldehyde. *Journal of Molecular Spectroscopy* **1971**, 38, 336.

(61) Kondo, J.; Ding, N.; Maruya, K.; Domen, K.; Yokoyama, T.; Fujita, N.; Maki, T., Infrared Study of Hydrogenation of Benzoic-Acid to Benzaldehyde on ZrO_2 Catalysts. *Bulletin of the Chemical Society of Japan* **1993**, 66, 3085.

(62) Butler, M. A., Infrared Study of Hydrogenation of Benzoic-Acid to Benzaldehyde on ZrO_2 Catalysts. *Journal of Applied Physics* **1977**, 48, 1914.

(63) Gomes, W. P.; Cardon, F., Electron-Energy Levels in Semiconductor Electrochemistry. *Progress in Surface Science* **1982**, 12, 155.

(64) Colavita, P. E.; Sun, B.; Tse, K. Y.; Hamers, R. J., Photochemical grafting of n-alkenes onto carbon surfaces: the role of photoelectron ejection. *Journal of the American Chemical Society* **2007**, 129, 13554.

(65) Wang, X. Y.; Ruther, R. E.; Streifer, J. A.; Hamers, R. J., UV-Induced Grafting of Alkenes to Silicon Surfaces: Photoemission versus Excitons. *Journal of the American Chemical Society* **2010**, 132, 4048.

(66) Wang, X. Y.; Colavita, P. E.; Streifer, J. A.; Butler, J. E.; Hamers, R. J., Photochemical Grafting of Alkenes onto Carbon Surfaces: Identifying the Roles of Electrons and Holes. *Journal of Physical Chemistry C* **2010**, 114, 4067.

(67) Wang, X. Y.; Landis, E. C.; Franking, R.; Hamers, R. J., Surface Chemistry for Stable and Smart Molecular and Biomolecular Interfaces via Photochemical Grafting of Alkenes. *Accounts of Chemical Research* **2010**, 43, 1205.

(68) Franking, R. A.; Landis, E. C.; Hamers, R. J., Highly Stable Molecular Layers on Nanocrystalline Anatase TiO_2 through Photochemical Grafting. *Langmuir* **2009**, 25, 10676.

(69) Kim, C. S.; Mowrey, R. C.; Butler, J. E.; Russell, J. N., Jr., Photochemical attachment of fluorobutyl moieties on a diamond (110)-oriented surface: A multiple internal reflection

infrared spectroscopic (MIRIRS) investigation. *Journal of Physical Chemistry B* **1998**, 102, 9290.

(70) Samskog, P. O.; Kispert, L. D., An Electron-Paramagnetic-Resonance Study of a Radical-Anion in X-Ray-Irradiated Trifluoroacetamide Single-Crystals at 3K. *Journal of Chemical Physics* **1983**, 78, 2129.

(71) Rogers, M. T.; Kispert, L. D., Trifluoromethyl and Other Radicals in Irradiated Single Crystals of Trifluoroacetamide. *Journal of Chemical Physics* **1967**, 46, 3193.

(72) Helmy, R.; Fadeev, A. Y., Self-assembled monolayers supported on TiO_2: Comparison of $C_{18}H_{37}SiX_3$ (X = H, Cl, OCH_3), $C_{18}H_{37}Si(CH_3)_2C1$, and $C_{18}H_{37}PO(OH)_2$. *Langmuir* **2002**, 18, 8924.

(73) Allen, C. G.; Baker, D. J.; Albin, J. M.; Oertli, H. E.; Gillaspie, D. T.; Olson, D. C.; Furtak, T. E.; Collins, R. T., Surface Modification of ZnO Using Triethoxysilane-Based Molecules. *Langmuir* **2008**, 24, 13393.

(74) Butler, M. A.; Nasby, R. D.; Quinn, R. K., Tungsten Trioxide as an Electrode for Photoelectrolysis of Water. *Solid State Communications* **1976**, 19, 1011.

(75) Schoonman, J.; Vos, K.; Blasse, G., Donor Densities in TiO_2 Photoelectrodes. *Journal of the Electrochemical Society* **1981**, 128, 1154.

(76) Mora-Sero, I.; Fabregat-Santiago, F.; Denier, B.; Bisquert, J.; Tena-Zaera, R.; Elias, J.; Levy-Clement, C., Determination of carrier density of ZnO nanowires by electrochemical techniques. Applied Physics Letters **2006**, 89, 203117.

(77) Oskam, G.; Vanmaekelbergh, D.; Kelly, J. J., A Reappraisal of the Frequency-Dependence of the Impedance of Semiconductor Electrodes. *Journal of Electroanalytical Chemistry* **1991**, 315, 65.

(78) Degryse, R.; Gomes, W. P.; Cardon, F.; Vennik, J., Interpretation Of Mott-Schottky Plots Determined At Semiconductor-Electrolyte Systems. *Journal of Electrochemical Society* **1975**, 122, 711.

Chapter 3

Highly Stable Redox-Active Molecular Layers by Covalent Grafting to Conductive Diamond

The work in the following chapter was done in collaboration with the Stahl group and published in an article in the *Journal of the American Chemical Society*, volume 133, issue 15, pages 5692-5694.

3.1 Introduction

The integration of electrochemically active molecular complexes with electrodes has great potential for the development of electrocatalytic interfaces for applications such as water splitting,[1-3] organic synthesis,[4-6] and solar energy conversion.[7-9] Extensive efforts have focused on tethering electrocatalytically active molecules to carbon-based surfaces;[6, 10] however, sp^2-hybridized materials such as graphite, glassy carbon, and carbon nanotubes are oxidized at modest potentials (>0.6 V vs. NHE at pH=1)[11, 12] and rapidly corrode at potentials >1 V vs. NHE.[12, 13] In contrast, diamond surfaces are stable to 1.7 V vs. NHE,[11, 14] suggesting that diamond may be an ideal candidate for anchoring molecules with the higher redox potentials necessary for applications such as water oxidation (typically > 1 V). Inexpensive conductive diamond substrates are available commercially in bulk and thin-film form. Here, we demonstrate a modular "click"-based approach to covalently link a Ru coordination complex to conductive diamond surfaces and show that the surface-tethered complex exhibits extraordinarily stable and reversible redox chemistry, able to withstand more than one million cycles to strongly oxidizing

potentials (approximately 1.5 V vs. NHE) in nonaqueous electrolytes and only slightly reduced stability in aqueous electrolyte solutions.

3.2 Experimental

3.2.1 Diamond Samples

Two types of diamond samples were used. Electrochemical grade ("EC") boron-doped diamond samples were purchased from Element VI Corporation. These samples are free-standing diamond substrates grown by chemical vapor deposition and boron-doped during growth; under the conditions of growth some non-diamond carbon is formed in the bulk, leaving the samples dark in appearance. A limited number of experiments were also performed using boron-doped diamond thin films (BDDTF) (1.53 um thick) grown on highly doped p-type silicon substrates at the U.S. Naval Research Laboratory. Boron concentrations are estimated at ~ 10^{21} cm^{-3} based upon the growth conditions used. We refer to these types of samples as "EC" diamond and "BDDTF", respectively.

Figure 3.1 shows the scheme for anchoring a redox-active Ru complex to diamond via the Cu^{I}-catalyzed azide-alkyne cycloaddition (CuAAC or "click") reaction.[15] We prepared the $[Ru(tpy)_2]^{2+}$ (tpy = 2,2':6',2"-terpyridyl) derivative bearing a pendant alkyne group (1), reported previously by Ziessel.[16] The unsubstituted parent complex has a Ru^{II}/Ru^{III} couple at a potential of 1260 mV vs. NHE in acetonitrile (1250 mV in H_2O),[17] presenting a stringent test of the stability of the interface. Azide functionalization of sp^2-hybridized carbon surfaces with IN_3 has been reported,[10] but this approach was not effective with the sp^3-hybridized diamond surface. Instead, we adapted a photochemical surface-functionalization method developed previously in our lab.[18, 19]

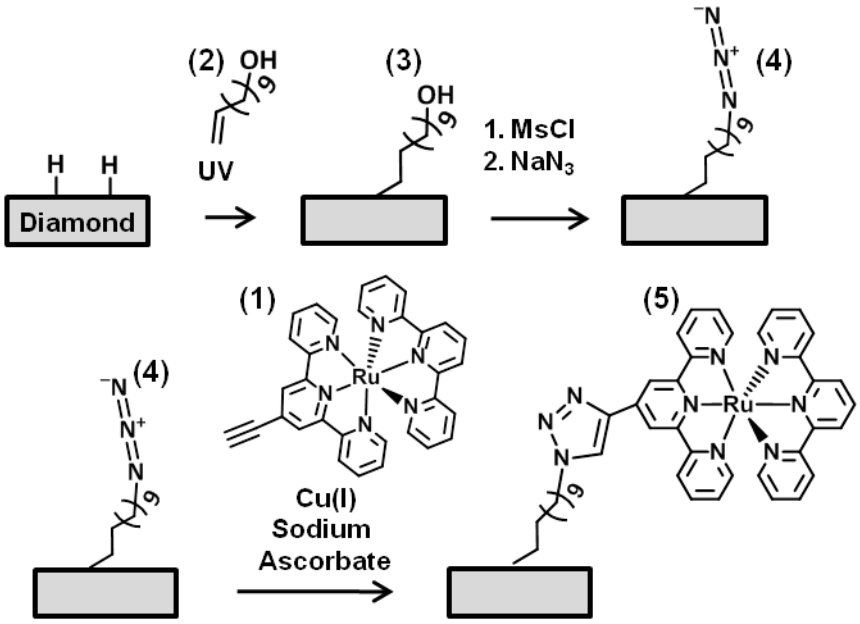

Figure 3.1: Reaction scheme for anchoring (1) to diamond

3.2.2 Azide Termination of Diamond

Diamond samples were hydrogen terminated prior to use by hydrogen plasma treatment in a manner similar to that developed by Thoms and co-workers.[20] The diamond samples were exposed to a radio-frequency hydrogen plasma (~20 Watts) of pure hydrogen (20 Torr), while heating to ~800^{o}C, for a period of approximately 30 minutes. XPS data (not shown) have established that this leaves the diamond samples terminated with C-H bonds. The resulting "hydrogen-terminated" diamond samples were removed from the vacuum system and covered with a layer of argon-purged 10-undecen-1-ol (Sigma Aldrich), covered with a fused silica window, and illuminated with UV light (254 nm, ~10 mW/cm^2) in a sealed cell under an argon atmosphere. The EC-grade bulk diamond and the BDDTF diamond graft at different rates; reaction times of 10-15 hours (EC grade) and ~ 4 hours (BDDTF) were used to achieve similar coverages of the 11-undecene-1-ol on the surfaces. After reaction the samples were sonicated in isopropanol and dried under N_2. To convert the alcohol-terminated surface into the mesylate, samples were placed in a solution containing 10 mL methylene chloride, 1 mL triethylamine, and 1 mL methane sulfonyl chloride. The samples were reacted for 1 h in an ice bath. After reaction, the samples were sonicated in methylene chloride and dried under N_2. Replacement of the mesylate intermediate with azide was accomplished by treating the samples overnight in a saturated solution of sodium azide in dry DMSO at 80^{o}C.

3.2.3 "Click" Functionalization of Azide-Terminated Diamond Surfaces

The azide-modified diamond samples were immersed in a solution of 100 μM alkyne-complex with 0.8 mM Cu(II)(tris-(benzyltriazolyl-methyl)amine)SO_4 (TBTA) and 15 mM sodium ascorbate in a 3:1 (v:v) DMSO:H_2O mixture for 5 hours. The samples were sonicated in

MeOH, $CHCl_3$, and isopropanol (IPA) for 30 seconds each and stored in isopropanol until further use

3.2.4 Electrochemical Characterization Methods:

Cyclic voltammetry measurements were performed using a three-electrode cell. The diamond samples were used as the working electrode with an exposed area of 0.275 cm^2 and a platinum wire was used as the counter-electrode. For measurements performed in aqueous electrolytes a Ag/AgCl reference electrode was used. For measurements performed in nonaqueous electrolytes a Ag/Ag^+ reference electrode (0.01 M $AgClO_4$ in supporting electrolyte) was used. The Ag/Ag^+ reference electrode was calibrated against a Ag/AgCl reference by direct potentiometric measurement; data reported in the main paper were corrected to compensate for this difference. The cell was capped to prevent evaporation over long periods of scanning. We also calibrated both reference electrodes again the ferrocene/ferrocinium couple by measuring E^0 of this redox couple in each solvent. The resulting values of E^0 were: 0.14 V vs. Ag/AgCl in 1M $LiClO_4$/ H_2O, 0.052 V vs. Ag/Ag^+ in 1M $LiClO_4$/Acetonitrile, and 0.035 V vs. Ag/Ag^+ in 1M $LiClO_4$ /propylene carbonate.

3.2.5 Spectroscopic Characterization Methods

3.2.5.1 X-ray Photoelectron Spectroscopy (XPS)

XPS data were obtained using a modified Physical Electronics system equipped with an aluminum K_α source, a quartz-crystal X-ray monochromator, and a 16-channel detector array. Surface coverage of ruthenium was determined using two methods, with equivalent results. In

the first method, the Ru and C signals from the same sample are used. The Ru covered can then be estimated from the ratio of the Ru($3d_{5/2}$) to C(1s) peaks according to:

$$Ru(atoms/cm^2) = \frac{A_{Ru(3d5/2)}}{A_{C(1s)}} \cdot \frac{S_{C(1s)}}{S_{Ru(3d5/2)}} \cdot \rho_{C,diamond} \cdot IMFP_{C,diamond} \cdot \cos(45°)$$

where *A* is the XPS peak area, *S* is the atomic sensitivity factor[21], ρ is the number density of carbon atoms in diamond, and *IMFP* is the inelastic mean free path of C(1s) photoelectrons in diamond (~2 nm).[22] Since the Ru($3d_{3/2}$) peak overlaps with the C(1s) peak, coverage was estimated using only the Ru($3d_{5/2}$) peak whose sensitivity factor was calculated to be 2.2 based on the 3:2 peak area ratio of the spin-orbit split pair.[21, 23] The cos(45^o) term compensates for the fact that electrons were collected at an angle of 45^o with respect to the surface normal. Since the Ru atoms are at the topmost surface, the Ru(3d) photoelectrons do not experience scattering; however, the underlying C(1s) photoelectrons do, and the factor of cos(45^o) is need to correctly calculate the effective number of C(1s) photoelectrons detected. Using a single sample minimizes errors arising from sample alignment, but makes the assumption that the C(1s) signals from the initial molecular layer and from the underlying diamond can be treated as being equivalent.

We also calculated the Ru coverage using a second approach using the Ru(3d) signal from a functionalized sample, but using the C(1s) signal from non-functionalized, H-terminated diamond. This approach requires careful placement of the samples to minimize any changes in C(1s) intensity due to changes in sample alignment with respect to the X-ray source and the input lens of the hemispherical analyzer. Both methods of calculation yielded the same coverage.

3.2.5.2 Fourier-transform Infrared (FTIR) Spectroscopy

FTIR spectra were collected using a Bruker Vertex 70 instrument in a single-bounce external-reflection geometry using p-polarized light at a 50° angle of incidence, with a liquid nitrogen-cooled HgCdTe detector. Clean, hydrogen-terminated samples were used for the background.

3.3 Results and Discussion

3.3.1 Cyclic Voltammetry

Cyclic voltammetry (CV) data in Fig. 3.2a and 3.2b demonstrate the remarkable electrochemical stability of the $Ru(tpy)_2$ complex covalently bound to diamond. Figure 2a shows overlaid cyclic voltammograms measured in 1 M $LiClO_4$ propylene carbonate (PC) out to one million cycles (scan rate 10 V/sec, 0.85 to 1.36 V vs. Ag/AgCl). The surface complex shows stable, well defined oxidation and reduction waves with $E_{1/2}$=1.18 V vs. Ag/AgCl (~1.36 V vs. NHE) at cycle 10^6, close to the 1.26 V of the unsubstituted parent compound in CH_3CN. The peak-to-peak splitting of only 45 mV after 10^6 cycles indicates highly reversible electron-transfer kinetics. The peak area of 2.5 μC with our 0.275 cm^2 sample area yields $6x10^{13}$ redox groups/cm^2, in excellent agreement with the XPS results. Similar voltammograms were obtained in $LiClO_4$/acetonitrile (AN) (Fig. 3.3), with slightly increasing peak-to-peak splitting. While the redox peak potential undergoes a larger shift during the experiment in acetonitrile compared to propylene carbonate, the total area under the redox peaks remains nearly unchanged over the 1 million cycles. It is not known whether the shift arises from a change in the redox-active layers or whether it arises from changes in the semiconductor band-bending. Changes in band-bending

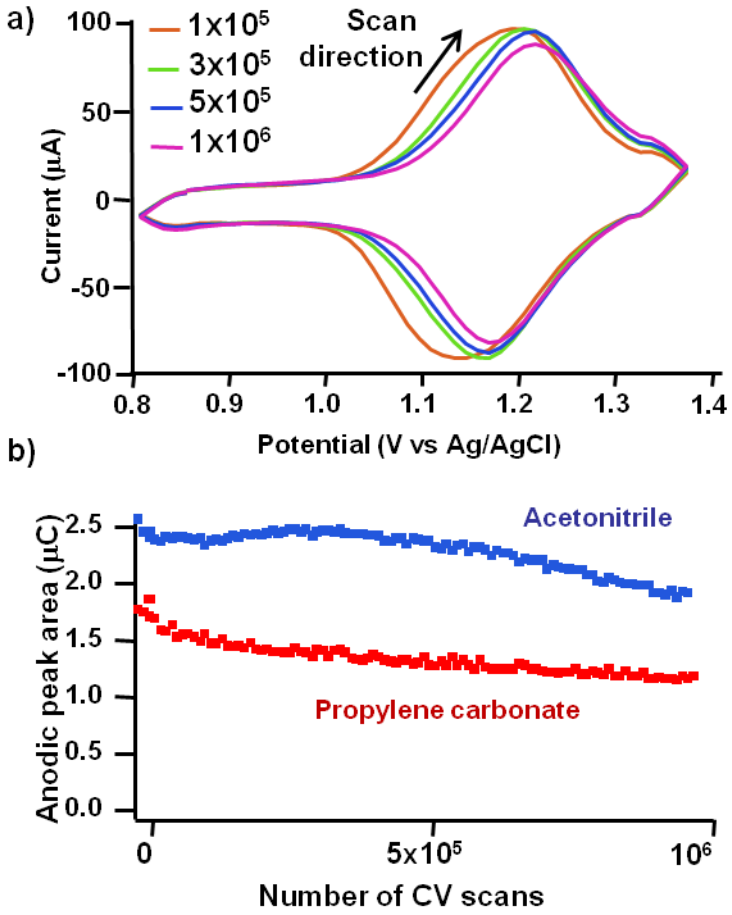

Figure 3.2: a) cyclic voltammograms of $Ru(tpy)_2$ tethered to EC diamond in propylene carbonate solution, b) anodic peak areas for 10^6 cyclic voltammetry scans in acetonitrile and propylene carbonate.

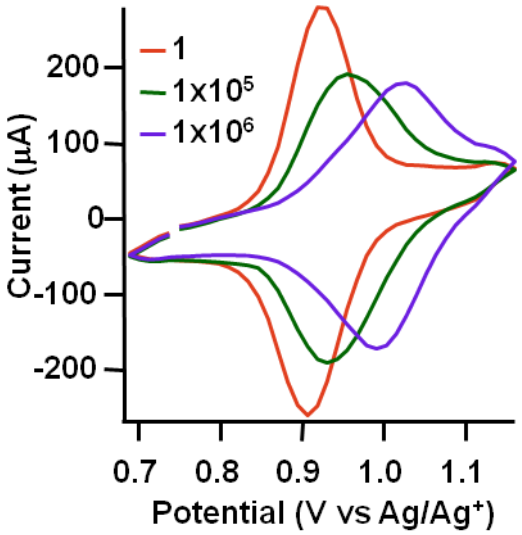

Figure 3.3: Cyclic voltammograms of $Ru(tpy)_2$ tethered to EC diamond in 1 M $LiClO_4$ in acetonitrile. CVs are shown after 1 cycle; 100,000 cycles; and 1,000,000 cycles. Analysis of the peak areas is shown in Figure 3.2b.

might arise from partial oxidation of the diamond surface or other changes in the surface electronic structure.

Figure 3.2b summarizes the anodic peak areas in PC and AN. In both cases, after an initial loss (presumably due to molecules bonded at less stable surface sites such as steps or defects), the CVs are remarkably stable for more than 1 million cycles.

Diamond's unusually large window of electrochemical stability suggests that surface-tethered complexes might also exhibit stable behavior in water. To test this hypothesis, CVs were obtained in aqueous solutions of 1 M $LiClO_4$. Figure 3.4a shows CVs out to 1.3 V vs. Ag/AgCl, while Fig. 3.4b shows the area under the oxidation wave vs. cycle number. The CVs show reversible behavior with $E_{1/2}$=1.08 V vs. Ag/AgCl or ~1.27 vs. NHE, close to the previously reported value of 1.250 V vs. NHE of the unsubstituted $Ru(tpy)_2$ compound.[17] There is a small initial loss of activity, but this is followed by extraordinarily high stability out to >500,000 cycles. Fig. 3.5a shows CVs measured at different scan rates, and Fig. 3.5b summarizes the peak-to-peak splitting (E_{pp}) and peak current (I_{peak}) vs. scan rate (R, in V/s). For a surface-tethered redox couple, the peak current should be linear in R and E_{pp} should go to zero at R = 0.[24] Fig. 5b shows I_{peak} is indeed linear in scan rate (R) with zero intercept, following I_{peak} = $(5.2\pm0.1)\text{x}10^{-5}R + (1.0\pm1.2)\text{x}10^{-5}$ with regression coefficient $r^2 = 0.99$. However, at zero scan rate E_{pp} is ~100 mV rather than zero. This difference could arise from space-charge effects in the (semiconducting) diamond or from imperfections in the molecular layer. The standard electrochemical charge-transfer rate k^0_{ct} can be estimated as $k^0_{ct} = \Delta E_{pp}/R$. Using the slope of E_{pp} vs. R from the 5 points at highest rate yields $k^0_{ct} = 620\pm30\ s^{-1}$.

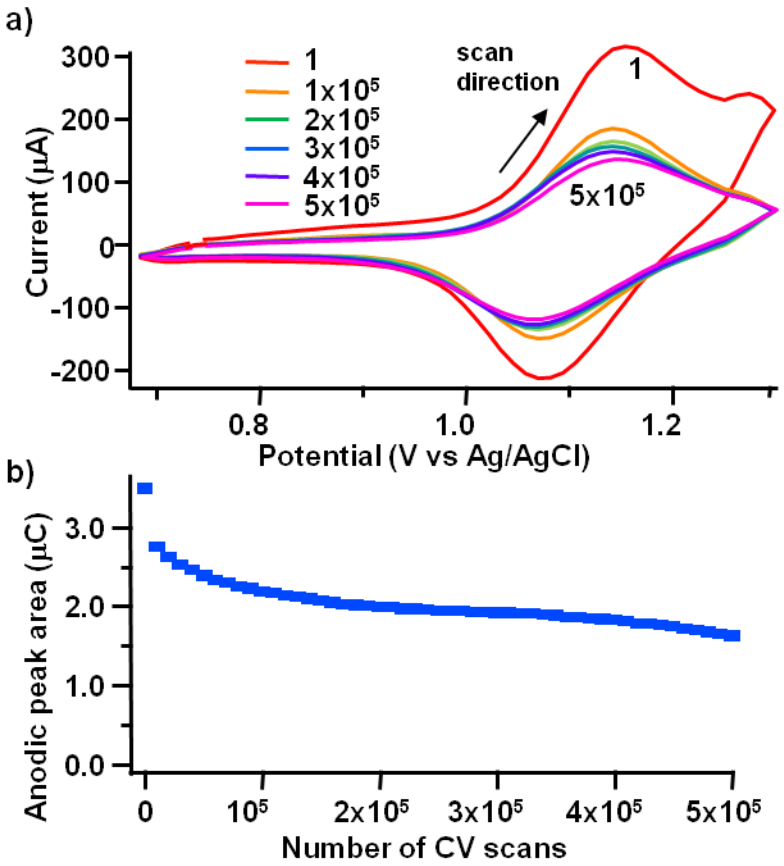

Figure 3.4: Electrochemical data for $Ru(tpy)_2$ tethered to EC diamond in 1 M $LiClO_4$. a) cyclic voltammograms; b) anodic peak area vs. time

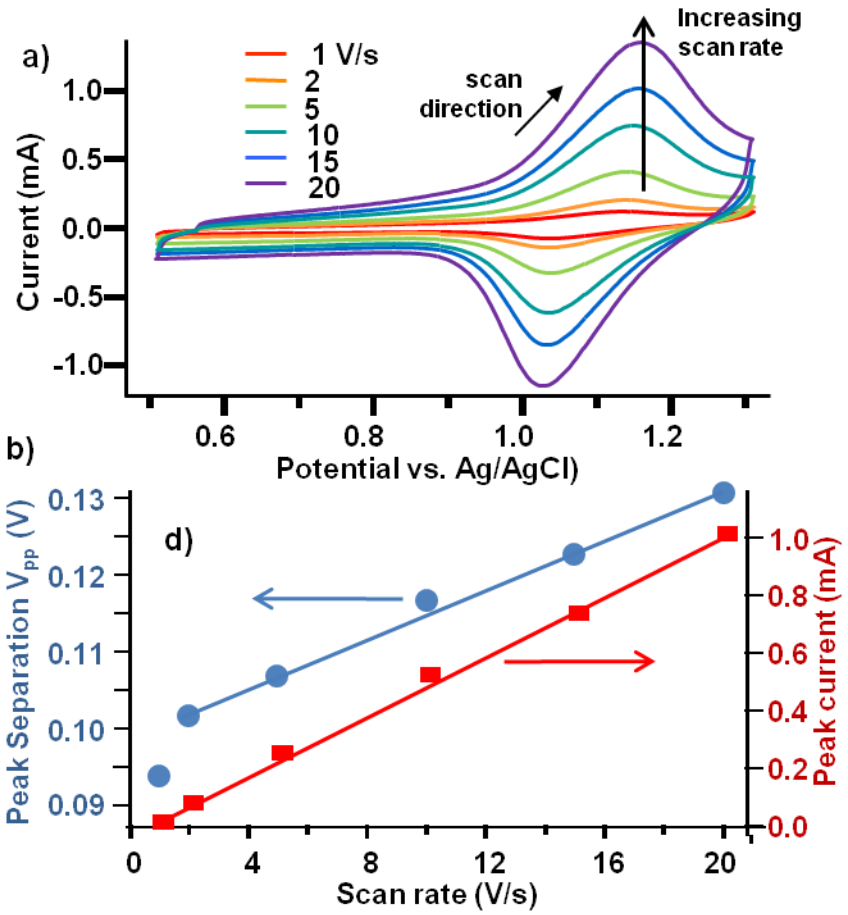

Figure 3.5: a) voltammograms at different scan rates in 1M $HClO_4$, b) peak-to-peak separation and peak current vs. scan rate.

To establish that the outstanding stability of the electrochemical grade diamond is not unique to this specific type of diamond, we also performed a more limited number of experiments using boron-doped diamond thin films grown by chemical vapor deposition at the U.S. Naval Research Laboratory. These samples were functionalized as described above. Fig. 3.6 shows cyclic voltammograms of the tethered $Ru(tpy)_2$ complex on boron-doped diamond thin films, measured in 1 M $LiClO_4$ in acetonitrile. The samples once again show excellent stability.

3.3.2 Raman Characterization of Black Diamond Substrates

Fig. 3.7 shows a Raman spectrum of the EC grade diamond sample using 532 nm incident light. The sharp 1332 cm^{-1} peak of diamond can be observed, along with additional broad peaks due to non-diamond (graphitic or amorphous) phases. Raman spectroscopy is highly sensitive to trace amounts of non-diamond carbon impurities, which gives rise to intense features at 1000-1600 cm^{-1}. The Raman cross-sections for graphitic and amorphous carbons are much stronger than those of diamond because they are resonantly enhanced by the π-π^* electronic transitions of sp^2-hybridized carbon.[25] The spectrum shown in Fig. 3.7 is similar to spectra reported previously from synthetic diamond produced by chemical vapor deposition methods.[26] The hydrogen-termination process used in our studies (below) is also known to selectively remove graphite contamination,[20] so that the amount of graphite at the surface of the diamond is expected to be significantly smaller than that in the bulk.

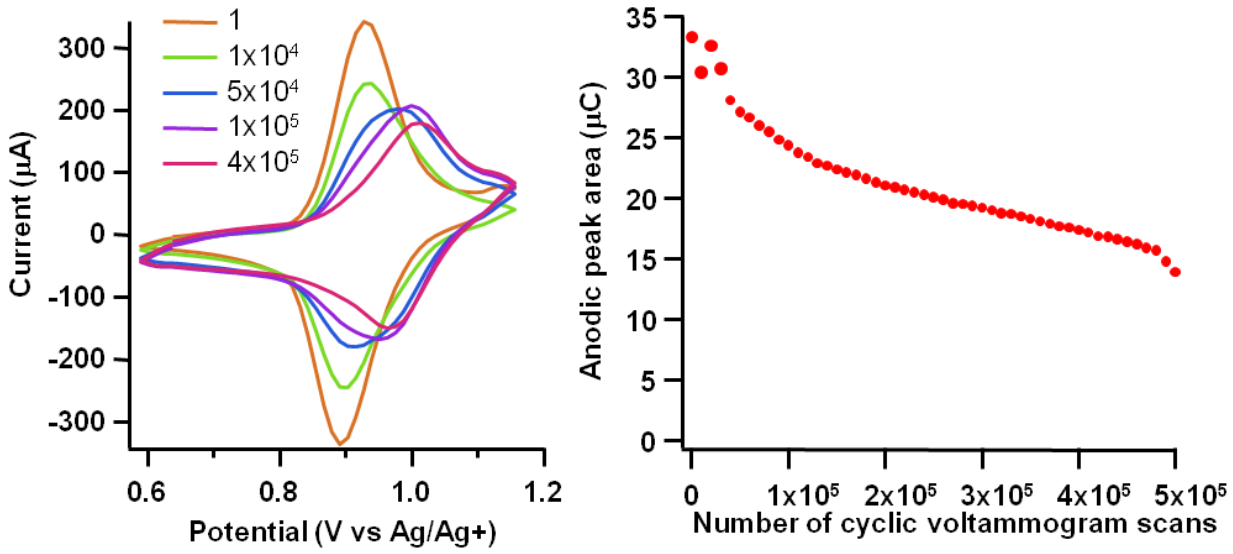

Figure 3.6: Left: Cyclic voltammograms of Ru(tpy)2 tethered to boron doped diamond electrodes obtained in 1 M LiClO4 in acetonitrile. Right: The anodic peak area as a function of the number of CV cycles for the same sample.

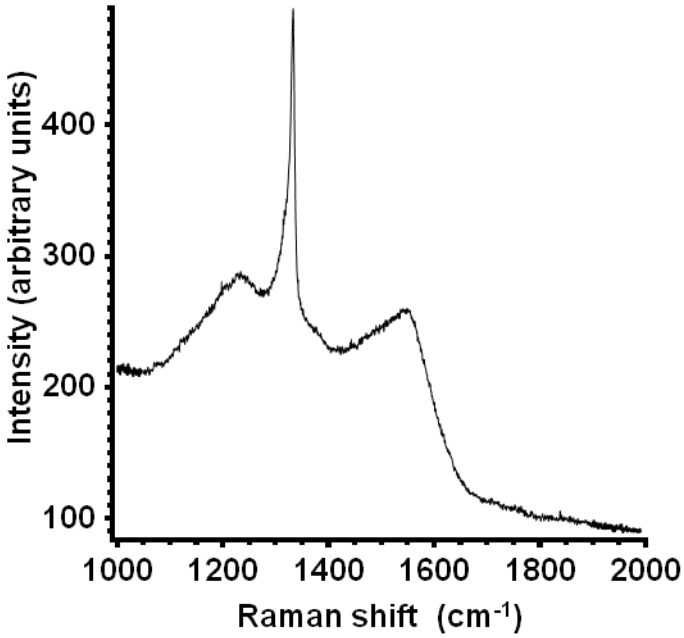

Figure 3.7: Raman spectrum of electrochemical grade ("EC") diamond using excitation at 532 nm.

3.3.3 XPS and FTIR Characterization of Surface Functionalization

3.3.3.1 FTIR Characterization of Azide Formation on Diamond

One challenge in functionalization of the surfaces is making the azide-terminated surface. To demonstrate that the initial photochemical grafting to produce a hydroxyl-terminated surface is important to the overall functionalization scheme, we collected infrared spectra of samples after that azidization step, and a comparable sample that was treated in the same manner except that the initial photochemical grafting step was eliminated.

Figure 3.8 shows infrared spectra of two samples at intermediate stages of functionalization. One sample was functionalized with 10-undecen-1-ol as the first step, then mesylated and finally converted to the azide. The second sample was not functionalized by 10-undecene-1-ol but was otherwise treated in the same manner as the first. Only the first sample shows the 2090 cm^{-1} vibrational mode that is characteristic of the azide group. The results demonstrate that formation of surface –OH groups is important to achieving azide functionalization of the diamond surface and that azide groups do not otherwise bind to the diamond surfaces.

3.3.3.2 XPS Characterization of "Click" Reaction

XPS spectra were obtained of the azide-modified diamond before and after the Cu^{I}-catalyzed azide-alkyne cycloaddition (CuAAC) ("click") reaction. Fig. 3.9 shows spectra of the C(1s) and Ru($3d_{5/2}$) region (Fig. 3.9a), an enlarged view of the Ru($3d_{5/2}$) region (Fig. 3.9b), and the N(1s) region (Fig. 3.9c).

After the click reaction with the $Ru(tpy)_2$ complex, the C(1s) spectrum shows one main peak from the bulk diamond with a smaller shoulder at higher binding energy that arises from the

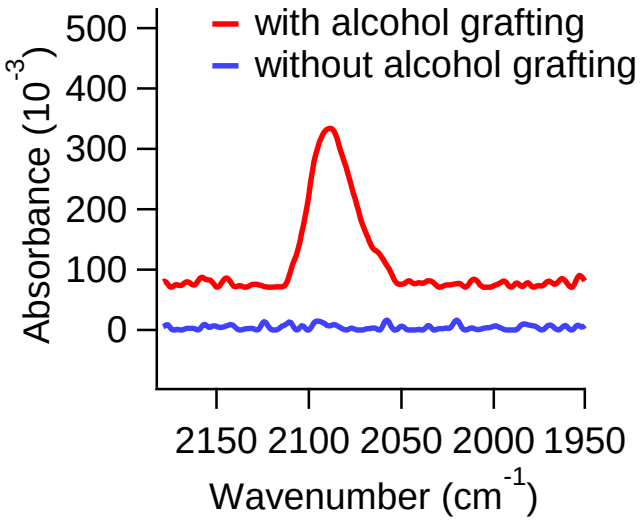

Figure 3.8: FTIR spectrum of EC diamond sample after azide treatment (top trace, in red). The lower (blue) trace shows a control sample prepared in an identical fashion but omitting the initial photochemical grafting of the alcohol group.

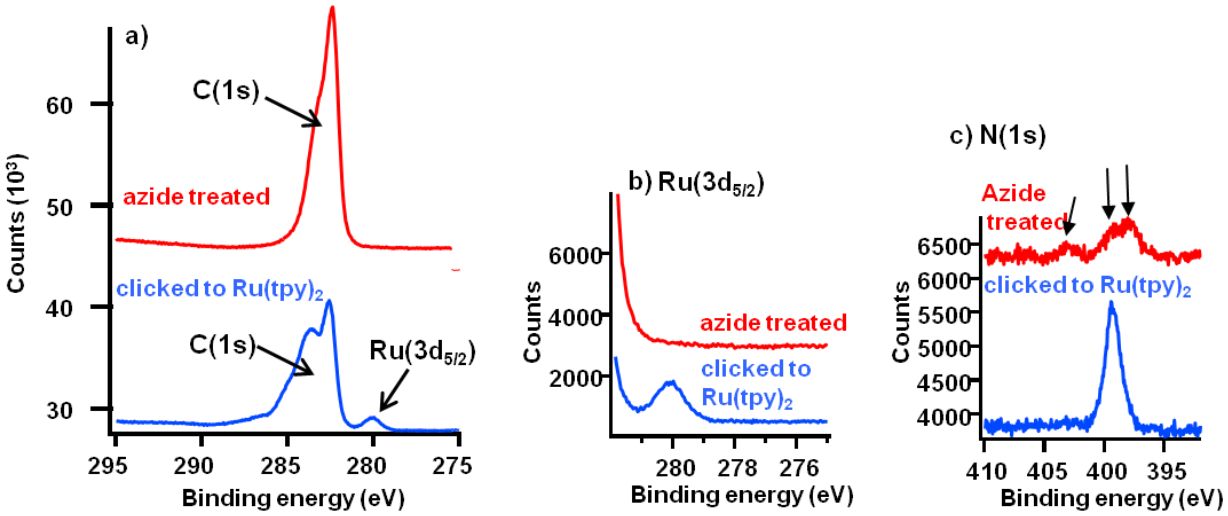

Figure 3.9: XPS spectra of azide-modified EC-grade diamond before and after "click" reaction with Ru(tpy)2 complex. a) C(1s) and Ru(3d5/2) region; b) enlarged view of Ru(3d5/2) region; c) N(1s) region.

molecular layer grafted to the surface. After exposure to the Ru(tpy)2 complex under conditions optimized for the click reaction, a new peak is observed at lower binding energy, near 279-280 eV that arises from the photoemission from the 3d5/2 level of the Ru atoms in the Ru(typ)2 complex. The corresponding Ru(3d3/2) spin-orbit component should occur ~ 4 eV higher in binding energy than the 3d5/2 component, placing the 3d3/2 component directly under the main C(1s) peak. Further confirmation that the CuAAC reaction was successful comes from the N(1s) spectra. Fig. 3.9c shows that the azide-modified diamond has three broad N(1s) features that correspond to the three N(1s) nitrogen atoms within the azide group, in agreement with the FTIR data presented above; the azide group is sensitive to electron damage and difficult to detect reliably by XPS. However, after the CuAAC reaction the N(1s) signal increases substantially in intensity, as expected from the N atoms within the terpyridine ligands.

Quantitative measurements of the Ru($3d_{3/2}$) and C(1s) peaks were made on several different samples to establish an average number density of grafted $Ru(tpy)_2$ molecules. Analysis of the Ru($3d_{5/2}$) peaks yields a typical surface coverage of $(6 \pm 1)x10^{13}$ molecules/cm^2. This value is in agreement with the electrochemical current measurements.

3.3.3.3 Infrared Characterization of CuAAC ("Click") Reaction

FTIR spectra were obtained of the diamond sample before and after the cycloaddition reaction (Fig. 3.10). The azide group gives rise to a reasonably sharp feature near 2090 cm^{-1}. Although the signal is weak (only ~10^{-4} absorbance units), it can be detected. After reaction, this peak is reduced in intensity by 70%, suggesting that ~70% of the surface azide groups react during the cycloaddition step.

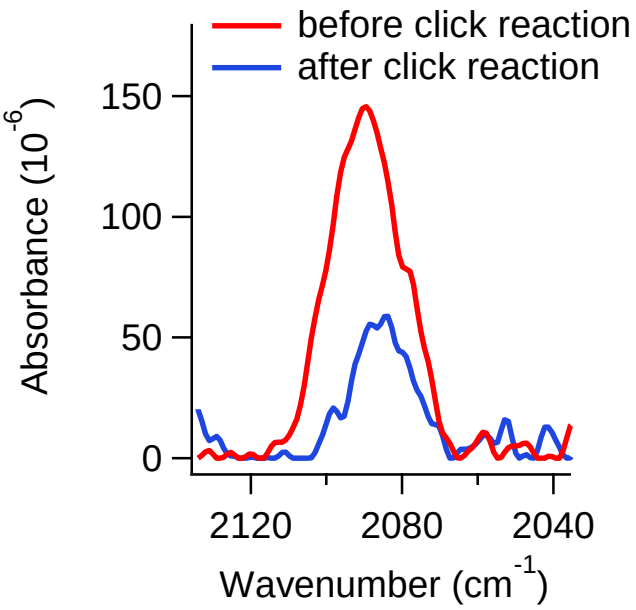

Figure 3.10: FTIR of the azide asymmetric stretching region before and after the CuAAC reaction

3.3.3.4 Control Samples for CuAAC Reaction

Two control experiments were run in which the exposure to sodium azide was eliminated, with all other steps carried out normally. This study effectively compares the reactivity of the azide-terminated diamond compared to that of the alcohol-terminated diamond when both are subjected to the CuAAC reaction conditions.

The XPS data (Fig. 3.11) show that without the azide step, there is no evidence for Ru on the surface (left) and also no evidence for nitrogen. Since the $Ru(tpy)_2$ complex has 6 nitrogen atoms per molecule, the absence of any detectable nitrogen shows that the $Ru(tpy)_2$ complex does not have any detectable physisorption or other non-covalent bonding to the surface.

This result is further corroborated by electrochemical measurements examining the cyclic voltammograms of a sample in which the azide step was eliminated but all other steps carried out as normal. The resulting CV (Fig. 3.12) shows no evidence for a redox peak; the small separation between forward and reverse sweeps is due to the interfacial capacitance.

3.3.4 Effect of Cycling One Million Times on Chemical Composition

3.3.4.1 Cycling in Non-aqueous Electrolytes

We obtained XPS spectra of an electrochemical-grade diamond functionalized with the $Ru(tpy)_2$ complex before and after cycling for 10^6 times in 1 M $LiClO_4$/acetonitrile, yielding the result shown in Fig. 3.13. Analysis of the Ru $3d_{5/2}$ peaks yields a surface coverage of $(6 \pm 1)\times10^{13}$ molecules/cm^2 before cycling and $(6.5\pm1)\times10^{13}$ molecules/cm^2 after cycling. Thus, within the experimental error no significant changes are observed in the total N(1s) or O(1s) signals. Similar experiments were performed in 1M $LiClO_4$/propylene carbonate, yielding the results shown in Fig. 3.14.

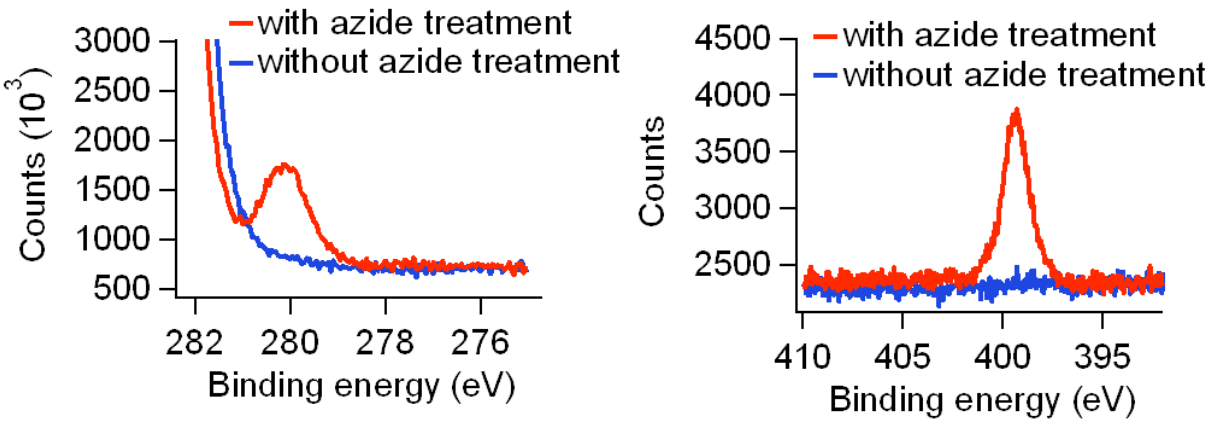

Figure 3.11: XPS data showing the Ru(3d5/2) region (left) and the N(1s) region (right) after cycloaddition reaction on EC grade diamond samples. The red trace is the result of the cycloaddition reaction with an azide terminated sample prepared as described above. The blue trace is the result of a control experiment where the azide treatment was omitted and the click reaction was performed on the alcohol terminated surface.

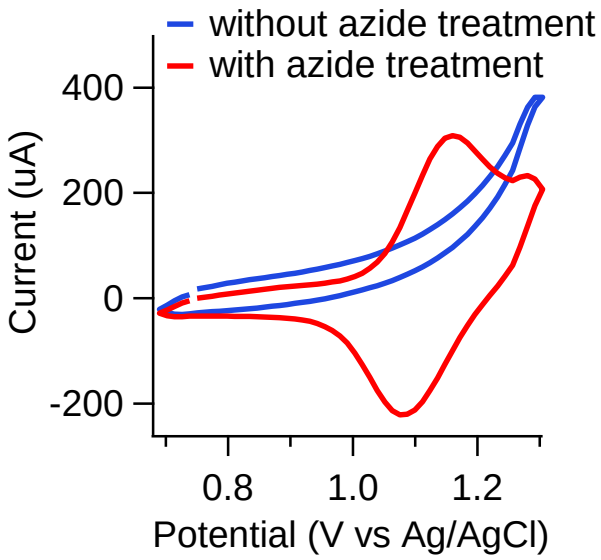

Figure 3.12: Cyclic voltammograms of sample with complete cycloaddition reaction including azide step (blue) and a control eliminating the azide step (blue)

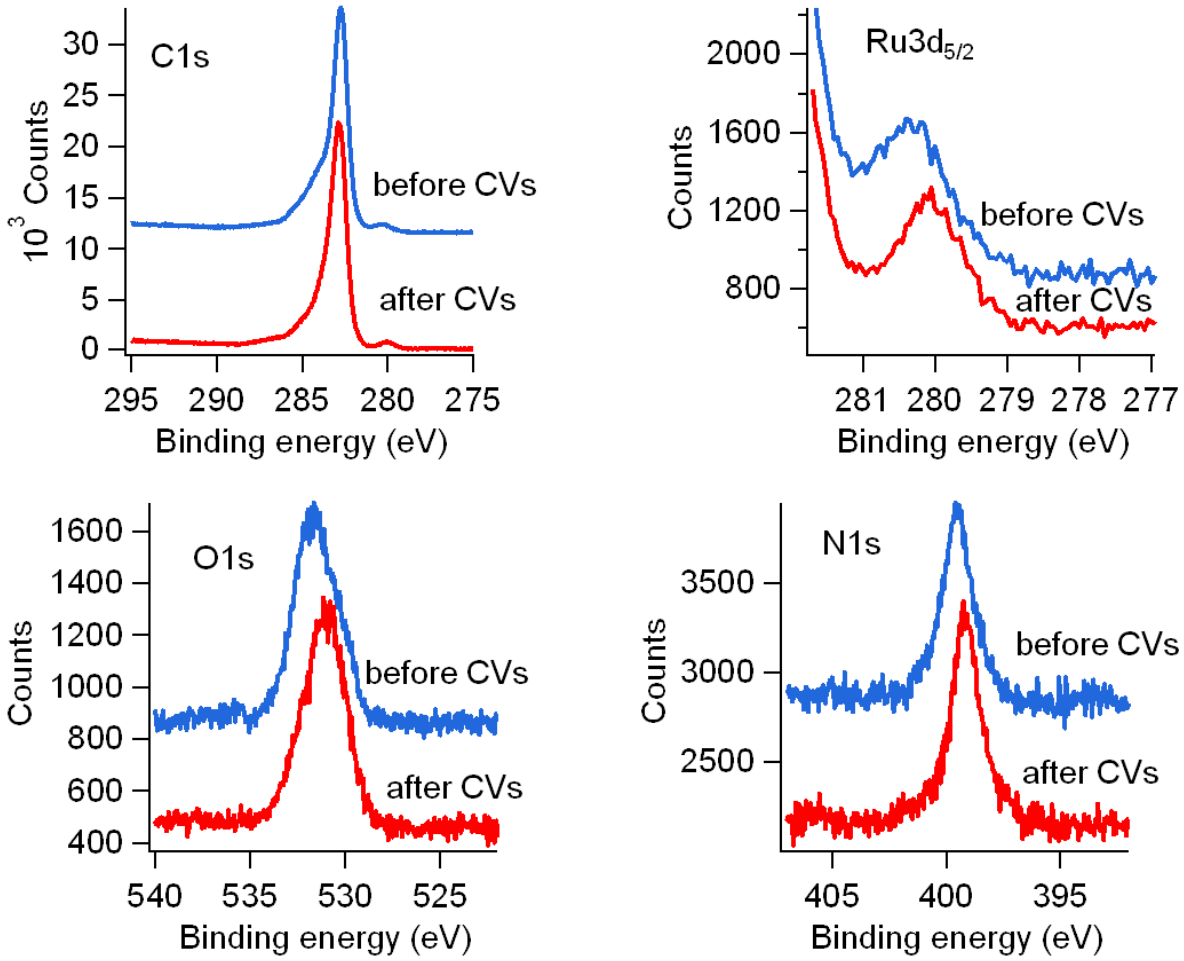

Figure 3.13: XPS spectra of EC diamond sample before and after 1 million cyclic voltammograms in 1 M $LiClO_4$ in propylene carbonate.

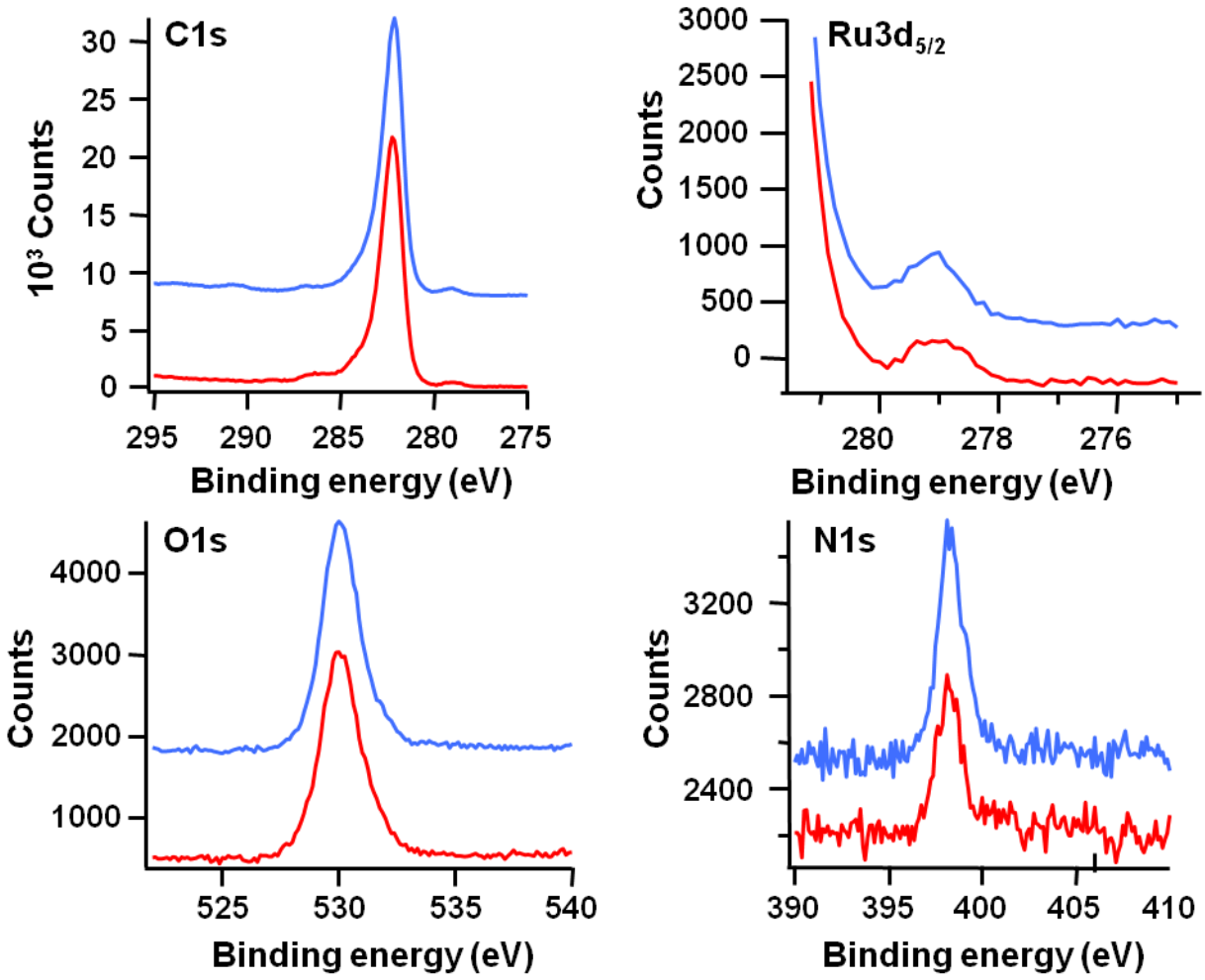

Figure 3.14: XPS spectra of EC diamond sample before and after 1 million cyclic voltammograms in 1 M $LiClO_4$ in propylene carbonate.

3.3.4.2 Cycling in Aqueous Electrolyte

The electrochemical response of a $Ru(tpy)_2$-modified electrochemical grade diamond was measured for 10^6 cycles in 1 M $LiClO_4$ in water. Fig. 3.15 shows the electrochemical response. The sample exhibits excellent stability for at least $5x10^5$ cycles, but undergoes some slow degradation at more extended times.

XPS data were obtained before and after cycling to identify any chemical changes that occurred in the sample. XPS spectra before and after (Fig. 3.16) show that the loss in electrochemical activity is accompanied by reduction in the amount of Ru on the surface. There is also a small shift toward lower binding energy for both the Ru($3d_{5/2}$) and N(1s) features after cycling. These observations demonstrate that there is partial loss of the ligands after extended cycling in water. Because the N(1s) peak arises from unreacted azide groups, the triazole linkage, and the (tpy) groups of the ligand, the signal-to-noise ratio of the experiment is not sufficient to determine whether there is loss of the initial functionalization layer or loss of only the Ru(tpy) moieties.

3.4 Conclusions

Our results demonstrate that molecular complexes can be robustly linked to inexpensive diamond substrates to yield redox-active surfaces with unprecedented electrochemical stability and only minimal perturbation of the complex's redox properties compared to the parent complex in solution. We anticipate that general routes to highly stable, electrochemically active electrodes, such as the one described here, will provide a convenient way to combine the high selectivity and activity of molecular catalysts with the stability and convenience of inorganic electrodes.

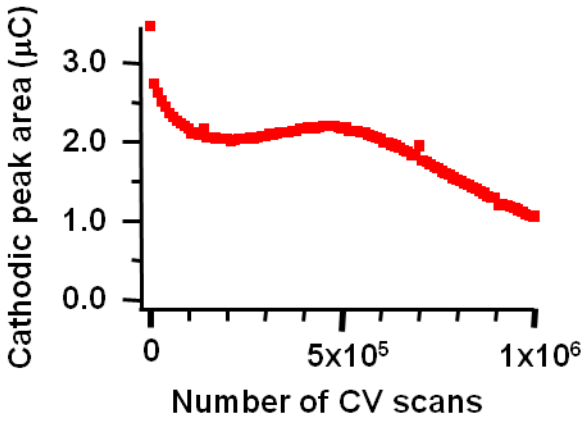

Figure 3.15: Cathodic peak area during 10^6 cyclic voltammograms of $Ru(tpy)_2$-modified EC diamond in aqueous 1 M $LiClO_4$.

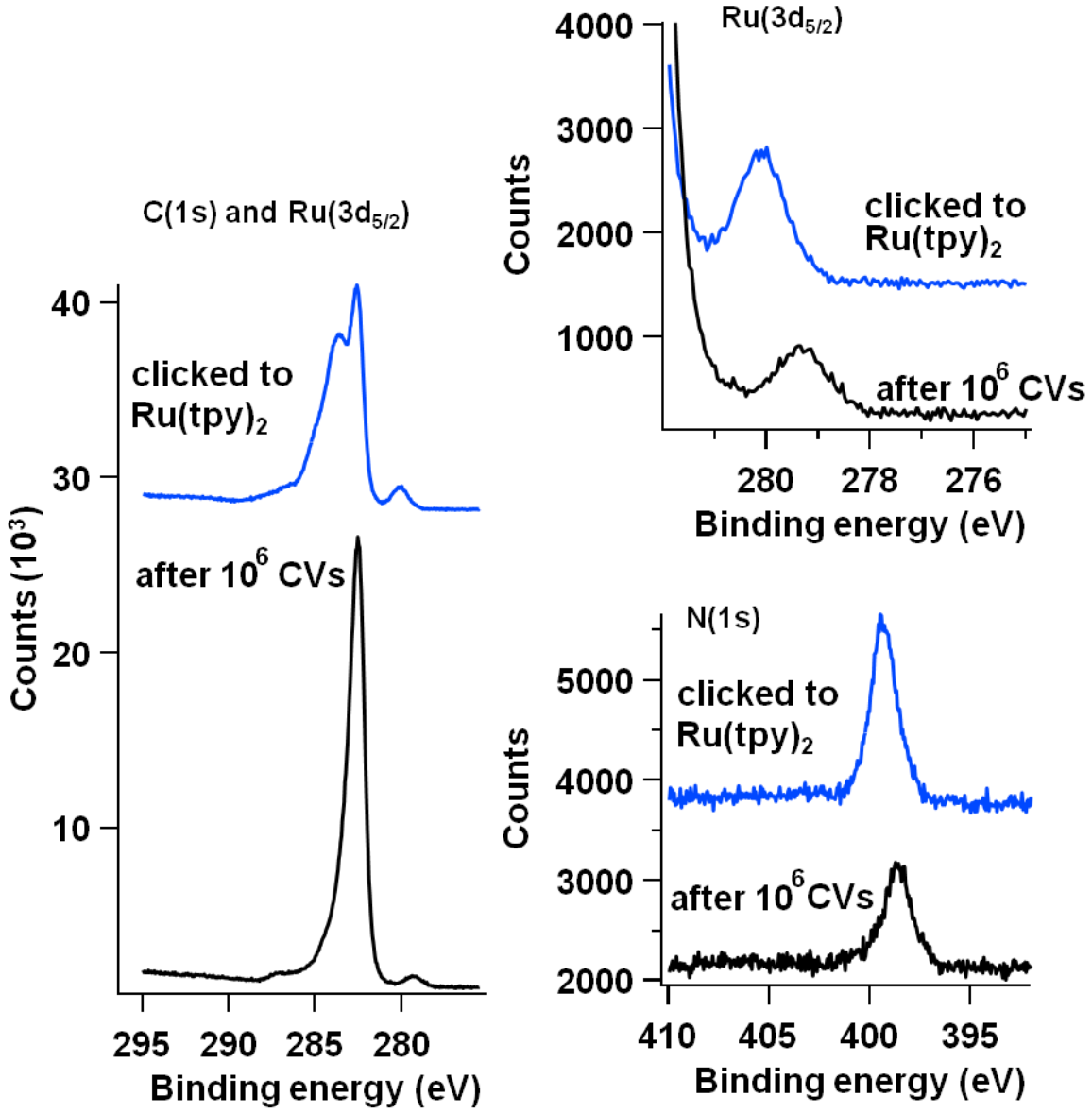

Figure 3.16: XPS data for $Ru(tpy)_2$-modified EC diamond before and after million cyclic voltammograms in 1M $LiClO_4$ in water.

3.5 References

1. Concepcion, J. J.; Jurss, J. W.; Brennaman, M. K.; Hoertz, P. G.; Patrocinio, A. O. T.; Murakami Iha, N. Y.; Templeton, J. L.; Meyer, T. J., Making Oxygen with Ruthenium Complexes. *Accounts Of Chemical Research* **2009**, 42, 1954.

2. Wasylenko, D. J.; Ganesamoorthy, C.; Henderson, M. A.; Koivisto, B. D.; Osthoff, H. D.; Berlinguette, C. P., Electronic Modification of the [Ru(II)(tpy)(bpy)(OH(2))](2+) Scaffold: Effects on Catalytic Water Oxidation. *Journal Of The American Chemical Society* **2010,** 132, 16094.

3. Liu, F.; Concepcion, J. J.; Jurss, J. W.; Cardolaccia, T.; Templeton, J. L.; Meyer, T. J., Mechanisms of water oxidation from the blue dimer to photosystem II. *Inorganic Chemistry* **2008**, 47, 1727.

4. Tucker, J. W.; Narayanam, J. M. R.; Krabbe, S. W.; Stephenson, C. R. J., Electron Transfer Photoredox Catalysis: Intramolecular Radical Addition to Indoles and Pyrroles. *Organic Letters* **2010,** 12, 368.

5. Ischay, M. A.; Anzovino, M. E.; Du, J.; Yoon, T. P., Efficient visible light photocatalysis of [2+2] enone cycloadditions. *Journal Of The American Chemical Society* **2008**, 130, 12886.

6. Murray, R. W., Chemically Modified Electrodes. Electroanalytical Chemistry: A Series of Advances. Vol. 13, p 191-368.

7. Grätzel, M., Dye-sensitized solar cells. *Journal of Photochemistry and Photobiology C-Photochemistry Reviews* **2003**, 4, 145.

8. Kalyanasundaram, K., Photophysics, Photochemistry and Solar-Energy Conversion with Tris(Bipyridyl)Ruthenium(II) and Its Analogs. *Coordination Chemistry Reviews* **1982**, 46, 159.

9. Campagna, S.; Puntoriero, F.; Nastasi, F.; Bergamini, G.; Balzani, V., Photochemistry and Photophysics of Coordination Compounds I. Vol. 280. Springer-Verlag Berlin: 2007.

10. Devadoss, A.; Chidsey, C. E. D., Azide-modified graphitic surfaces for covalent attachment of alkyne-terminated molecules by "click" chemistry. *Journal of the American Chemical Society* **2007**, 129, 5370.

11. Swain, G. M.; Ramesham, R., The Electrochemical Activity of Boron-Doped Polycrystalline Diamond Thin-Film Electrodes. *Analytical Chemistry* **1993**, 65, 345.

12. Choo, H.-S.; Kinumoto, T.; Jeong, S.-K.; Iriyama, Y.; Abe, T.; Ogumi, Z., Mechanism for electrochemical oxidation of highly oriented pyrolytic graphite in sulfuric acid solution. *Journal of the Electrochemical Society* **2007**, 154, B1017.

13. Besenhard, J. O.; Fritz, H. P., The Electrochemistry of Black Carbons. *Angewandte Chemie-International Edition In English* **1983**, 22, 950.

14. Martin, H. B.; Argoitia, A.; Landau, U.; Anderson, A. B.; Angus, J. C., Hydrogen and oxygen evolution on boron-doped diamond electrodes. *Journal of the Electrochemical Society* **1996**, 143, L133.

15. Collman, J. P.; Devaraj, N. K.; Chidsey, C. E. D., "Clicking" functionality onto electrode surfaces. *Langmuir* **2004**, 20, 1051.

16. Ziessel, R.; Grosshenny, V.; Hissler, M.; Stroh, C., cis-[Ru(2,2':6',2"-terpyridine)(DMSO)Cl_2]: Useful precursor for the synthesis of heteroleptic terpyridine complexes under mild conditions. *Inorganic Chemistry* **2004**, 43, 4262.

17. Juris, A.; Balzani, V.; Barigelletti, F.; Campagna, S.; Belser, P.; Vonzelewsky, A., Ru(Ii) Polypyridine Complexes - Photophysics, Photochemistry, Electrochemistry, and Chemi-Luminescence. *Coordination Chemistry Reviews* **1988**, 84, 85.

18. Strother, T.; Knickerbocker, T.; Russell, J. N.; Butler, J. E.; Smith, L. M.; Hamers, R. J., Photochemical functionalization of diamond films. *Langmuir* **2002**, 18, 968.

19. Wang, X.; Landis, E. C.; Franking, R.; Hamers, R. J., Surface Chemistry for Stable and Smart Molecular and Biomolecular Interfaces via Photochemical Grafting of Alkenes. *Accounts of Chemical Research* **2010,** 43, 1205.

20. Thoms, B. D.; Owens, M. S.; Butler, J. E.; Spiro, C., Production and Characterization of Smooth, Hydrogen-Terminated Diamond C(100). *Applied Physics Letters* **1994**, 65, 2957.

21. Wagner, C. D.; Davis, L. E.; Zeller, M. V.; Taylor, J. A.; Raymond, R. H.; Gale, L. H., Empirical Atomic Sensitivity Factors for Quantitative Analysis by Electron Spectroscopy for Chemical Analysis. *Surface and Interface Analysis* **1981**, 3, 211.

22. Zemek, J.; Potmesil, J.; Vanecek, M.; Lesiak, B.; Jablonski, A., Inelastic mean-free path of electrons at nanocrystalline diamond surfaces. *Applied Physics Letters.* **2005**, 87, 262114.

23. Moulder, J. F.; Stickle, W. F.; Sobol, P. E.; Bomben, K. D., *Handbook of X-ray Photoelectron Spectroscopy*. Perkin-Elmer Corporation: Eden Prairie, MN, 1992.

24. Laviron, E., General Expression of the Linear Potential Sweep Voltammogram in the Case of Diffusionless Electrochemical Systems. *Journal of Electroanalytical Chemistry* **1979**, 101, 19.

25. Wada, N.; Solin, S. A., Raman Efficiency Measurements of Graphite. *Physica B & C* **1981**, 105, 353.

26. Yoshikawa, M.; Katagiri, G.; Ishida, H.; Ishitani, A.; Ono, M.; Matsumura, K., Characterization of Crystalline Quality of Diamond Films by Raman-Spectroscopy. *Applied Physics Letters* **1989**, 55, 2608.

Chapter 4

Electron Transfer Properties of Ferrocene Covalently Attached to Diamond Electrodes

4.1 Introduction

Diamond electrodes are very promising materials for electrochemistry and electrocatalysis due to their high conductivity, wide potential window, high stability, and low and stable background currents.[1-7] While sp^2 bonded carbon (activated carbon, carbon black, and graphitic carbon) are the most commonly used catalyst support materials, they corrode at elevated temperatures, in harsh chemical environments, and under high operating potentials. Boron-doped diamond electrodes, in contrast, offer extreme corrosion resistance.[3-5] Recently we showed that redox-active molecular complexes could be covalently attached to the surface of conductive diamond electrodes to yield very stable, electroactive surfaces at strongly oxidizing potentials (1.5 V vs. NHE).[8]

In addition to stability, the electronic properties of the interface are important in designing electroactive and catalytic surfaces. In this paper, we report the electron transfer rate of ferrocene covalently linked to the surface of diamond electrodes. Ferrocene has been widely used as a model system for understanding charge transfer across molecular interfaces to electrodes.[9-34] Most measurements of electron transfer rates across molecular layers have used self-assembled monolayers on metal surfaces, especially gold[9-19, 22, 33-49] while fewer studies have investigated electron transfer rates on other substrates such as silicon[23, 26, 27, 29, 30, 49], ITO[28], or carbon-based electrodes.[20, 25]

The structure of the monolayer can dramatically change electron transfer kinetics. While effects such as chain length, packing density, and defect density have been studied extensively for self-assembled monolayers on gold[10, 12, 14, 15, 17-19, 22, 32, 37, 38, 43, 47-49], fewer systematic studies have been carried out for other types of electrodes.[25, 26, 29, 30] Our method for anchoring molecular complexes to the diamond surface uses saturated alkyl chains, and electron transfer rates are studied as a function of both the density and length of the alkyl groups. The results provide insight into the structure of the molecular layers on diamond and to their suitability as platforms for electron transfer and electrocatalysis.

4.2 Experimental Methods

4.2.1 Covalent Attachment of Ferrocene to Boron-doped Diamond Electrodes

Free-standing electrochemical grade ("EC") boron-doped diamond electrodes (Element VI Corporation) were used for all measurements except AFM characterization. AFM characterization was carried out using a cleaved natural single crystal of boron-doped diamond. Ferrocene groups were tethered to the diamond surfaces using previously published procedures (Scheme 1).[8, 50] The following alkenes were used for surface functionalization: 3-buten-1-ol (Sigma Aldrich), 5-hexen-1-ol (Sigma Aldrich), 7-octen-1-ol (TCI), and 11-undecen-1-ol (Sigma Aldrich). Diamond samples were hydrogen terminated prior to use by hydrogen plasma treatment.[51] Hydrogen-terminated diamond samples were covered with a thin layer of the argon-purged alkene, covered with a fused silica window, and illuminated with UV light (254 nm, ~10 mW/cm^2) in a sealed cell under an argon atmosphere. Typical illumination times were between 4 and 16 hours. After reaction the samples were sonicated in isopropanol and dried under N_2. To convert the surface alcohol groups into the mesylate, samples were placed in a solution

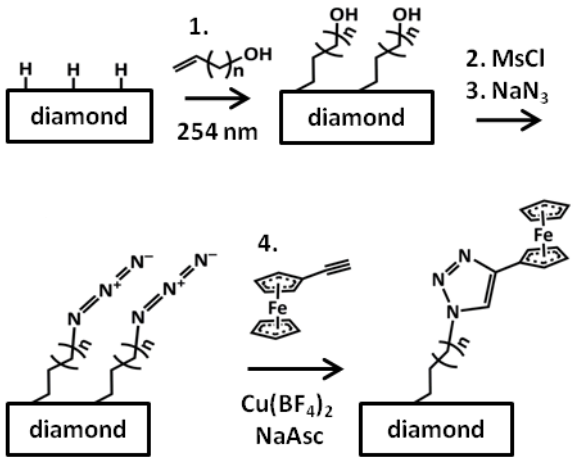

Scheme 4.1: Covalent attachment of ferrocene groups to diamond surface through click chemistry.

containing 10 mL methylene chloride, 1 mL triethylamine, and 1 mL methane sulfonyl chloride. The samples were reacted for 1 h in an ice bath. After reaction, the samples were sonicated in methylene chloride and dried under N_2. Replacement of the mesylate intermediate with azide was accomplished by treating the samples overnight in a saturated solution of sodium azide in dry DMSO at 80^{o}C. After reaction with sodium azide the samples were sonicated in water, acetone, and again in water and dried under N_2. The click reaction with ethynyl ferrocene was carried out in a solution of 4 mM ethynyl ferrocene, 2 mM Cu(BF_4), and 8 mM sodium ascorbate in a 3:1 (v:v) DMSO:H_2O mixture for 3 hours. The samples were sonicated in water, acetone, and methylene chloride for 5 minutes each and stored in isopropanol until further use.

4.2.2 X-ray Photoelectron Spectroscopy (XPS) Measurements

XPS data were obtained using a modified Physical Electronics system equipped with a monochromatized aluminum K_α source (1486.6 eV), a quartz-crystal X-ray monochromator, and a 16-channel detector array. Spectra were obtained using a takeoff angle of 45°. For quantitative analysis the peaks were fit with Voigt functions after subtracting a Shirley background to compensate for inelastic scattering. All fit parameters were adjustable.

4.2.3 Fourier Transform Infrared Spectroscopy (FTIR) Measurements

Infrared spectra were collected using an FTIR spectrometer (Vertex 70, Bruker Optics) with a liquid nitrogen-cooled HgCdTe detector. FTIR spectra were collected at a resolution of 4 cm^{-1} in single-bounce external reflection mode using a variable angle specular reflectance accessory with a wire grid polarizer (VeeMAX II, Pike Technologies). All reflection spectra were collected with p-polarized light at an incident angle of 50° from the surface normal. FTIR

spectra of functionalized surfaces were measured using a clean hydrogen-terminated sample as the background. Residual sloping baselines were removed to improve the clarity of the spectra.

4.2.4 Atomic Force Microscopy (AFM) Measurements

AFM measurements were taken with a Veeco Nanoscope IVa instrument. Tapping mode diamond-like-carbon coated tips (Tap300Al-G-DLC, Budget Sensors) were used for both imaging and scratching. The scratching was carried out in contact mode and tapping mode was used to image a larger area than the scratched rectangle.

4.2.5 Electrochemical Characterization

All electrochemical measurements were performed using an Autolab potentiostat (PGSTAT302N, Metrohm Autolab B.V.) and a three-electrode cell. The diamond samples were used as the working electrode with an exposed area of 0.275 cm^2 and a platinum wire was used as the counter-electrode. The reference electrode was Ag/AgCl/3M NaCl (BASi). All reported voltages are with respect to this reference. 1 M $HClO_4$ was used as the electrolyte unless stated otherwise. Impedance spectroscopy measurements were taken with a 10 mV RMS amplitude at frequencies typically between 0.1 and 100,000 Hz. Nova software was used to fit impedance data to circuit models.

4.3 Results

4.3.1 Characterization of the Click Reaction

Successful covalent attachment of ferrocene groups to the diamond surface was followed using FTIR, XPS, and cyclic voltammetry. Figure 4.1 shows FTIR spectra of an azide terminated diamond sample before and after reaction with ethynyl ferrocene. The data shown are for a

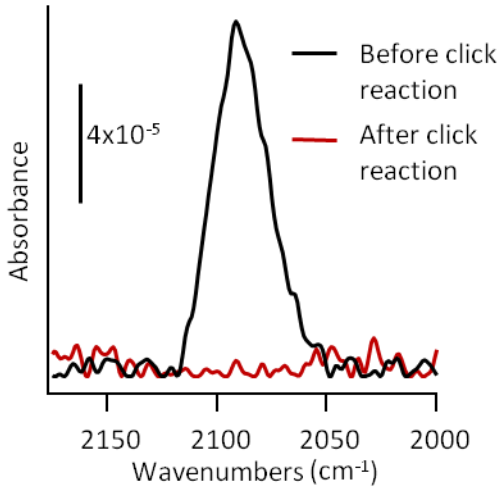

Figure 4.1: FTIR of an azide terminated diamond sample before and after click reaction. The stretch at 2090 cm^{-1} is the asymmetric stretch of the azide group. The disappearance of the stretch is consistent with a successful click reaction.

sample that was initially reacted with 3-buten-1-ol for 16 hours, although similar results were obtained with the longer chain alcohols. The stretch at 2090 cm^{-1} is characteristic of the asymmetric stretch of the azide group. This stretch disappears after reaction with ethynyl ferrocene, consistent with a successful click reaction.

Figure 4.2a shows XPS measurements of the azide terminated surface before (red trace) and after (blue trace) the click reaction with ethynyl ferrocene. The N(1s) signal of the unreacted azide groups appears as a characteristic 2:1 doublet at 400 and 404 eV.[13] The higher binding energy N(1s) peak is from the electron-deficient central N atom in the azide group. After the click reaction this higher binding energy peak disappears and the N(1s) spectrum shows only a single broad peak around 400 eV, consistent with the conversion of the azide group into the triazole ring.

To rule out the contribution of physisorbed ferrocene molecules, control experiments were done by reacting the intermediate alcohol-terminated diamond surface (Scheme 4.1) with alkynyl ferrocene under identical click reaction conditions. XPS measurements of the Fe(2p) region are shown in Figure 4.2b. Only measurements of the initially azide-terminated surface show sharp peaks at 708 and 720 eV characteristic of ferrocene with iron in the 2+ oxidation state. Interestingly, XPS measurements of both the alcohol-terminated surface and the azide-terminated surface show much broader peaks at 711 and 725 eV. These broader peaks are characteristic of ferrocenium where the iron is in the 3+ oxidation state.[21, 27] The XPS results suggest that ferrocene is specifically bound to the surface through the click reaction, but some non-specifically bound ferrocenium is also present. Coverage of $1.3x10^{14} Fe^{2+}/cm^2$ was calculated from the XPS peak areas. The theoretical maximum coverage of ferrocene groups has been

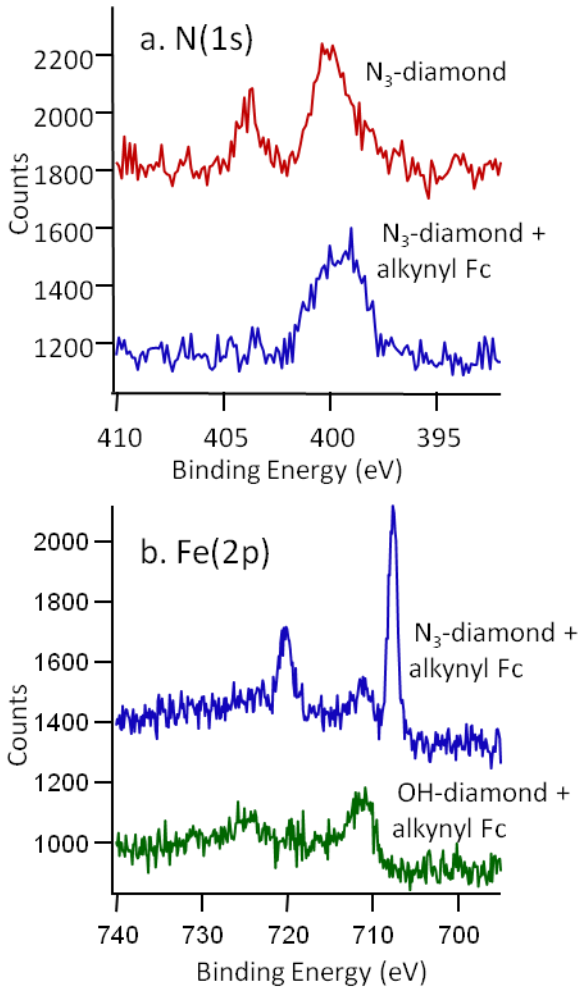

Figure 4.2: XPS of azide terminated diamond before (red trace) and after (blue trace) reaction with alkynyl ferrocene. As a control the alcohol terminated surface was also reacted with alkynyl ferrocene under identical conditions (green trace).

estimated to be $2.7x10^{14}$ cm^{-2} based on a close-packed layer of spheres with 6.6Å diameter[12] and an experimental maximum coverage of $2.6x10^{14}$ was measured for ferrocene terminated monolayers on gold.[13] The coverage measured here is ~50% of the expected maximum coverage. This result is typical for samples that have been illuminated for long times (16 hours) in the initial photochemical grafting step.

To see if the physisorbed ferrocenium is electrochemically active cyclic voltammograms were taken. Figure 4.3 shows CVs of the azide-terminated surface (black trace) and alcohol-terminated surface (red trace) after click reaction with the ethynyl ferrocene. Clear redox peaks ($E° = 0.39$ V) are seen for the sample which was initially terminated with azide groups. The control sample shows no evidence of redox peaks; the very small separation between forward and reverse sweeps is due to the interfacial capacitance. Therefore any physisorbed ferrocenium appears to be removed from the surface under the CV conditions and is not electrochemically active. Coverage of electrochemically active ferrocene was calculated by integrating the peak areas[10] yielding $1.6x10^{14}$ ferrocene/cm^2 consistent with the results from XPS.

4.3.2 Cyclic Voltammetry of Ferrocene Covalently Attached to Diamond

Figure 4.4 shows cyclic voltammograms obtained at different scan rates for ferrocene groups attached to the diamond surface. The data shown are for a sample that was initially reacted with 3-buten-1-ol for 16 hours, with similar results obtained for the longer chain alcohols. The formal potential is 0.39 V vs. Ag/AgCl similar to values reported for other types of electrodes modified with ferrocene through click chemistry[23, 52, 53] and somewhat higher than that reported for unmodified ferrocene in solution (~0.2 V vs. Ag/AgCl).[54] The triazole ring formed by the click reaction is an electron-withdrawing group and is expected to shift the formal

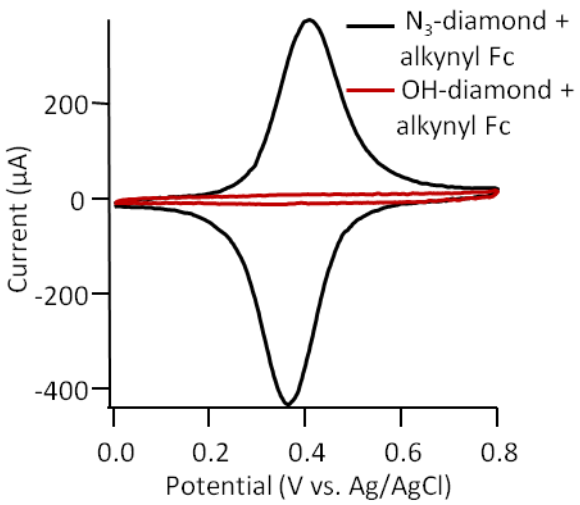

Figure 4.3: Cyclic voltammetry (scan rate 10 V/s) after the click reaction. The black trace is the azide-terminated surface after reaction with alkynyl ferrocene. The red trace is the alcohol terminated surface after undergoing the identical reaction with alkynyl ferrocene.

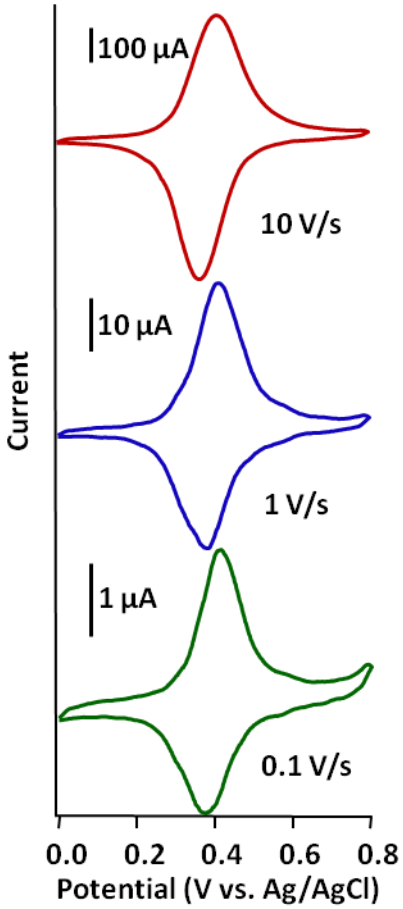

Figure 4.4: Cyclic voltammograms of diamond electrodes after reaction with ferrocene taken at different scan rates.

potential towards more oxidizing potentials.[55, 56] The shift towards higher potentials may also be partly explained by the non-polar monolayer destabilizing the ferrocenium with respect to the ferrocene.[57]

The peak half-width ΔE_{FWHM} is ideally 3.53RT/nF or 91 mV for a one-electron transfer at 25°C.[10, 58] The observed peak half-widths are significantly larger than the ideal value ranging from 120 mV at 0.1 V/s to 150 mV at 10 V/s for the anodic peak. This broadening is not uncommon and has been attributed to different local environments of the redox couple, variations in surface charge, and interactions between redox couples.[10]

The peak splitting ΔE_p is ~ 40 mV and is independent of scan rate between 0.1 and 10 V/s. While ideally ΔE_p is zero, this is seldom observed experimentally. A nonzero ΔE_p has been attributed to changes in the solvation of the redox centers or structure of the monolayer with changing oxidation state.[10] For example, ferrocenium is known to specifically ion pair with perchlorate anions.[57] Peak splitting tends to increase as the scan rate becomes comparable to or greater than the electron transfer rate. Since we observe that ΔE_p is independent of scan rate for the scan rates used here, this suggests that the electron transfer rate is fast relative to the scan rate.

Interestingly, we found no correlation between peak splitting and the length of the alkene used in the initial photochemical grafting step. Figure 4.5 shows cyclic voltammograms taken at 10 V/s for ferrocene tethered to diamond using different alkyl chain lengths. ΔE_p is 70 - 80 mV independent of chain length for the CVs shown. This suggests that the electron transfer rate is not significantly slowed by longer chains, at least for scan rates up to 10 V/s. There is some variability in the value of ΔE_p sample to sample, which typically ranges between 40 and 100 mV.

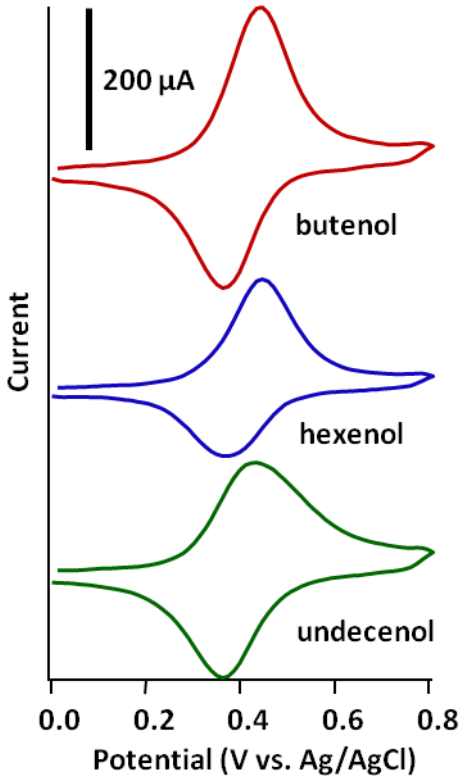

Figure 4.5: Cyclic voltammograms of ferrocene tethered to diamond with alkyl chains of different lengths. All scan rates were 10 V/s. Top trace (red) is for an initial photochemical grafting step with butenol. Middle trace (blue) used hexenol and bottom trace (green) used undecenol. All photochemical reaction times were 16 h.

This can most likely be attributed to differences in ferrocene coverage.[26, 49] A more detailed analysis of electron transfer rate which explicitly includes coverage effects was measured by electrochemical impedance spectroscopy.

4.3.3 Impedance Analysis of Standard Electron Transfer Rates k°.

Electrochemical impedance spectroscopy was used to measure the electron transfer rates. The equivalent circuit for redox couples strongly adsorbed to an electrode surface has been given by Laviron[59] (Figure 4.6a). It includes the solution resistance, R_S, and the double-layer capacitance, C_{DL}. The redox couple contributes an additional charge transfer resistance, $R_{CT,}$ and pseudocapacitance, $C_{A.}$ The solution resistance is in series with the other circuit elements and can be subtracted to yield the simpler Debye equivalent circuit[41, 60] (Figure 4.6b). The Debye circuit has a single relaxation time constant, τ, which is inversely related to the standard electron transfer rate, k°:

$$\tau = R_{CT}C_A = (2k°)^{-1}$$

The Debye circuit yields a perfect semi-circle in a Nyquist plot of the dielectric constant with the center of the circle positioned along the real axis. The dielectric constant, ε, is given by:

$$\varepsilon = (j\omega Z)^{-1}$$

where j is the imaginary unit, ω is the angular frequency, and Z is the impedance. The magnitude of the imaginary component of the dielectric constant reaches a maximum at a frequency, $\omega°$ inversely related to the relaxation time constant of the system:

$$\omega° = \tau^{-1}$$

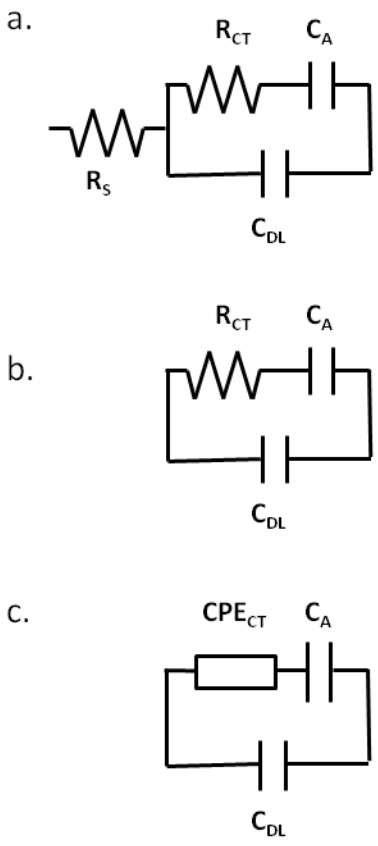

Figure 4.6: a.) Laviron's equivalent circuit for a redox couple strongly adsorbed to an electrode surface. R_S is the solution resistance and C_{DL} is the double layer capacitance. R_{CT} and C_A are the charge transfer resistance and pseudocapacitance. b.) Debye equivalent circuit. c.) Cole-Cole equivalent circuit. Here the charge transfer resistance has been replaced by a constant phase element.

Often systems display a distribution of time constants, rather than a single relaxation time constant.[22, 43, 61] This is commonly modeled by the Cole-Cole circuit where R_{CT}, a pure resistor, is replaced with a constant phase element (Figure 4.6c).[41, 42, 44, 60, 61] The impedance of a constant phase element (CPE) is given by:

$$Z_{CPE} = A(j\omega)^{-\alpha}$$

where A and α are adjustable parameters. The CPE is a simple distributed circuit element which is often used to model frequency-dependent effects that arise from microscopic inhomogeneity of the macroscopic electrode.[62] This can include effects such as surface roughness, local charge inhomogeneities, or a distribution of activation energies for charge transfer. The Cole-Cole circuit also yields a single, circular arc in a Nyquist plot of the dielectric constant, but the center of the circle lies below the real axis. Broader distributions of relaxation times result in greater depression of this arc below the real axis and are also reflected in larger values for the α parameter (an α value of 0 corresponds to the impedance of a pure resistor).

The redox potential of the surface bound ferrocene groups, E°, was measured using cyclic voltammetry for each sample and impedance data were collected at E° (~0.39 V vs. Ag/AgCl). The solution resistance was measured by taking impedance data at 0.8 V vs. Ag/AgCl, a potential far from the redox potential of the ferrocene where the diamond electrode behaves as a simple blocking electrode (solution resistance in series with a double layer capacitance). The solution resistance was subtracted from the impedance data taken at E° and the data was displayed as Cole-Cole plots (Nyquist plots of the dielectric constant). Figure 4.7 shows typical Cole-Cole plots for ferrocene tethered to diamond electrodes by the four different alkyl chain lengths investigated. Data were collected at frequencies from 1 Hz to 100,000 Hz. The data is

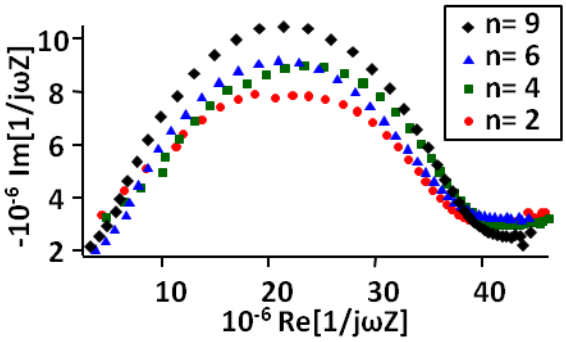

Figure 4.7: Cole-Cole plots for ferrocene tethered to the diamond surface through different alkyl chain lengths. Data were collected at frequencies between 1 and 100,000 Hz.

reasonably well fit by the Cole-Cole circuit shown in figure 5.5c. Figure 4.8 compares experimental data with the best fit to the Cole-Cole circuit. Modestly better fits can be obtained by replacing the double layer capacitance C_{DL} with a CPE. In all cases the data show a very broad distribution of relaxation times with α values for CPE_{CT} typically between 0.3 and 0.4. Electron transfer rates were taken directly from the frequency corresponding to the maxima in the Cole-Cole plots. These values were found to correlate well with values obtained through more detailed fitting to circuit models. Surprisingly, no correlation between chain length and electron transfer rate were found. Rather, a strong correlation between ferrocene coverage and electron transfer rater was measured.

Ferrocene coverage was varied by changing the length of illumination time for the initial photochemical grafting step (step 1, scheme 1) between 4 and 16 h. Shorter illumination times yield sparser, submonolayer coverage while longer reaction times yield full monolayer coverage.[63] Ferrocene coverage was measured by integrating the peak areas in the cyclic voltammograms. Electron transfer rates as a function of ferrocene coverage for three different alkyl chain lengths are shown in figure 4.9. The electron transfer is typically fast (~10^3-10^4 s^{-1}) with higher ferrocene coverage resulting in slower electron transfer rates.

4.3.4 Measurements of Interfacial Capacitance and Monolayer Structure

To gain insight into monolayer structure the double layer capacitance of a bare, hydrogen-terminated diamond electrode was compared to the capacitance of electrodes after functionalization with undecenol and ferrocene groups. The double layer capacitance was measured by impedance spectroscopy at 0.0 V and 0.8 V vs. Ag/AgCl, potentials far from $E°_{ferrocene}$ to avoid contributions from the charge transfer pseudocapacitance in the sample

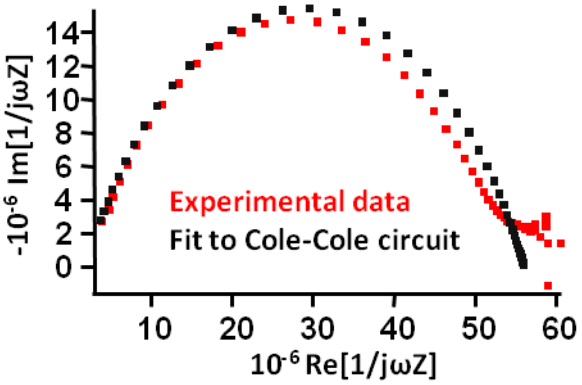

Figure 4.8: Red trace: Cole-Cole plot of experimental data for ferrocene tethered to diamond. Black trace: Fit to Cole-Cole circuit shown in figure 4c.

Fit parameters: C_{DL}= 2.1x10^{-6}μF ; C_A = 5.4x10^{-5} μF ; Z_{CPE} = 1.9x10^{-2} (jω)$^{-0.34}$ Ω

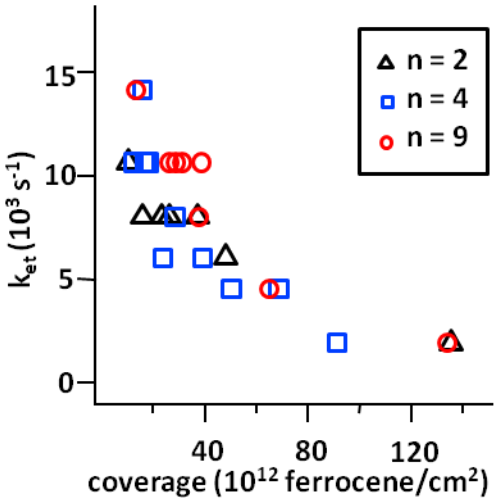

Figure 4.9: Standard electron transfer rates as a function of ferrocene coverage for different alkyl chain lengths

functionalized with ferrocene groups. Figure 4.10 shows Nyquist plots of the admittance at 0.8 V for a bare, hydrogen-terminated diamond electrode, a diamond electrode grafted with undecenol for 16 hours, and a diamond electrode after functionalization with ferrocene groups. Impedance data were modeled by series R-CPE circuits, where R is the solution resistance (typically ~ 4 Ω) and the CPE represents the double layer capacitance.[64, 65] Table 4.1 shows values for the CPE parameters for all three surfaces. All parameters at each voltage are the same within the error of the fits, with the exception of an ~ 40% increase in A after grafting with undecenol compared to the bare surface.

Cyclic voltammetry is another method of characterizing the double-layer capacitance.[6, 66] In the absence of faradaic processes the only current that flows is that required to charge the double-layer. Figure 4.11 shows cyclic voltammograms taken at 1 V/s with a bare, hydrogen-terminated diamond electrode and a diamond electrode grafted with undecenol. There is a small increase in separation between forward and reverse scans after modification with undecenol, suggesting a small increase in the interfacial capacitance. Both cyclic voltammetry and impedance measurements indicate that the molecular layers do not result in a decrease in the interfacial capacitance. This is different from results for self-assembled monolayers on gold where the SAM-modified electrodes show much lower capacitance than the bare electrodes.[10] The change in interfacial capacitance is highly dependent on the degree of structural order in the SAM. A well-ordered SAM on gold formed using alkane thiols of similar chain length to the undecenol would decrease the interfacial capacitance by a factor of ~50 relative to the bare electrode[14]. SAMs with more defects and higher ion permeability show a much higher capacitance than well-ordered SAMs.[48]

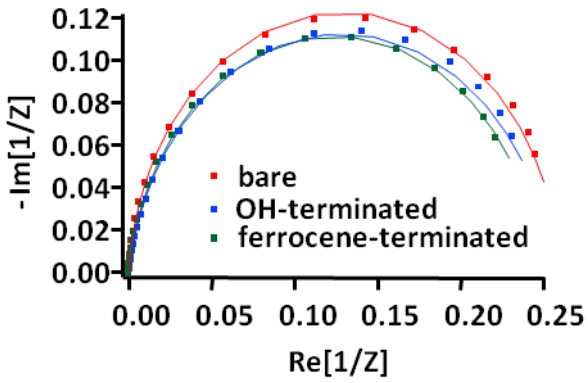

Figure 4.10: Nyquist plots of the admittance for a bare, hydrogen-terminated diamond electrode (red), a diamond electrode after photochemical grafting with undecenol (blue), and a diamond electrode functionalized with ferrocene (green). All data were collected at 0.8 V vs. Ag/AgCl. Markers are experimental data. Lines are for best fits to a series R-CPE circuit.

	0.0 V		0.8 V	
	A (10^{-6})	α	A (10^{-6})	α
bare, hydrogen-terminated	1.90	0.96	3.86	0.96
grafted with undecenol	1.74	0.94	5.33	0.92
ferrocene terminated	1.84	0.93	3.88	0.94

Table 4.1: Values for CPE Fitting parameters

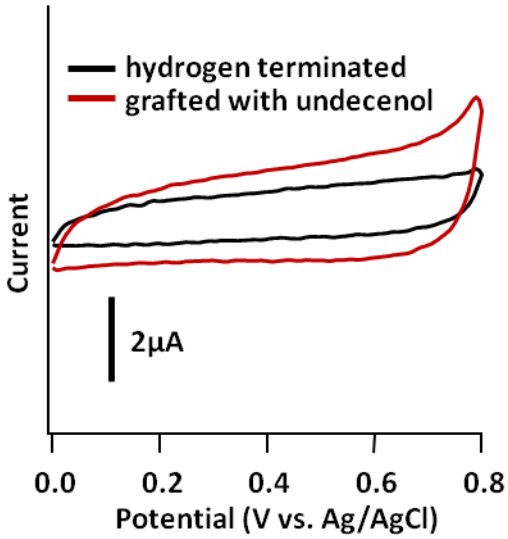

Figure 4.11: Cyclic voltammograms of a bare, hydrogen-terminated diamond electrode and a diamond electrode grafted with undecenol for 16 h. Scan rate 1 V/s.

AFM scratching[67] was used to further investigate the structure of the molecular layers. The CVD diamond used for electrochemical characterization is too rough for AFM measurements. Therefore, a cleaved, natural single crystal of boron-doped diamond was used for characterization by AFM. The natural crystal exposes atomically flat (111) crystal planes. The natural diamond was grafted for 16 hours with undecenol. A portion of the monolayer was removed by the AFM tip in contact mode and then the sample was reimaged in tapping mode (figure 4.12). The height of the molecular layer on this sample is 1.3 nm, which is very similar to what has been reported for SAMs on gold formed from thiols with alkyl chains of similar length to undecenol.[14] The height of the fully extended hydrocarbon chain in undecanol is 1.5 nm, but some tilting of the alkyl chains or disorder in the layer would be expected to decrease the thickness.

4.4 Discussion

Many factors influence electron transfer rate from redox-active monolayers including the structure of the monolayer[12, 17, 38, 48], the nature of the substrate[20], the density of redox active groups[26, 31, 49, 68], and the choice of electrolyte, solvent, and pH.[43, 69, 70] Many studies have been performed on thiol SAMs on gold where the chain length in the monolayer is systematically varied. The electron transfer rate has been found to decrease exponentially with increasing distance or chain length:[19, 22, 32-34, 37, 38, 45, 71]

$$k°_{app}=k°\exp(-\beta d)$$

where $k°_{app}$ is the apparent rate constant, β is the tunneling parameter, and d is the distance between the electrode and the redox couple. The value of the tunneling parameter β has been

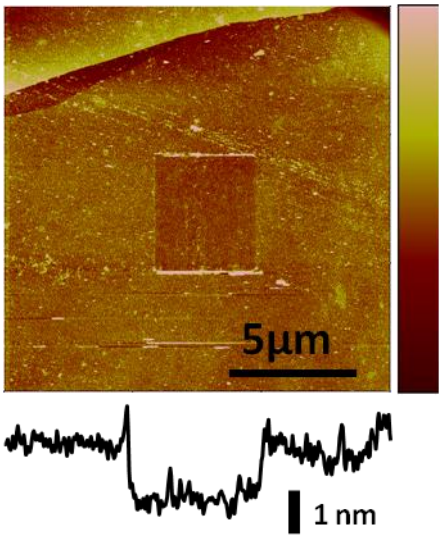

Figure 4.12: AFM image of cleaved single crystal diamond grafted with undecenol for 16 h. The center rectangle is where the undecenol has been removed by the AFM tip. The vertical scale bar is 20 nm.

shown to depend on the conjugation of the spacer and the environment of the redox couple which reflect changes in tunneling rate and mechanism.[33, 38]

A few studies have not found an exponential dependence on rate constant with the length of the spacer.[17, 25, 29, 30, 46, 47, 69, 72] Electron transfer rates that are independent of chain length have been explained by a rate-limiting step that is not electron tunneling. Rather, conformational changes[46, 47, 72], counterion motion[17, 73], or electron hopping between redox centers[29, 30] determine the electron transfer rate. It seems unlikely that conformational changes are the rate limiting step in our system. Ferrocene is a simple, outer sphere redox couple and little structural change takes place between the two oxidation states. Rather, the dominant contribution to the activation barrier is the solvent reorganization energy.[11, 74] An adiabatic electron transfer rate of 2.4×10^{8} s^{-1} has been calculated for electron transfer between ferrocene and gold.[33] This is 4-5 orders of magnitude faster than the rates measured here which indicates that conformational changes or solvent reorganization are unlikely to be rate limiting.

A detailed understanding of the role of counterion motion is beyond the scope of this study. However, measurements of interfacial capacitance indicate that the molecular layers formed on diamond are very permeable to solvent and ions, making it unlikely that counterion motion is rate-limiting. Moreover, one would expect that longer alkyl chains could more effectively bury the ferrocene groups than shorter tethers. Since the electron transfer rates are independent of chain length, it seems unlikely that ion migration and ion pairing are kinetically limiting.

Similarly, a mechanism of electron hopping between redox centers does not satisfactorily explain our results. Electron exchange between redox centers has been proposed to be an

important pathway for electron transfer in monolayers with high densities of redox-active groups.[12, 29-31] This model, however, predicts faster electron transfer rates with higher coverage of redox moieties.[68, 75] The opposite trend is observed here, with higher densities of redox active groups resulting in slower electron transfer rates.

Electron transfer rates that decrease with increasing surface coverage have been reported for ferrocene monolayers on Si[26] and for porphyrin monolayers on Si and gold.[49] Changes in adsorption geometry and orientation as a function of surface concentration were given as one possible explanation for this trend. In other words, the average distance between the redox couple and the surface is a function of coverage. At lower coverage the redox couples may approach the surface more closely and electronic interactions could occur directly between the redox center and the surface. This interpretation is consistent with our previous results for ferrocene groups linked to carbon nanofibers, where we argued that an electron tunneling mechanism did not describe electron transfer rates through sparse and disordered monolayers.[25]

Electron transfer rates between gold electrodes and ferrocene SAMs are on the order of $10^6 – 10^3$ s^{-1} for 5-10 methylene groups in the aliphatic chain.[19, 34] These values are comparable to the electron transfer rates we measured on diamond electrodes, typically 10^3-10^4 s^{-1}. The electron transfer rates on diamond do not surpass the electron transfer rates on gold for short chain lengths. This result is not surprising since the heterogeneous electron transfer rate between ferrocene in solution and gold electrodes is 1-2 orders of magnitude higher than what has been measured at diamond electrodes.[3, 76] This is likely due to the lower density of states in diamond relative to gold.[77] Nonetheless, the electron transfer rates are considerably faster than the turnover frequency of many catalysts of interest[78-81] and also 2-4 orders of magnitude faster than

electron transfer rates measured on other carbon-based electrodes.[20, 25] These results highlight that diamond electrodes are especially promising as platforms for challenging electrocatalytic reactions such as water oxidation or CO_2 reduction where high electrode stability is essential and catalyst turnover frequency is likely to be rate-limiting.

4.5 Conclusions

We have measured electron transfer rates between ferrocene monolayers and diamond electrodes as a function of chain length and found that the kinetics are independent of the length of the linker. In contrast to self-assembled monolayers formed on gold electrodes, the monolayers formed on diamond are relatively disordered, as evidenced by their permeability to ion and solvent. Therefore, the average distance between the redox couple and the surface is not simply the length of the tether. Similarly, a lower coverage of ferrocene results in faster electron transfer rates because the ferrocene can approach the surface more closely. These results highlight the importance of monolayer structure in the determining the mechanism of charge transport.

Our results show that there is a trade-off between high surface coverage and fast electron transfer rates. However, even at the highest coverage (~50% of a close-packed monolayer) the electron transfer rates measured here are considerably faster than what has been previously been measured on carbon-based electrodes. The attachment chemistry we have developed for diamond electrodes shows both high stability and fast electron transfer kinetics and is a promising platform for electron transfer and electrocatalysis.

4.6 References

1. Martin, H. B.; Argoitia, A.; Landau, U.; Anderson, A. B.; Angus, J. C., Hydrogen and oxygen evolution on boron-doped diamond electrodes. *Journal of the Electrochemical Society* **1996,** 143, L133.

2. Granger, M. C.; Witek, M.; Xu, J. S.; Wang, J.; Hupert, M.; Hanks, A.; Koppang, M. D.; Butler, J. E.; Lucazeau, G.; Mermoux, M.; Strojek, J. W.; Swain, G. M., Standard electrochemical behavior of high-quality, boron-doped polycrystalline diamond thin-film electrodes. *Analytical Chemistry* **2000,** 72, 3793.

3. Hupert, M.; Muck, A.; Wang, R.; Stotter, J.; Cvackova, Z.; Haymond, S.; Show, Y.; Swain, G. M., Conductive diamond thin-films in electrochemistry. *Diamond and Related Materials* **2003,** 12, 1940.

4. Swain, G. M., Electrically Conducting Diamond Thin Films: Advanced Electrode Materials for Electrochemical Technologies. Electroanalytical Chemistry: A Series of Advances. Vol. 22, p 181-277.

5. Swain, G. M., The Susceptibility to Surface Corrosion in Acidic Fluoride Media - A Comparison of Diamond, HOPG, and Glassy Carbon Electrodes. *Journal of the Electrochemical Society* **1994,** 141, 3382.

6. Swain, G. M.; Ramesham, R., The Electrochemical Activity of Boron-Doped Polycrystalline Diamond Thin-Film Electrodes. *Analytical Chemistry* **1993,** 65, 345.

7. Xu, J. S.; Granger, M. C.; Chen, Q. Y.; Strojek, J. W.; Lister, T. E.; Swain, G. M., Boron-doped diamond thin-film electrodes. *Analytical Chemistry* **1997,** 69, A591.

8. Ruther, R. E.; Rigsby, M. L.; Gerken, J. B.; Hogendoorn, S. R.; Landis, E. C.; Stahl, S. S.; Hamers, R. J., Highly Stable Redox-Active Molecular Layers by Covalent Grafting to Conductive Diamond. *Journal of the American Chemical Society* **2011,** 133, 5692.

9. Devaraj, N. K.; Decreau, R. A.; Ebina, W.; Collman, J. P.; Chidsey, C. E. D., Rate of interfacial electron transfer through the 1,2,3-triazole linkage. *Journal of Physical Chemistry B* **2006,** 110, 15955.

10. Finklea, H. O., Electrochemistry of organized monolayers of thiols and related molecules on electrodes. Electroanalytical Chemistry: A Series of Advances. Vol. 19, p 109-335.

11. Chidsey, C. E. D., Free-Energy and Temperature-Dependence of Electron-Transfer at the Metal-Electrolyte Interface. *Science* **1991,** 251, 919.

12. Chidsey, C. E. D.; Bertozzi, C. R.; Putvinski, T. M.; Mujsce, A. M., Coadsorption of Ferrocene-Terminated and Unsubstituted Alkanethiols on Gold - Electroactive Self-Assembled Monolayers. *Journal of the American Chemical Society* **1990,** 112, 4301.

13. Collman, J. P.; Devaraj, N. K.; Eberspacher, T. P. A.; Chidsey, C. E. D., Mixed azide-terminated monolayers: A platform for modifying electrode surfaces. *Langmuir* **2006,** 22, 2457.

14. Porter, M. D.; Bright, T. B.; Allara, D. L.; Chidsey, C. E. D., Spontaneously Organized Molecular Assemblies. 4. Structural Characterization of Normal-Alkyl Thiol Monolayers on Gold by Optical Ellipsometry, Infrared-Spectroscopy, and Electrochemistry. *Journal of the American Chemical Society* **1987,** 109, 3559.

15. Smalley, J. F.; Finklea, H. O.; Chidsey, C. E. D.; Linford, M. R.; Creager, S. E.; Ferraris, J. P.; Chalfant, K.; Zawodzinsk, T.; Feldberg, S. W.; Newton, M. D., Heterogeneous electron-transfer kinetics for ruthenium and ferrocene redox moieties through alkanethiol monolayers on gold. *Journal of the American Chemical Society* **2003,** 125, 2004.

16. Creager, S. E.; Wooster, T. T., A new way of using ac voltammetry to study redox kinetics in electroactive monolayers. *Analytical Chemistry* **1998,** 70, 4257.

17. Sumner, J. J.; Creager, S. E., Redox kinetics in monolayers on electrodes: Electron transfer is sluggish for ferrocene groups buried within the monolayer interior. *Journal of Physical Chemistry B* **2001,** 105, 8739.

18. Sumner, J. J.; Weber, K. S.; Hockett, L. A.; Creager, S. E., Long-range heterogeneous electron transfer between ferrocene and gold mediated by n-alkane and N-alkyl-carboxamide bridges. *Journal of Physical Chemistry B* **2000,** 104, 7449.

19. Weber, K.; Hockett, L.; Creager, S., Long-range electronic coupling between ferrocene and gold in alkanethiolate-based monolayers on electrodes. *Journal of Physical Chemistry B* **1997,** 101, 8286.

20. Liu, G. Z.; Liu, J. Q.; Bocking, T.; Eggers, P. K.; Gooding, J. J., The modification of glassy carbon and gold electrodes with aryl diazonium salt: The impact of the electrode materials on the rate of heterogeneous electron transfer. *Chemical Physics* **2005,** 319, 136.

21. Umana, M.; Rolison, D. R.; Nowak, R.; Daum, P.; Murray, R. W., X-Ray Photoelectron-Spectroscopy of Metal, Metal-Oxide, and Carbon Electrode Surfaces Chemically Modified with Ferrocene and Ferricenium. *Surface Science* **1980,** 101, 295.

22. Rowe, G. K.; Carter, M. T.; Richardson, J. N.; Murray, R. W., Consequences of Kinetic Dispersion on the Electrochemistry of an Adsorbed Redox-Active Monolayer. *Langmuir* **1995,** 11, 1797.

23. Marrani, A. G.; Dalchiele, E. A.; Zanoni, R.; Decker, F.; Cattaruzza, F.; Bonifazi, D.; Pratoc, M., Functionalization of Si(100) with ferrocene derivatives via "click" chemistry. *Electrochimica Acta* **2008,** 53, 3903.

24. Evrard, D.; Lambert, F.; Policar, C.; Balland, V.; Limoges, B., Electrochemical Functionalization of Carbon Surfaces by Aromatic Azide or Alkyne Molecules: A Versatile Platform for Click Chemistry. *Chemistry-A European Journal* **2008,** 14, 9286.

25. Landis, E. C.; Hamers, R. J., Covalent Grafting of Ferrocene to Vertically Aligned Carbon Nanofibers: Electron-transfer Processes at Nanostructured Electrodes. *Journal of Physical Chemistry C* **2008,** 112, 16910.

26. Roth, K. M.; Yasseri, A. A.; Liu, Z. M.; Dabke, R. B.; Malinovskii, V.; Schweikart, K. H.; Yu, L. H.; Tiznado, H.; Zaera, F.; Lindsey, J. S.; Kuhr, W. G.; Bocian, D. F., Measurements of electron-transfer rates of charge-storage molecular monolayers on Si(100). Toward hybrid molecular/semiconductor information storage devices. *Journal of the American Chemical Society* **2003,** 125, 505.

27. Dalchiele, E. A.; Aurora, A.; Bernardini, G.; Cattaruzza, F.; Flamini, A.; Pallavicini, P.; Zanoni, R.; Decker, F., XPS and electrochemical studies of ferrocene derivatives anchored on n- and p-Si(100) by Si-O or Si-C bonds. *Journal of Electroanalytical Chemistry* **2005,** 579, 133.

28. Li, C. Q.; Ren, B. Y.; Zhang, Y.; Cheng, Z. Y.; Liu, X. X.; Tong, Z., A Novel Ferroceneylazobenzene Self-Assembled Monolayer on an ITO Electrode: Photochemical and Electrochemical Behaviors. *Langmuir* **2008,** 24, 12911.

29. Riveros, G.; Meneses, S.; Escobar, S.; Garin, C.; Chornik, B., Electron Transfer Rates of Alkyl-Ferrocene Molecules Forming Incomplete Monolayer on Silicon Electrodes. *Journal of the Chilean Chemical Society* **2010**, 55, 61.

30. Riveros, G.; Garin, C.; Meneses, S.; Escobar, S., Silicon Modification with Molecules Derived from Ferrocene: Effect of the Crystallographic Orientation of Silicon in the Electron-Transfer Rates. *Molecular Crystals and Liquid Crystals* **2010**, 521, 187.

31. Hauquier, F.; Ghilane, J.; Fabre, B.; Hapiot, P., Conducting ferrocene monolayers on nonconducting surfaces. *Journal of the American Chemical Society* **2008,** 130, 2748.

32. Sachs, S. B.; Dudek, S. P.; Hsung, R. P.; Sita, L. R.; Smalley, J. F.; Newton, M. D.; Feldberg, S. W.; Chidsey, C. E. D., Rates of interfacial electron transfer through pi-conjugated spacers. *Journal of the American Chemical Society* **1997,** 119, 10563.

33. Creager, S.; Yu, C. J.; Bamdad, C.; O'Connor, S.; MacLean, T.; Lam, E.; Chong, Y.; Olsen, G. T.; Luo, J. Y.; Gozin, M.; Kayyem, J. F., Electron transfer at electrodes through conjugated "molecular wire" bridges. *Journal of the American Chemical Society* **1999,** 121, 1059.

34. Smalley, J. F.; Feldberg, S. W.; Chidsey, C. E. D.; Linford, M. R.; Newton, M. D.; Liu, Y. P., The Kinetics of Electron-Transfer Through Ferrocene-Terminated Alkanethiol Monolayers on Gold. *Journal of Physical Chemistry* **1995,** 99, 13141.

35. Eckermann, A. L.; Feld, D. J.; Shaw, J. A.; Meade, T. J., Electrochemistry of redox-active self-assembled monolayers. *Coordination Chemistry Reviews* **2010,** 254, 1769.

36. Creager, S. E.; Weber, K., On the Interplay Between Interfacial Potential Distribution and Electron-Transfer Kinetics in Organized Monolayers on Electrodes. *Langmuir* **1993,** 9, 844.

37. Finklea, H. O.; Hanshew, D. D., Electron-Transfer Kinetics in Organized Thiol Monolayers with Attached Pentaammine(Pyridine)Ruthenium Redox Centers. *Journal of the American Chemical Society* **1992,** 114, 3173.

38. Finklea, H. O.; Liu, L.; Ravenscroft, M. S.; Punturi, S., Multiple electron tunneling paths across self-assembled monolayers alkanethiols with attached ruthenium(II/III) redox centers. *Journal of Physical Chemistry* **1996,** 100, 18852.

39. Finklea, H. O.; Ravenscroft, M. S.; Snider, D. A., Electrolyte and Temperature Effects on Long-Range Electron-Transfer Across Self-Assembled Monolayers. *Langmuir* **1993,** 9, 223.

40. Groat, K. A.; Creager, S. E., Self-Assembled Monolayers in Organic-Solvents - Electrochemistry at Alkanethiolate-Coated Gold in Propylene Carbonate. *Langmuir* **1993,** 9, 3668.

41. Nahir, T. M.; Bowden, E. F., The distribution of standard rate constants for electron transfer between thiol-modified gold electrodes and adsorbed cytochrome c. *Journal of Electroanalytical Chemistry* **1996,** 410, 9.

42. Nahir, T. M.; Bowden, E. F., Measurement of the rate of adsorption of electroactive cytochrome c to modified gold electrodes by electrochemical impedance spectroscopy. *Langmuir* **2002,** 18, 5283.

43. Ravenscroft, M. S.; Finklea, H. O., Kinetics of Electron-Transfer to Attached Redox Centers on Gold Electrodes in Nonaqueous Electrolytes. *Journal of Physical Chemistry* **1994,** 98, 3843.

44. Wang, Q.; Zhi, F. P.; Wang, W. T.; Xia, X. H.; Liu, X. H.; Meng, F. F.; Song, Y. Y.; Yang, C.; Lu, X. Q., Direct Electron Transfer of Thiol-Derivatized Tetraphenylporphyrin Assembled on Gold Electrodes in an Aqueous Solution. *Journal of Physical Chemistry C* **2009,** 113, 9359.

45. Brevnov, D. A.; Finklea, H. O.; Van Ryswyk, H., AC voltammetry studies of electron transfer kinetics for a redox couple attached via short alkanethiols to a gold electrode. *Journal of Electroanalytical Chemistry* **2001,** 500, 100.

46. Feng, Z. Q.; Imabayashi, S.; Kakiuchi, T.; Niki, K., Long-range electron-transfer reaction rates to cytochrome c across long- and short-chain alkanethiol self-assembled monolayers: Electroreflectance studies. *Journal of the Chemical Society-Faraday Transactions* **1997,** 93, 1367.

47. Avila, A.; Gregory, B. W.; Niki, K.; Cotton, T. M., An electrochemical approach to investigate gated electron transfer using a physiological model system: Cytochrome c immobilized on carboxylic acid-terminated alkanethiol self-assembled monolayers on gold electrodes. *Journal of Physical Chemistry B* **2000,** 104, 2759.

48. Hockett, L. A.; Creager, S. E., Redox Kinetics for Ferrocene Groups Immobilized in Impermeable and Permeable Self-Assembled Monolayers. *Langmuir* **1995,** 11, 2318.

49. Roth, K. M.; Gryko, D. T.; Clausen, C.; Li, J. Z.; Lindsey, J. S.; Kuhr, W. G.; Bocian, D. F., Comparison of electron-transfer and charge-retention characteristics of porphyrin-containing self-assembled monolayers designed for molecular information storage. *Journal of Physical Chemistry B* **2002,** 106, 8639.

50. Benson, M. C.; Ruther, R. E.; Gerken, J. B.; Rigsby, M. L.; Bishop, L. M.; Tan, Y. Z.; Stahl, S. S.; Hamers, R. J., Modular "Click" Chemistry for Electrochemically and Photoelectrochemically Active Molecular Interfaces to Tin Oxide Surfaces. *ACS Applied Materials & Interfaces* **2011,** 3, 3110.

51. Thoms, B. D.; Owens, M. S.; Butler, J. E.; Spiro, C., Production And Characterization Of Smooth, Hydrogen-Terminated Diamond C(100). *Applied Physics Letters* **1994,** 65, 2957.

52. Collman, J. P.; Devaraj, N. K.; Chidsey, C. E. D., "Clicking" functionality onto electrode surfaces. *Langmuir* **2004,** 20, 1051.

53. Devadoss, A.; Chidsey, C. E. D., Azide-modified graphitic surfaces for covalent attachment of alkyne-terminated molecules by "click" chemistry. *Journal of the American Chemical Society* **2007,** 129, 5370.

54. Gagne, R. R.; Koval, C. A.; Lisensky, G. C., Ferrocene as an internal standard for electrochemical measurements. *Inorganic Chemistry* **1980,** 19, 2854.

55. Ganesh, V.; Sudhir, V. S.; Kundu, T.; Chandrasekaran, S., 10 Years of Click Chemistry: Synthesis and Applications of Ferrocene-Derived Triazoles. *Chemistry-An Asian Journal* 6, 2670.

56. McCrory, C. C. L.; Devadoss, A.; Ottenwaelder, X.; Lowe, R. D.; Stack, T. D. P.; Chidsey, C. E. D., Electrocatalytic O_2 Reduction by Covalently Immobilized Mononuclear Copper(I) Complexes: Evidence for a Binuclear Cu_2O_2 Intermediate. *Journal of the American Chemical Society* 133, 3696.

57. Rowe, G. K.; Creager, S. E., Redox and Ion-Pairing Thermodynamics in Self-Assembled Monolayers. *Langmuir* **1991,** 7, 2307.

58. Laviron, E., Adsorption, Autoinhibition and Autocatalysis in Polarography and in Linear Potential Sweep Voltammetry. *Journal of Electroanalytical Chemistry* **1974,** 52, 355.

59. Laviron, E., AC Polarography and Faradaic Impedance of Strongly Adsorbed Electroactive Species. 3. Theoretical Complex-Plane Analysis for a Surface Redox Reaction. *Journal of Electroanalytical Chemistry* **1979,** 105, 35.

60. MacDonald, J. R., *Impedance Spectroscopy. Emphasizing Solid Materials and Systems.* Wiley-Interscience: New York, 1987.

61. Cole, K. S.; Cole, R. H., Dispersion and Absorption in Dielectrics. I. Alternating Current Characteristics. *Journal of Chemical Physics* **1941,** 9, 341.

62. Hurt, R. L.; Macdonald, J. R., Distributed Circuit Elements in Impedance Spectroscopy - A Unified Treatment of Conductive and Dielectric Systems. *Solid State Ionics* **1986,** 20, 111.

63. Nichols, B. M.; Butler, J. E.; Russell, J. N.; Hamers, R. J., Photochemical functionalization of hydrogen-terminated diamond surfaces: A structural and mechanistic study. *Journal of Physical Chemistry B* **2005,** 109, 20938.

64. Brug, G. J.; Vandeneeden, A. L. G.; Sluytersrehbach, M.; Sluyters, J. H., The Analysis of Electrode Impedances Complicated by the Presence of a Constant Phase Element. *Journal of Electroanalytical Chemistry* **1984,** 176, 275.

65. Pajkossy, T., Impedance of Rough Capacitive Electrodes. *Journal of Electroanalytical Chemistry* **1994,** 364, 111.

66. Hamann, C. H.; Hamnett, A.; Vielstich, W., *Electrochemistry*. Wiley: Weinheim, 1998.

67. Anariba, F.; DuVall, S. H.; McCreery, R. L., Mono- and multilayer formation by diazonium reduction on carbon surfaces monitored with atomic force microscopy "scratching". *Analytical Chemistry* **2003,** 75, 3837.

68. Blauch, D. N.; Saveant, J. M., Dynamics of Electron Hopping in Assemblies of Redox Centers - Percolation and Diffusion. *Journal of the American Chemical Society* **1992,** 114, 3323.

69. Hong, H. G.; Park, W., Unusual electron tunneling constant for long range electron transfer in hydroquinone (H_2Q)-terminated self-assembled monolayers on gold in alkaline solution. *Bulletin of the Korean Chemical Society* **2005,** 26, 1885.

70. Forster, R. J.; Faulkner, L. R., Electrochemistry of Spontaneously Adsorbed Monolayers - Effects of Solvent, Potential, and Temperature on Electron-Transfer Dynamics. *Journal of the American Chemical Society* **1994,** 116, 5453.

71. Dubois, L. H.; Nuzzo, R. G., Synthesis, Structure, And Properties Of Model Organic-Surfaces. *Annual Review of Physical Chemistry* **1992,** 43, 437.

72. Niki, K.; Sprinkle, J. R.; Margoliash, E., Intermolecular biological electron transfer: an electrochemical approach. *Bioelectrochemistry* **2002,** 55, 37.

73. Amatore, C.; Maisonhaute, E.; Schollhorn, B.; Wadhawan, J., Ultrafast voltammetry for probing interfacial electron transfer in molecular wires. *Chemphyschem* **2007,** 8, 1321.

74. Gennett, T.; Milner, D. F.; Weaver, M. J., Role of Solvent Reorganization Dynamics in Electron-Transfer Processes - Theory Experiment Comparisons for Electrochemical and Homogeneous Electron Exchange Involving Metallocene Redox Couples. *Journal of Physical Chemistry* **1985,** 89, 2787.

75. George, C. B.; Szleifer, I.; Ratner, M. A., Lateral electron transport in monolayers of short chains at interfaces: A Monte Carlo study. *Chemical Physics* **2010**, 375, 503.

76. Wipf, D. O.; Kristensen, E. W.; Deakin, M. R.; Wightman, R. M., Fast-Scan Cyclic Voltammetry as a Method to Measure Rapid, Heterogeneous Electron-Transfer Kinetics. *Analytical Chemistry* **1988,** 60, 306.

77. Haymond, S.; Babcock, G. T.; Swain, G. M., Electron transfer kinetics of ferrocene at microcrystalline boron-doped diamond electrodes: Effect of solvent and electrolyte. *Electroanalysis* **2003,** 15, 249.

78. Duan, L.; Bozoglian, F.; Mandal, S.; Stewart, B.; Privalov, T.; Llobet, A.; Sun, L., A molecular ruthenium catalyst with water-oxidation activity comparable to that of photosystem II. *Nature Chemistry* **2012,** advance on-line publication.

79. Yin, Q.; Tan, J. M.; Besson, C.; Geletii, Y. V.; Musaev, D. G.; Kuznetsov, A. E.; Luo, Z.; Hardcastle, K. I.; Hill, C. L., A Fast Soluble Carbon-Free Molecular Water Oxidation Catalyst Based on Abundant Metals. *Science* **2010,** 328, 342.

80. Geletii, Y. V.; Botar, B.; Koegerler, P.; Hillesheim, D. A.; Musaev, D. G.; Hill, C. L., An all-inorganic, stable, and highly active tetraruthenium homogeneous catalyst for water oxidation. *Angewandte Chemie-International Edition* **2008,** 47, 3896.

81. Laitar, D. S.; Muller, P.; Sadighi, J. P., Efficient homogeneous catalysis in the reduction of CO_2 to CO. *Journal of the American Chemical Society* **2005,** 127, 17196.

Chapter 5

Future Directions

5.1 ZnO

One great limitation of ZnO is its susceptibility to corrosion in aqueous solutions. Photochemical grafting of long alkyl chains creates a very hydrophobic surface. The work done here suggests that these alkyl groups may act as a protective coating which could greatly improve the hydrolytic stability of the material. It would be interesting to explore this effect in more detail using either AFM or SEM or possibly electrochemically by measuring corrosion currents.

The functional groups grafted to the surface of ZnO were limited here to simple esters and protected amines. While amide coupling or the Schiff's base reaction provide a route to introducing other functional groups, these reactions may suffer from low yield. It would be interesting to explore the possibility of doing click chemistry on the ZnO surface. The same general procedure used for introducing azide groups to the diamond surface should be transferable to ZnO. Some modifications of reaction times, temperatures, or solvents may be needed to prevent surface etching. The mesylation step could be replaced with a gas-phase thionyl chloride treatment which might also limit corrosion.

5.2 Diamond

The work done here shows that diamond holds great promise as a substrate for electrocatalysis. In collaboration with the Stahl group two different ruthenium-based oxidation catalysts have been successfully tethered to the diamond surface. Both of these complexes show

significant loss of activity under controlled potential electrolysis (CPE) and potential cycling. While the surface-bound $Ru(tpy)_2$ demonstrates greater stability, it too slowly degrades under potential cycling. The degradation is accelerated in aqueous solution. It would be valuable to understand the mechanism of this decomposition in order to design more robust systems.

Less work has been done with reduction catalysts tethered to the diamond surface, and it would be interesting to explore the stability of the surface chemistry under reducing potentials. In collaboration with the Berry group, a cobalt porphyrin CO_2 reduction catalyst was successfully tethered to the diamond surface. The ability to tether porphyrins to the diamond surface opens up the possibility to do interesting spectroelectrochemical studies of surface chemistry and catalysis.